Factors Affecting Fuel Transport of Firefighting Foam

Rezawana Islam

Dissertation submitted to the faculty of Virginia Polytechnic Institute and State University in partial fulfillment of the requirements for the degree of

Doctor of Philosophy

in

Materials Science & Engineering

Brian Y. Lattimer (Chair)

Rui Qiao

Alex Aning

Bill Reynolds

Feb 16th, 2024

Blacksburg, VA

Keywords: Aqueous film forming foam (AFFF), fuel transport, surfactants, microstructure, surfactant concentration, convection effect, ignition time.

Copyright

Factors Affecting Fuel Transport of Firefighting Foam

Rezawana Islam

Abstract

Aqueous film-forming foam (AFFF) used for fuel firefighting contains polyfluoroalkyl substances (PFAS) that have been identified as environmentally persistent and bioaccumulative resulting in phase out of AFFF. Currently, there are no environmentally friendly foams available that can perform at the same level as AFFF. Fuel transport has been recognized as a potential mechanism behind poor fire extinguishment, but the key features are yet unidentified. To fill these knowledge gaps, identifying the properties and features of surfactants used in firefighting foam that will prevent the transport of liquid fuel through the surfactant solution was imperative. To achieve that, this research was performed exclusively on single surfactants that have applications in firefighting foam. Impact of single surfactants on fuel transport was evaluated. Thermodynamics of the interaction between single surfactants and fuel; and kinetics of fuel transport through single surfactant solutions was observed.

It was hypothesized that the liquid fuel transport would influence microstructure in the bulk of the surfactant solution. Experiments were conducted for different single surfactant structures. Various methods were applied to identify the microstructure and interfacial properties of surfactants with and without exposure to liquid fuel. The factor affecting microstructure, identified through this study was further used to evaluate the firefighting performance of single surfactants through ignition test.

The thermodynamics of the interaction between fuel and single surfactants helped us to understand the fuel transport mechanism and role of micelle on fuel transport. Surfactant and fuel interaction has been studied below, at, and above the critical micelle concentration of surfactants. The effect of surfactant concentration, convection, and surfactant types were observed on the fuel transport. Moreover, an ignition test was conducted to evaluate the firefighting performance of single surfactants for various fuel types. Overall, the findings from this study will help design a new type of superefficient, environmentally acceptable surfactant for firefighting foam application.

Factors Affecting Fuel Transport of Firefighting Foam

Rezawana Islam

GENERAL AUDIENCE ABSTRACT

Aqueous film-forming foam (AFFF) used for fuel firefighting contains fluorinated compounds which are environmentally persistent and bioaccumulative. Therefore, AFFF has been phased out. There are no environmentally friendly foams available as efficient as current AFFF. Researchers have found that fuel transport through surfactant foam solution is the reason for foam collapse and poor fire extinguishment performance. However, the key parameters affecting fuel transport through foam solution have not been identified. Therefore, new formulations have become challenging, and it is important to identify the parameters affecting fuel transport through the firefighting foams. Surfactants are the key components of firefighting foam. The liquid fuel transport affects the microstructure of the surfactants in the bulk solution. Through this research microstructural and interfacial properties of single surfactants have been studied with and without exposure to liquid fuel. The factors affecting microstructure and firefighting performance of surfactants have been identified. Moreover, the interaction between fuel and single surfactants has been evaluated. The effect of surfactant concentration and fuel type on fuel transport has been observed. Moreover, the effect of convection (at the foam-fuel interface) on fuel transport has been observed. Overall, an understanding of factors affecting fuel transport of firefighting foam is achieved through this research, which can guide new types of efficient, environmentally friendly surfactant design.

Acknowledgements

My family members and their continuous support are my inspiration for this Ph.D. degree. I am thankful to my parents, my strength towards achieving this degree, and my brother for always believing in me. I'm thankful to my husband, Dr. Kazi Moshiur Rahman, for his complete support in my day-to-day life and for sharing this journey with me with our 2 years old son, Radeen Mahyar Kazi, my motivation to face all the challenges.

I would like to thank my advisor, Dr. Brian Lattimer, for giving me the opportunity to work in the EXTREME Environments and Materials Lab. His guidance and critiques at times gave me the drive to grow as a researcher. I am extremely grateful for his mentoring, support, and trust throughout my PhD journey. I acknowledge my Ph.D. advisory committee members Dr. Rui Qiao, Dr. Bill Reynolds, Dr. Alex Aning for their suggestions to improve my research. I am especially thankful to Dr. Rui Qiao for his beneficial and insightful comments and knowledge sharing in conducting my research. To my lab mates Dr. Steven Wong, Aysenur Ates, Mehrnoush Farhadi, Mehran Islam, Manjunath, thank you all for making my journey a memorable one. Our everyday interactions and conversations have always boosted my confidence and productivity, and I am thankful for that.

I would like to thank the Strategic Environmental Research and Development Program (SERDP) for funding my research. I would like to acknowledge the assistance from Dr. Alexis Williams, and Dr. Jong K. Keum from the Center for Nanophase Materials Sciences (CNMS) at Oak ridge national laboratory (ORNL). Dr. Gergely Nagy from Spallation Neutron Source (SNS) facility at ORNL. Patrick Finley from Materials Characterization Lab (MCL) at Virginia Tech. Dr. Weinan Leng from the Nanoscale Characterization and Fabrication Laboratory (NCFL) at Virginia Tech.

Finally, I am deeply thankful to Materials Science & Engineering Department's graduate coordinator Ms. Kim Grandstaff for her continuous support and motivation during my PhD journey. I am thankful to Mechanical Engineering Department staff Ms. Alida Spaulding, Ms. Amanda Collins, Ms. Amanda Maccoy, Mr. Johnny Underwood.

Table of Contents

Abstract ii
GENERAL AUDIENCE ABSTRACT iii
Acknowledgements iv
List of figures viii
List of Tables x
CHAPTER 1 1
Background and Motivation 1
1.1. Aqueous Film Forming Foam (AFFF) 1
1.2. Overall Research Goal 2
1.3. Research Objectives 3
1.3.1. Research Objectives: Impact of fuel on surfactant microstructure 3
1.3.2. Research Objectives: The interaction between fuel and single surfactants 3
1.3.3. Research Objectives: The effect of convection on fuel transport 4
1.4. Dissertation Roadmap 4
References 5
CHAPTER 2 6
Abstract 6
2.1. Introduction 6
2.2. Experimental details 9
2.2.1. Materials 9
2.2.2. Methods 12
2.3. Results 17
2.3.1. Packing parameter 17
2.3.2. Microstructural Features of Surfactants 18
2.3.3. Interfacial properties 23
2.3.4. Impact of surfactants on fuel solubility 27
2.3.5. Ignition test 31
2.4. Discussion 33
2.5. Conclusions 37
Appendix A. Supplementary information 41
A.1. Packing parameter 41
A.2. Small Angle neutron Scattering (SANS) 41
CHAPTER 3 46

Abstract 46
3.1. Introduction 47
3.2. Experimental 49
3.2.1. Materials 49
3.2.2. Methods 51
3.3. Results 53
3.3.1. Fuel Transport 53
3.3.2. Microstructural characterization 55
3.3.3. Thermodynamic characterization 57
3.3.3.1. Heptane 57
3.3.3.2. TMB 64
3.3.3.3. 25%TMB-Heptane 67
3.4. Discussion 70
3.5. Conclusions 74
References 75
Chapter 4 77
Abstract 77
4.1. Introduction 77
4.2. Experimental Details 80
4.2.1. Materials 80
4.2.2. Methods 81
4.3. Results 83
4.3.1. Fuel Transport 83
4.3.1.1. Heptane 83
4.3.1.2. TMB 85
4.3.1.3. 25%TMB/Heptane 87
4.3.2. Ignition test 89
4.4. Discussion 90
4.5. Conclusions 93
References 94
Appendix B. Supplementary Information 96
UV-Vis Spectroscopy 96
CHAPTER 5 98
5.1. Summary 98
5.2. Conclusions 99

5.3. Future Work 100
5.4. Publications 102
Appendix C 103
Abstract 103
C.1. Introduction 103
C.2. Experimental methods 106
C.2.1. Materials and Preparation 106
C.2.2. Characterization 108
C.3. Results 109
C.3.1 FTIR 109
C.3.1.1 Polyethylene 109
C.3.1.2. Polypropylene 111
C.3.1.3. Nylon 112
C.3.2. Raman Spectroscopy 114
C.3.2.1. Polyethylene 114
C.3.2.2. Polypropylene 116
C.3.2.3. Nylon 118
C.4. Discussion 119
C.5. Conclusion 122
References 124

List of figures

Figure 1 Aqueous film forming foam. 2
Figure 2. Surfactant structures a) Capstone 1157 b) Glucopon 600 CS UP c) Gelest 6185. 11
Figure 3. Experimental setup. 12
Figure 4. UV-Vis spectra a) absorbance versus wavelength b) standard graph. 15
Figure 5. Ignition test set up. 17
Figure 6. Cryo-TEM for a) Capstone b) Capstone- TMB. 19
Figure 7. Cryo-TEM for a) Glucopon b) Glucopon-TMB c) illustration of worm-like micelle. 20
Figure 8. a) Multilamellar vesicle b) d_spacing for vesicles. 21
Figure 9. DLS results a) Capstone b) Glucopon with and without fuel exposure. 23
Figure 10. Surface tension (SFT) and Interfacial tension (IFT) values. 24
Figure 11. CMC for surfactants i) Siloxane ii) Glucopon iii) Capstone. 25
Figure 12. CMC in the presence of fuel a) Capstone b) Glucopon c) Siloxane. 26
Figure 13. Surface excess with or without fuel exposure. 27
Figure 14. Solubility of fuel into surfactant solution a) Capstone b) Glucopon c) Siloxane. 29
Figure 15. Solubility of TMB in Capstone, Glucopon, and siloxane solution. 30
Figure 16. Solubility of 25% TMB-heptane in Capstone and Glucopon surfactant solution with and without stirring. 31
Figure 17. Bubble diameter. 32
Figure 18. Ignition test results. 33
Figure 19. Comparison of interfacial properties at air/solution and fuel/solution interface for Capstone, Glucopon, and siloxane to their microstructural properties. 35
Figure 20. Fuel solubilization mechanism a) nonpolar fuel b) polar fuel. 48
Figure 21. Experimental setup. 53
Figure 22. TMB and heptane concentration measurements in Glucopon below, at, and 5x CMC concentration for 15 minutes. 54
Figure 23. TMB, 25%TMB-heptane, and heptane concentration in a) Capstone and b) Glucopon solution at 5x CMC for 15 minutes 3 mm distance. 55
Figure 24. DLS results below, at, and above CMC concentrations of surfactants with and without fuel exposure a) Glucopon b) Capstone. 56
Figure 25. ITC thermogram (Heat flow versus time) after titration of heptane into sample cell with water. 57
Figure 26. ITC thermogram (Heat flow versus time) after titration of heptane into Glucopon solution a) 2x below CMC b) at CMC c) 5x above CMC. 59
Figure 27. Thermodynamic parameters enthalpy, Gibbs free energy, and entropy for heptane. 60
Figure 28. Fuel solubilization mechanism a) water-heptane b) Glucopon 2x below CMC c) Glucopon at CMC, and d) Glucopon 5x above CMC. 60
Figure 29. ITC thermogram (Heat flow versus time) after titration of heptane into Capstone solution a) below CMC b) at CMC c) 5x CMC. 63
Figure 30. ITC thermogram (Heat flow versus time) after titration of TMB into a) sample cell with water b) Capstone 5x CMC solution c) Glucopon 5x CMC solution. 66
Figure 31. Thermodynamic parameters enthalpy, Gibbs free energy, and entropy for TMB. 67
Figure 32. ITC thermogram (Heat flow versus time) after titration of 25% TMB-heptane into a) sample cell with water b) Glucopon 5x CMC solution c) Capstone 5x CMC solution. 69
Figure 33. Thermodynamic parameters enthalpy, Gibbs free energy, and entropy for 25% TMB-heptane. 70

Figure 34. Gibbs free energy versus fuel concentration and micelle size with heptane exposure 2x below, at and 5x above CMC concentration for a) Glucopon b) Capstone. 72
Figure 35. a) Single lamellar vesicle formed by Capstone b) Wormlike micelles formed by Glucopon [32]. 72
Figure 36. Illustration of convection effect at the foam-fuel interface. 79
Figure 37. Experimental setup. 82
Figure 38. Ignition test set up. 83
Figure 39. Heptane concentration measurement in Glucopon solution at four different distances away from the interface and times for a) natural and b) forced convection. 84
Figure 40. Heptane concentration measurement in Capstone solution at four different distances away from the interface and times for a) natural and b) forced convection. 85
Figure 41. TMB concentration measurement in Glucopon solution for a) natural and b) forced convection at four different distances away from the interface and times. 86
Figure 42. TMB concentration measurement in Capstone solution for a) natural and b) forced convection at different distances away from the interface and times. 87
Figure 43. 25%TMB-Heptane concentration measurement in Glucopon solution at four different distances away from the interface and times for a) natural and b) forced convection. 88
Figure 44. 25%TMB-Heptane concentration measurement in Capstone solution at four different distances away from the interface and times for a) natural and b) forced convection. 89
Figure 45. Ignition test result. 89
Figure 46. Values for fuel concentration change across the distance for forced convection at 60 min in a) Glucopon b) Capstone solution. 91
Figure 47. Fuel concentration versus time at 3 mm distance from the interface for forced convection in Capstone and Glucopon solution. 92
Figure 48. Absorbance versus wavelength plots and standard graph for fuel concentration measurment in Glucopon solution a) & b) TMB; c) & d)heptane; e) & f) 25%TMB-heptane. 97
Figure 49: Accelerated aging sample in AFFF concentrate. 108
Figure 50: Comparison of FTIR spectra of different polyethylene samples a) exposed to AFFF and b) after ultrasonic cleaning. 110
Figure 51: Comparison of FTIR spectra of different polypropylene samples a) exposed to AFFF and b) after ultrasonic cleaning. 112
Figure 52: Comparison of infrared spectra of different nylon samples a) exposed to AFFF and b) after ultrasonic cleaning. 114
Figure 53: Raman Spectra polyethylene samples a) exposed to AFFF and b) after ultrasonic cleaning. 115
Figure 54: Raman Spectra standard deviation for three different reading of PE Accld 3 yr Sample. 116
Figure 55: Raman Spectra polypropylene samples a) with AFFF exposure and b) following ultrasonic cleaning. 117
Figure 56: Raman spectra for nylon samples a) with AFFF exposure and b) following ultrasonic cleaning. 119
Figure 57: Comparison of intensity for different exposure durations for peak: Ny (1306 cm^{-1}), PE (1297 cm^{-1}), PP (1327 cm^{-1}). 121
Figure 58: Comparison of intensity at fluorinated peak for ultrasonic cleaned samples fluorinated peak: Ny (1306 cm^{-1}), PE (1297 cm^{-1}), PP (1327 cm^{-1}). 122
Figure 59: Intensity reduction from fluorinated to Ultrasonicated cleaned samples fluorinated peak: Ny (1306 cm^{-1}), PE (1297 cm^{-1}), PP (1327 cm^{-1}) 122

List of Tables

Table 1. Physical properties of fuel 10
Table 2. Surfactant Properties. 11
Table 3. calculated P value and graphical representation of self-assembly structure 18
Table 4 SANS measurement for Capstone 21
Table 5. SANS measurement for Glucopon 21
Table 6. radius for Siloxane from SANS (bottom phase) 22
Table 7. Radius for Siloxane from SANS (top phase) 22
Table 8. Water solubility of fuel 27
Table 9. Foam properties 32
Table 10. Physical properties of fuels. 50
Table 11. Surfactant Properties [5, 26]. 50
Table 12. Affinity value for Water-heptane, Glucopon-heptane below, at, and above CMC concentrations. 60
Table 13. Affinity value for Water-heptane, Capstone-heptane below, at, and above CMC concentrations. 64
Table 14. Affinity value for water-TMB, Capstone- TMB and Glucopon- TMB. 67
Table 15. Affinity value for water-25%TMB-heptane, Capstone-25%TMB-heptane and Glucopon-25%TMB-heptane. 70
Table 16. Surfactant Properties [21, 22]. 80
Table 17. Physical properties of fuel. 81
Table 18: Sample Composition 107
Table 19: FTIR peak assignment and description for polyethylene samples. 110
Table 20: FTIR peak assignment and description for polypropylene samples. 111
Table 21. FTIR peak assignment and description of nylon samples. 113
Table 22: Raman spectroscopy for polyethylene samples with assignment. 116
Table 23: Raman spectroscopy of polypropylene samples with assignment. 118
Table 24: Raman spectroscopy of nylon with assignment. 119

CHAPTER 1

Introduction

Background and Motivation

1.1. Aqueous Film Forming Foam (AFFF)

Aqueous film forming foams (AFFF) suppress liquid pool fires by spreading over and covering the fuel surface, acting as a physical barrier between fuel vapors and the flame above. AFFF has been in use by fire departments for fire extinguishing, fire-fighter drills and equipment analysis due to it being the most effective agent at suppressing large hydrocarbon fuel fires [1-3]. This is a concentrate of fluorocarbon surfactants, hydrocarbon surfactants, additive and water and the most efficient firefighting foam due to fluorocarbon surfactants in its formulations which can lower the surface tension of the foam solution significantly. Its high effectiveness in fire extinguishment is provided by not only foam layer but also an aqueous film layer on the surface of liquid fuel upon AFFF application [4].

The fire extinguishing mechanism of traditional AFFF is insulation of liquid fuel from oxygen by foam layer and aqueous film, as described in Figure 1. During AFFF extinguishing fire, a large amount of liquid drained out of foams due to the relative bad foam stability, and the liquid drained can form an aqueous film on the surface of liquid fuel relying on the very low surface tension of the liquid containing fluorocarbon surfactant [4]. The criterion for film formation is based upon the spreading coefficient given by Harkins and Feldman [5] as

$$\text{Spreading coefficient } (S) = \sigma_{\text{fuel}} - \sigma_{\text{foamsolution}} - \sigma_{\text{interfacial}}$$

σ_{fuel} and σ_{foam} solution are the surface tensions of the fuel and aqueous surfactant solution respectively and $\sigma_{Interfacial}$ is the interfacial tension between the fuel and solution. A zero or negative value for the spreading coefficient indicates an inability to form the aqueous film.

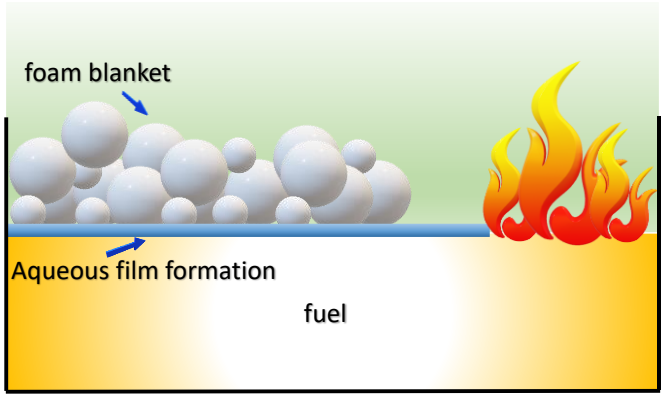

Figure 1 Aqueous film forming foam.

Now, fluorinated surfactants in AFFF are bio-persistence, bio-accumulative in nature. Due to this reason, they are being banned internationally. This includes a complete phase-out of AFFF from the U.S. DoD by October 1, 2024. Phase out of AFFF leads to finding an environmentally friendly alternative for current AFFF. The key features/properties of a successful surfactant solution that can lead to superior foams have not been identified. To date, the effects of fuel transport into the foam solution as well as surfactant transport out of the foam into the liquid fuel have not been fully quantified or demonstrated. Hence, the focus will be understanding the factors affecting liquid fuel transport through the surfactant solution in firefighting foam.

1.2. Overall Research Goal

The key features of a successful surfactant solution that can lead to superior foams have not been identified, thereby making the development of replacement foam is difficult.

Overall Research Goal
Factors affecting fuel transport of firefighting foam

Formulation of new types of environmentally friendly firefighting surfactant depends heavily on identifying the reasons behind fuel transport through surfactant foam solution. Therefore, a comprehensive understanding of the fuel-surfactant interaction is necessary. The overall Goal of this research is to understand the factors affecting fuel transport for firefighting foam.

1.3. Research Objectives

1.3.1. Research Objectives: Impact of fuel on surfactant microstructure

In this study, a liquid-liquid two phase system was investigated for different surfactant types. The hypothesis was that the liquid fuel layer affects surfactant microstructure in the bulk solution of firefighting foams.

Research Objectives

To understand:

I. **impact of liquid fuel transport on surfactant microstructures.**

II. **impact of liquid fuel transport on interfacial properties.**

III. **the factors affecting microstructure and interfacial properties.**

IV. **the implications of these factors on ignition time.**

The objective of this study was to identify the factors affecting fuel transport. Initially, the effect of liquid fuel transport on the microstructure was observed. Moreover, the effect of liquid fuel transport was observed on the interfacial properties. Later, fuel concentration in surfactant solution was quantified to identify the reason behind the fuel transport. Finally, the effect of liquid fuel properties on ignition time was observed.

1.3.2. Research Objectives: The interaction between fuel and single surfactants

In this work, single surfactant and fuel interaction was investigated for different surfactant and fuel types. The hypothesis was that presence of micelle in surfactant solution would impact fuel transport of firefighting foam.

Research Objectives

To understand:

I. **role of micelle during fuel transport.**

II. **implications of fuel types on fuel transport.**

Through this study, we observed the thermodynamic of the interaction between fuel and single surfactant. By changing surfactant concentrations in solutions, we evaluated the role of micelle on fuel transport. By varying the fuel types, we evaluated the effect of fuel types on fuel transport through surfactant solution.

1.3.3. Research Objectives: The effect of convection on fuel transport

In this work, a liquid-liquid two phase system was assessed for different types of surfactants and fuels. The hypothesis was that convection at the foam-fuel interface would impact fuel transport of firefighting foam.

Research Objectives

To understand

I. **the effect of convection during fuel transport.**

II. **the effect of fuel transport kinetic on ignition time.**

Through this work, experiments were conducted with and without stirring to observe the convection effect on fuel transport. Moreover, fuel transport kinetics were assessed and its effect on ignition time was observed for different fuel and surfactant types. To evaluate the kinetics of fuel transport through surfactant solution, experiments were done at different times and distances.

1.4. Dissertation Roadmap

To adequately address the research objectives towards achieving the overall research goal, an individual chapter contains some primary research objectives.

Chapter 2 details the impact of fuel on surfactant microstructure.

In Chapter 3 details study on the interaction between fuel and single surfactants.

In Chapter 3 details the impact of convection on fuel transport.

Chapter 4 includes a summary of research and conclusions.

References

[1] C. Baduel, J. F. Mueller, A. Rotander, J. Corfield, and M. J. Gomez-Ramos, "Discovery of novel per- and polyfluoroalkyl substances (PFASs) at a fire fighting training ground and preliminary investigation of their fate and mobility," *Chemosphere,* vol. 185, pp. 1030-1038, Oct 2017, doi: 10.1016/j.chemosphere.2017.06.096.

[2] B. J. Place and J. A. Field, "Identification of novel fluorochemicals in aqueous film-forming foams used by the US military," *Environ Sci Technol,* vol. 46, no. 13, pp. 7120-7, Jul 3 2012, doi: 10.1021/es301465n.

[3] W. J. Backe, T. C. Day, and J. A. Field, "Zwitterionic, cationic, and anionic fluorinated chemicals in aqueous film forming foam formulations and groundwater from U.S. military bases by nonaqueous large-volume injection HPLC-MS/MS," *Environ Sci Technol,* vol. 47, no. 10, pp. 5226-34, May 21 2013, doi: 10.1021/es3034999.

[4] Y. Sheng, N. Jiang, S. Lu, Q. Wang, Y. Zhao, and X. Liu, "Study of environmental-friendly firefighting foam based on the mixture of hydrocarbon and silicone surfactants," *Fire Technology,* vol. 56, no. 3, pp. 1059-1075, 2020.

[5] R. Ananth, K. M. Hinnant, S. L. Giles, J. P. Farley, and A. W. Snow, "Environmentally Friendly Surfactants for Foams with Low Fuel Permeability Needed for Effective Pool Fire Suppression," NAVAL RESEARCH LAB WASHINGTON DC, 2020.

CHAPTER 2

Understanding the impact of fuel on surfactant microstructure of firefighting foam

Rezawana Islam[1] and Brian Y. Lattimer[2]

[1]Materials Science and Engineering, Virginia Tech

[2]Mechanical Engineering, Virginia Tech

Submitted to Fire and Technology Journal

Abstract

Aqueous film-forming foam (AFFF) is being phased out due to the environmental impacts of fluorinated surfactants contained in the firefighting foams. To develop an environmentally friendly firefighting foam, it is important to understand the factors controlling the firefighting performance of surfactants. Fuel transport through foam has been considered as a dominant mechanism for foam collapse. Therefore, the impact of fuels (heptane, octane, and trimethylbenzene(TMB)) on surfactant microstructure was studied for three different types of surfactants (Capstone, Glucopon, and siloxane) that have applications in firefighting foam. Multiple techniques were used to identify the microstructure and interfacial properties of surfactants with and without exposure to liquid fuel. The ignition time of fuel vapor through foam and solubility of fuel through liquid surfactant solution were measured as well. This work shows fuel solubility has an impact on the surfactant microstructure and interfacial properties. In addition, fuel solubility and vapor pressure affect the ignition time of fuel vapors.

2.1. Introduction

The foam industry introduced fluorine-free firefighting foams that eliminate the fluorocarbon surfactants and PFAS from the solution and rely only on the hydrocarbon surfactants and other additives. However, existing fluorine-free alternatives to AFFF are unable to perform at the same level as AFFF [1]. The first step in developing AFFF replacements is to understand factors affecting the fuel transport in the foam solution. During fuel transport into the foam solution microstructure in the bulk of the solution and

interfacial properties get affected. In controlling both the microstructure and surface excess surfactants play a key role here. Therefore, it is important to understand the surfactant's role against fuel transport. Changing the surfactant structure affects microstructure and surface excess.

Aqueous film formation is considered an important mechanism of foam fire suppression. However, previous research has demonstrated questionable relationships between this mechanism and fire extinguishment performance [6]. Instead of focusing on aqueous film formation and surfactants with very low surface tension, Hinnant et al. [7], showed that the foam layer formed by AFFF is very effective at suppressing fuel vapors formed on a fuel surface. This was shown by measuring fuel vapor concentration above two AFFF covered fuel pools (methylcyclohexane and isooctane) with and without the ability to form the aqueous film. Macroscopic features of the foam such as bubble size and distribution, gas properties (water solubility and diffusivity), surface tension, and solution rheology are important features of foam [8] [9]. The effects of varying the fuel type and temperature beneath the foam were shown to vary spreading coefficient and have demonstrated that forming a film (i.e., positive spreading coefficient) does not correlate to vapor blockage or fire performance [7, 10, 11]. Fuel structure was observed to play a role in fire extinguishment and foam layer degradation with aromatics being more difficult to extinguish compared with alkanes, cyclo-alkanes, and alkenes [12]. Snow et al. [13] revealed that surfactant chemical structure, hydrophilicity hydrophobicity balance has an effect on fire suppression. Fuel transport through the foam was proposed as being a dominant reason for foam collapse, especially with hydrocarbon surfactant where lamellae is more permeable to fuel [7].

The fuel transport mechanism can be divided into four different steps as illustrated in Figure 1: (1) solubility of the fuel into the foam solution, (2) vaporization in the gas bubble, (3) diffusion of fuel in the lamellae, and (4) re-dissolving in the solution around the bubble. Though fuel transport was identified as a potential mechanism that affects foam collapse and extinguishment performance, the parameters controlling these phenomena are unidentified.

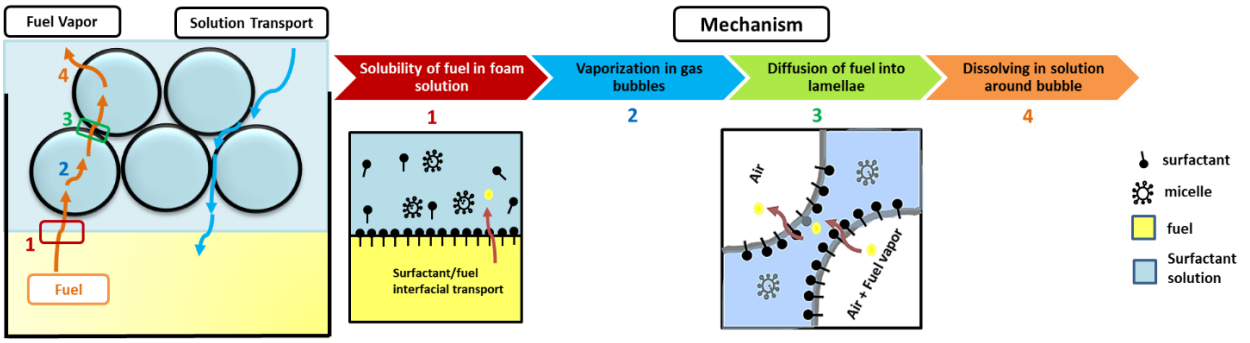

Figure 1. Fuel transport mechanism through a foam blanket.

It was hypothesized that fuel transport will impact surfactant microstructure. To understand fuel transport, a liquid-liquid setup was developed to study location 1 from figure 1, where a layer of fuel was placed at the top of surfactant solution as a second phase. The surfactant solution-fuel interface was used to study interfacial properties and samples were extracted from the surfactant solution side for microstructural study.

To date, the effects of fuel transport into the foam solution as well as surfactant transport out of the foam into the liquid fuel have not been fully quantified or demonstrated. For foam solution in air without the presence of fuel, a variety of advanced experimental methods were used in other applications to quantify and visualize the microscopic changes in surfactants and their effect on the solution transport properties. Surfactants exist on the nanoscale; therefore, cryogenic transmission electron microscopy (cryo-TEM) was used to visualize surfactant structure [2], micelle assembly [3], and changes in microstructure for fluorocarbon-hydrocarbon surfactant mixtures [2]. The micelles ranged from less than 5 nm up to 50 nm with some micelles being spherical while others are more wormlike in structure. SANS was used to quantify micelle assembly structure and surface concentration [4]. Measurements on single lamella or bubbles were used to isolate parameters affecting transport [5, 6]. Numerous studies have demonstrated that cryo-TEM and SANS can be used collectively to characterize the micelle microstructural details of surfactant solutions [2, 7, 8]. However, none of these studies have explored the changes in surfactant solution microstructure after exposure to liquid fuels. In addition, previous literature [9] has reported that hydrocarbon surfactants solubilizes more fuel than fluorocarbon. There is a lack of evidence on the impact of fuel solubility on microstructure in the bulk of firefighting foam.

This study aims to quantify the impact of liquid fuel diffusion on the surfactant solution microstructure. To assess these, three different types of surfactants (fluorocarbon, hydrocarbon, and siloxane into aqueous solution) and two types of fuel (n-alkane, aromatic) were explored. Various experiments were performed to observe micelle size and shape with or without exposure to fuel. Interfacial properties were measured for different surfactant solution/fuel interfaces. The quantity of fuel diffused into surfactant solution was measured. Ignition time was measured for fuel vapor that was transported through the foam. The results from this study will help us understand 1) the detailed microstructure of the Capstone, Glucopon, and siloxane, 2) impact of fuel on their microstructure 3) factors affecting the microstructure and ignition time.

2.2. Experimental details

2.2.1. Materials

In this study, our goal was to investigate the single surfactants (fluorosurfactant Capstone and hydrocarbon surfactant Glucopon) used in Ref-AFFF to evaluate the factors affecting fuel transport. Siloxane surfactant has been explored as a potential alternative to fluorosurfactant in firefighting foam formulation. In addition, Capstone, Glucopon, and siloxane were chosen as firefighting foam surfactants due to their greater ability to reduce surface tension. Gasoline was used as the fuel in a pool for fire extinction test in MilSpec standard, the most rigorous method for evaluating firefighting foam performance. However, the presence of TMB in gasoline makes it harder to extinguish [10]. Most other test protocols use heptane as fuel for fire extinction tests [10]. In this work, primarily we have studied TMB and heptane to understand the difference in fuel impact on surfactant microstructure. In addition, have studied octane from n-alkane category to observe the ignition time. TMB, heptane, and octane have a constant composition, unlike gasoline. These fuels represent two different categories of fuel: n-alkane (heptane, octane), and aromatic (TMB). Due to the higher flash point, it was challenging to ignite TMB at room temperature. Therefore, a two components (25% trimethylbenzene + 75% heptane) simulant for gasoline were used for evaluating ignition time in the presence of an aromatic component (TMB) since suppression time for this mixture of fuel is very close to the suppression time for gasoline [10].

Fuel

The physical properties of TMB, heptane, octane is presented in Table 1. All the physical properties are taken from the Safety data sheet for these fuels [11-13]. The calculated vapor pressure of 25%TMB-heptane is 37.9 mm Hg.

Table 1. Physical properties of fuel

Fuel	Chemical formula	Structure	Water Solubility (mg/L)	Vapor Pressure (mm Hg)	Flash Point (°C)
1,2,4 Tri-methylbenzene	C_9H_{12}	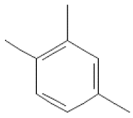	57	1.72	48
Octane	C_8H_{18}	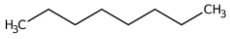	0.66	14	13
Heptane	C_7H_{16}	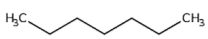	3.4	48	-4

Surfactant

Three different types of surfactants Capstone 1157, Glucopon 600 CS UP, and Gelest 6185 were used for this study with properties given in Table 2. Various experiments were done on surfactant solutions and characterized at a range of surfactant concentrations to determine interfacial properties. Ignition tests, fuel concentration measurements, Dynamic light scattering (DLS) have been done at 5 times the Critical micelle concentration (CMC) based on surfactant concentration, which is approximately the surfactant concentration used in Reference AFFF [14]. Cryo-TEM, SANS were done at 7 times higher than Capstone and 10 times higher than Glucopon surfactant concentration consecutively.

Table 2. Surfactant Properties.

Name	Molecular Weight (g/mol)	Molecular length (Å)	Tail length	Tail Type	Head Type
Capstone 1157	570	19.322	Long	Fluorocarbon	Zwitterionic
Glucopon 600 CS UP	386	18.779	Long	Hydrocarbon	Nonionic
Gelest 6185	550	39.945	Branched	Siloxane	Nonionic

a)

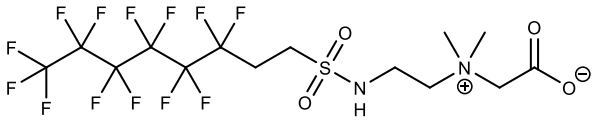

b)

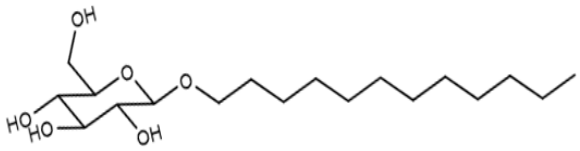

c)

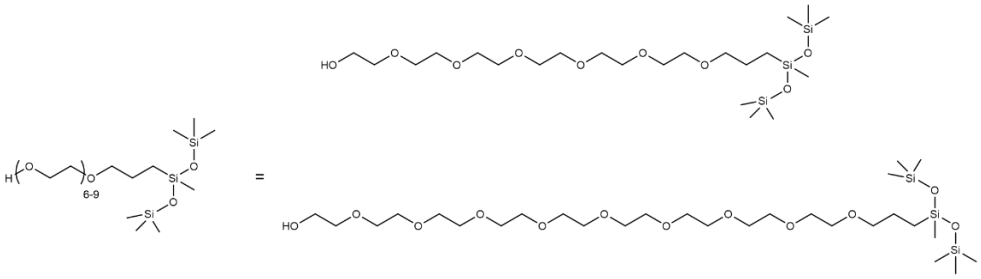

Figure 2. Surfactant structures a) Capstone 1157 b) Glucopon 600 CS UP c) Gelest 6185.

Sample Preparation

Figure 3 shows the sample extraction setup. The transport of fuel into the surfactant solution was quantified through a diffusion experiment with ~15 ml liquid fuel over a layer of ~ 15 ml surfactant solution. The fuel and surfactant solution two-phase system were prepared in a 20 ml glass vial. After pouring the surfactant solution in the glass vial, a syringe was inserted and then a fuel layer was added at the top of the surfactant solution to avoid any contamination on the needle while extracting the sample using the syringe. Before extracting the sample, waited 15 minutes for the fuel and surfactant solution to reach equilibrium at room

temperature, this will allow diffusion processes to equilibrate before measuring. The surfactant solution sample was extracted from 10 mm away from the interface. The extracted sample (referred to as two-layer interaction sample in this document) was used for microstructural and fuel concentration measurements.

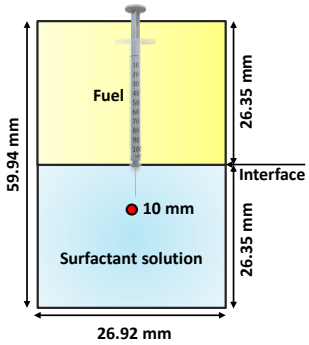

Figure 3. Experimental setup.

2.2.2. Methods

Small angle neutron scattering (SANS), Cryogenic transmission electron microscopy **(**Cryo-TEM), and Dynamic light scattering (DLS) were used to measure the surfactant microstructure in the bulk of the surfactant solution with or without exposure to fuel. Tensiometer was used to measure the interfacial properties (surface tension (SFT), interfacial tension (IFT), critical micelle concentration (CMC), surface excess, etc.). The concentration of fuel in the surfactant solution quantified using UV/Vis spectroscopy. An, ignition test was conducted to quantify the ignition time of fuel vapors transported through a layer of foam. For ignition tests foams were prepared using a Dynamic Foam Analyzer (DFA100).

Cryogenic Transmission Electron Microscopy (Cryo-TEM)

As shown in Figure 3 the samples were extracted and vitrified to visualize the micelle structure. Vitrification was done in a controlled environment vitrification system (CEVS) and plunged into liquid nitrogen at its freezing point using a lacey carbon grid. The vitrified specimens were stored under liquid nitrogen (−196°C). Then samples were observed in a ThermoFisher titan krios g4 with a direct electron detector (falcon 3EC). Cryo-TEM measurements were conducted at the CNMS facility of the Oak Ridge National Laboratory, Oak Ridge, TN.

Small Angle Neutron Scattering (SANS)

To observe the micelle size and shape in the bulk, a liquid-liquid interface was created by placing a fuel layer at the top of the surfactant solution as described in Figure 3. Two different locations away from the interface, one at the fuel side (top phase) and the liquid side (bottom phase) were chosen to study. Samples were prepared by dissolving precise quantities of surfactant in D_2O with stirring. Measurements were performed at 25 °C in 1 mm path length and quartz Hellma cells. Then raw scattering intensity profile I(q) versus q was captured. Intensity profile is a function of the scattering vector, q. The wavelength (λ) of the incident neutrons is 2.5 Å. Scattering was performed with the detector positioned separately at 3 and then 4 m from the sample environment, providing a q-range of approximately $0.004-1.4$ $Å^{-1}$. SANS measurements were conducted at beamline-6 of SNS facility, Oak Ridge National Laboratory, Oak Ridge, TN.

Dynamic light scattering (DLS)

DLS was performed to observe the micelle size in the bulk using a Malvern Zetasizer Nano ZS. The extracted sample (as shown in Figure 3) was placed in a Polystyrene cuvette at 25 °C. Data processing was carried out with a computer attached to the instrument. The average size distribution of the surfactant micelle was recorded. The measurements were repeated three times to check their reproducibility.

Tensiometer

Surface tension was measured at room temperature using a KRÜSS K100C tensiometer using the Wilhelmy plate method. Each measurement was an average of five surface tension measurements. Using the automatic dosing unit of the instrument, surface tension was measured at different surfactant concentrations. A plot of surface tension versus surfactant concentration was used to quantify the CMC, which is the lowest concentration where the surface tension does not change when there is an increase in surfactant concentration. Surface tension is linearly dependent on the logarithm of the concentration over a large range. The CMC results from the intersection between the regression straight line of the linearly dependent region and the straight line passing through the plateau. The data was also used to quantify the surface

excess. Surface excess is the area-related concentration of surfactant at the surface or interface. The concentration of surfactant at the surface is significantly higher compared to its concentration in the bulk phase. Surface excess has the unit of mol/m2 and is calculated based on the slope of the surface tension data at concentrations below the CMC using the Gibbs equation [15].

$$\Gamma = -\frac{1}{nRT} \cdot \frac{d\gamma}{d\ln(c)} \quad (1)$$

where n = 1 for non-ionic surfactants, neutral molecules, or ionic surfactants, Γ is the equilibrium surface excess (mol/m^2), R is the gas constant (8.314 J/mol-K), T is temperature (K), c is the bulk surfactant concentration (M), γ is surface tension (mN/m), and dγ/dln(c) is the slope of the surface tension and natural log of surfactant concentration. This was then used to calculate the area per molecule (nm^2)

$$A = -\frac{10^{18}}{N_A \Gamma} \quad (2)$$

where N_A is Avagadro's number (6.022×10^{23} molecules/mol). These measurements were conducted for all surfactants at an air interface and for select surfactants at the solution-fuel interface.

UV-Vis Spectroscopy

UV-Vis measurements were done to quantify the fuel concentration in the bulk using a Hitachi U4100 UV-VIS-NIR spectroscopy. In this work, we measured the TMB water solubility using UV-Vis spectroscopy as a verification of this method. In Figure 4a, the absorbance spectra for known concentrations of TMB in water were measured to prepare the standard curve in Figure 4b. TMB was added to surfactant solution in known concentrations of 0.4, 0.8, 1.2, 1.6, and 2 wt.%. A stirring plate and a magnetic stirring bar were used for approximately 10 minutes for mixing. Afterwards, waited for 15 minutes for sample equilibration and transferred it to the cuvette for analysis [16]. The absorption peak from 300 – 230 nm was used for the analysis of TMB. The absorbances of all the standard samples were recorded keeping water as the baseline presented in Figure 4a.

For TMB-water analysis, sample was extracted from a two-layer interaction sample of water (bottom phase) and TMB (top phase) as shown in Figure 3. The absorbance attained was placed into the standard curve

(absorbance versus Fuel concentrations Figure 4b) to quantify the concentration of TMB in water. The value was 0.006 wt.% which is close to the reported value of 57 mg/l or 0.0057 wt.% in water [17].

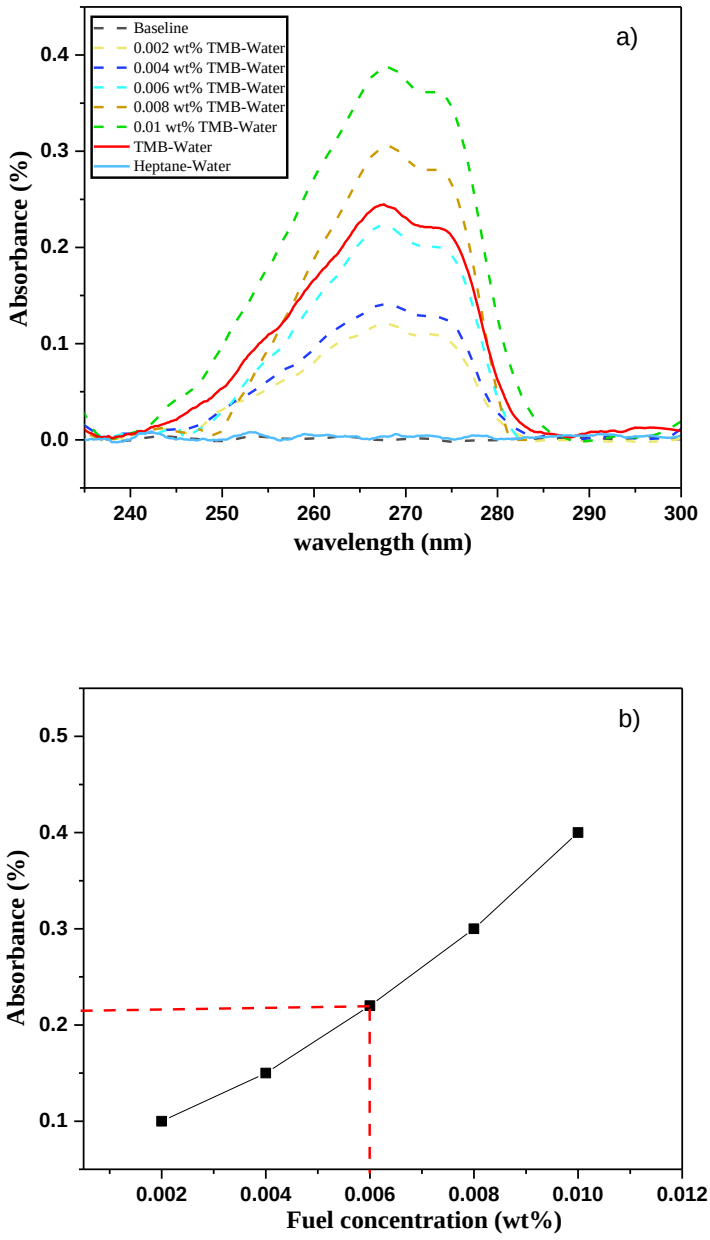

Figure 4. UV-Vis spectra a) absorbance versus wavelength b) standard graph.

Dynamic foam analyzer (DFA)

The Dynamic Foam Analyzer (DFA100 – KRÜSS) was used to quantify the foam quality on a bench scale. We intended to use a consistent way to generate foam. DFA is such a method that can produce foam in a consistent and reliable way and provide all the foam properties for various surfactants studied in the laboratory. In this method, a surfactant solution (35 mL) was introduced into the DFA glass cylinder container, which has a porous disk with a pore size ranging from 16 µm to 40 µm at the bottom of the cylinder. Air then flows through the sparger at a rate of 0.2 L/min for 40 seconds. The expansion ratio of each surfactant is calculated by measuring the foam volume using a line sensor after 40 seconds of air addition. After foam generation, the initial bubble diameter, initial bubble distribution, liquid drainage from the foam, and expansion ratio are studied for each of the foams generated. The bubble sizes were directly obtained from ADVANCE software.

Ignition test

An ignition test was developed (Figure 5) to quantify the ignition time of fuel vapors transported through a layer of foam. The test was developed with inspiration from the open-cup flashpoint test that is commonly used to assess the flammability of fuels. For the ignition test, a 75 mm diameter, 25 mm deep glass dish was filled with a 15 mm thick layer of foam, then 25 mL of fuel was injected with a syringe through the foam so that the foam height was close to the top of the dish. After the fuel was injected through the foam, a pilot flame igniter was positioned over the top of the foam in the center of the pan. The changes in foam during the experiment were captured using a high-resolution video camera.

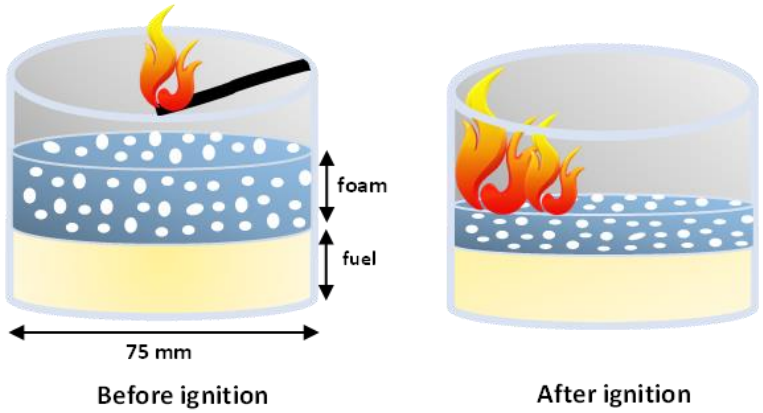

Figure 5. Ignition test set up.

2.3. Results

2.3.1. Packing parameter

Surfactants tend to self-assemble themselves into micelle above their critical micelle concentration (CMC). The molecular packing parameter (p), a theory developed by Israelachvili et al. to describe or calculate the shape of molecular self-assembled structures in a surfactant solution [18]. p can be estimated using the following equation:

$$p = \frac{v}{a_0 l} \quad (3)$$

Where, v and l are the volume (nm^3) and length (nm) of the hydrophobic tail, a_0 = the effective head group area (nm^3) at the interface of the hydrophobic core−hydrophilic media.

This parameter allows a simple and intuitive insight into the relationship between molecular structures and the shape of self-assembly. For example, $0 < p \leq 1/3$ is for spherical micelles, $1/3 < p \leq 1/2$ is for cylindrical ones, $1/2 < p \leq 1$ is for bilayer structures, such as vesicles, and $p > 1$ is for inverted structures [19] [20, 21].

The chemical structures of surfactants used in this study were drawn using Chem sketch. Tail length and volume for the surfactant structures were attained using the Avogadro software [22]. Effective head group area was calculated from tensiometer discussed in the Interfacial properties section of this paper. The calculated p values indicated the shape of the micelles formed (i.e., vesicles, worm-like and inverted

structure for Capstone, Glucopon and siloxane surfactants respectively) [21]. See supporting information (Table S1) for more details.

Table 3. calculated P value and graphical representation of self-assembly structure

	Surfactant	$p = \frac{v}{a_0 l}$	Structure formed	
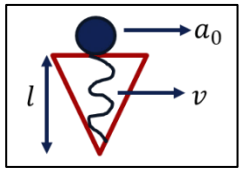	Capstone	>1/2	Vesicles	
	Glucopon	1/2	Worm-like	
	Siloxane	>1	Inverted structure	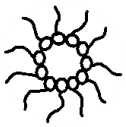

2.3.2. Microstructural Features of Surfactants

2.3.2.1. Cryogenic transmission electron microscopy (Cryo-TEM)

Cryo-TEM has been used to observe the size and shape of micelles. Samples were extracted from the surfactant solution side for microstructural study.

Capstone

The self-assembly behavior of Capstone with or without exposure to liquid TMB was observed by cryo-TEM. As shown in Figure 6a, it was noticeable that Capstone molecules self-assemble into vesicles in solution rather than forming micelles consistent with literature [23]. At a concentration higher than CMC (7 times higher than CMC based on surfactant concentration), observed single lamellar vesicles formed by Capstone molecules, and the diameters of vesicles are ~37 nm. In Capstone-TMB (Figure 6b), the size of vesicles increased and diameter is around 194 nm. In some cases, they formed multilamellar vesicles can be observed clearly in Figure 6b. Cryo-TEM images showed the impact of Trimethylbenzene (TMB) on the Capstone vesicle and revealed that adding TMB results in two changes 1) an increase in aggregation/grouping of the vesicles and 2) an increase in the diameter and (sometimes) membrane layers.

Most likely Capstone was solubilizing TMB and forming swollen micelle but the location of fuel molecules was not confirmed for Capstone-TMB from this analysis.

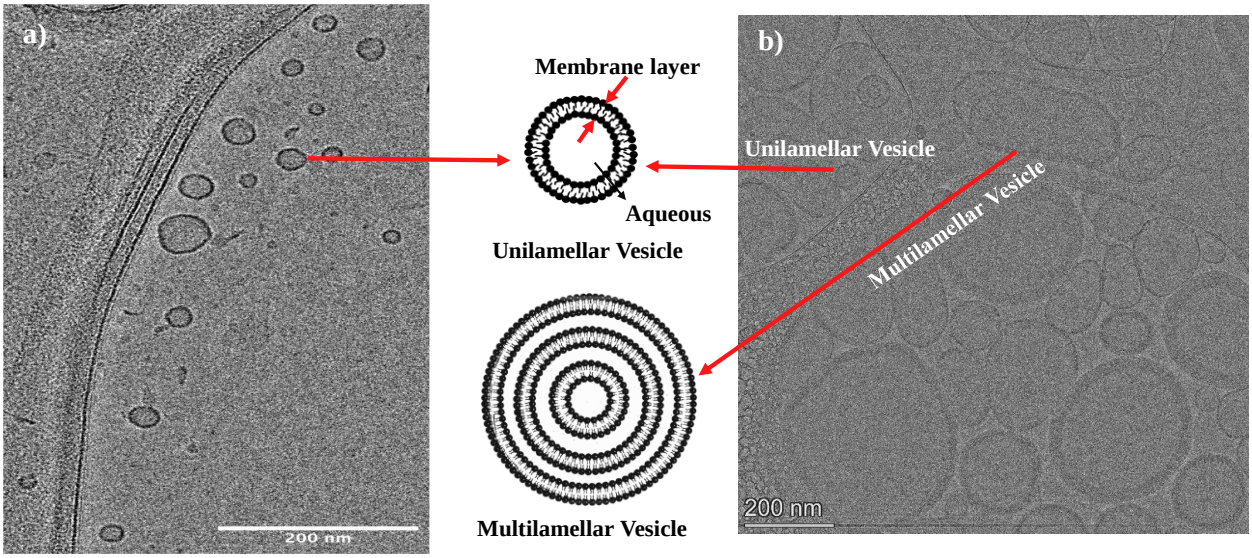

Figure 6. Cryo-TEM for a) Capstone b) Capstone- TMB.

Glucopon

Cryo-TEM reveals self assembly behavior of Glucopon 600 CS UP in aqoueous solution. Glucopon formed worm like micelles as shown in Figure 7**,** at a concentration higher than CMC (10 times higher than CMC based on surfactant concentration). We observed worm like micelle for Glucopon-TMB presented in Figure 7. Visually from cryo-TEM no difference was observed in terms of micelle size and shape between Glucopon and Glucopon-TMB.

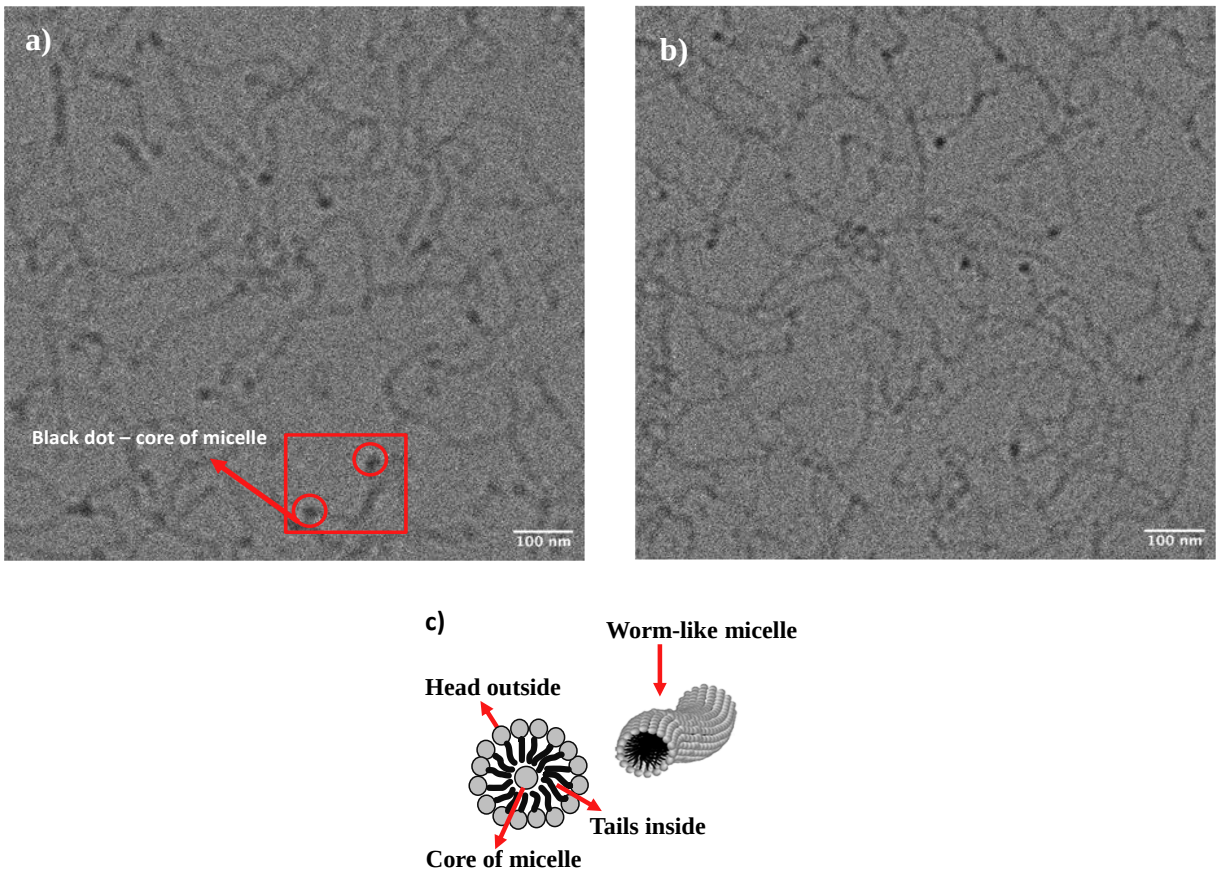

Figure 7. Cryo-TEM for a) Glucopon b) Glucopon-TMB c) illustration of worm-like micelle.

2.3.2.2. SANS

For in-situ observation of structures in the bulk and fuel phase, measurements were performed using SANS. Scattering profiles are included in the supporting information section.

Capstone

The scattering profile (see Figure S1 for supporting information) indicated that Capstone 1157 formed a lamellar structure. The form factor "lamellar structure paracrystal" was the representation of large multilamellar vesicles. Sheet thickness (t) was ~28 Å and similar for Capstone, Capstone-heptane, and Capstone-TMB. However, the d_spacing occurred to increase for the Capstone-TMB (Table 4). It was confirmed from the Cryo-TEM images that the presence of TMB increased the vesicle size and membrane layers (Figure 6). Therefore, it was likely that the d_spacing would increase (Figure 8). The d_spacing

(Table 4) was similar for Capstone and Capstone-heptane indicating that heptane did not impact the vesicle size.

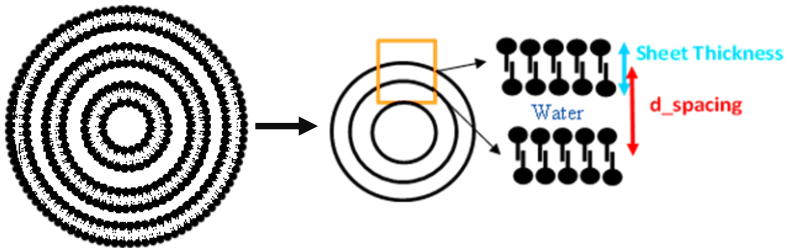

Figure 8. a) Multilamellar vesicle b) d_spacing for vesicles.

Table 4 SANS measurement for Capstone

Sample	thickness (Å)	d_spacing (Å)
Capstone	28 ± 0.2	325 ± 9.08
Capstone-heptane	27 ± 0.19	331 ± 6.92
Capstone-TMB	28 ± 0.22	373 ± 8.92

Glucopon

The scattering profile (see Figure S2 for supporting information) from SANS result showed that Glucopon formed worm like micelle. The form factor "flexible cylinder elliptical" was a representation of a worm-like micelle. The radius was ~ 14 Å for Glucopon. The overall length of the micelle was 654 ± 14 Å (Table 5). In the two-layer sample, due to the presence of heptane on the top phase length of the micelles in the bulk of the solution was somewhat decreased. In this case, more surfactants were traveling to the interface, thereby decreasing the micelle length. For the case of TMB on the top phase, micelles were increasing in length by 100 Å (Table 5). The characteristic of worm-like micelles is that they grow in length to accommodate fuel molecules [24]. As a result, the increasing length of the worm like micelle indicated fuel solubilization.

Table 5. SANS measurement for Glucopon

Sample	Radius (Å)	Length (Å)
Glucopon	14.78 ± 0.11	654 ± 14
Glucopon-heptane	14.81 ± 0.07	633 ± 13
Glucopon-TMB	14.66 ± 0.08	728 ± 16

Siloxane

According to SANS fitted model (see Figure S3 for supporting information), siloxane surfactant was ellipsoidalu. In the presence of heptane and TMB on the top phase (Table 6), micelles in the bulk of the solution did not change shape and radius. Therefore, TMB and heptane did not affect the microstructure of the siloxane surfactant. However, the scattering data (see Figure S4 from supporting information) indicated the presence of structures in the heptane phase (top phase in Figure 3) for Siloxane-heptane. This confirmed the formation of reverse micelle. SANS data was fitted using sphere model and radius was around 363 Å (Table 7).

Table 6. radius for Siloxane from SANS (bottom phase)

Name	radius (Å)
Siloxane	20 ± 0.03
Siloxane-heptane	20 ± 0.03
Siloxane- TMB	20 ± 0.04

Table 7. Radius for Siloxane from SANS (top phase)

Name	Model	radius (A)
Siloxane- Heptane	Sphere	363 ± 11

2.3.2.3. DLS

Dynamic light scattering (DLS) measurements were performed to assess the change of micelle size in the bulk of the surfactant solution due to fuel exposure. For different surfactant micelles with fuel exposure resulted in increased size and sometimes two different size distributions were observed, see Figure 9. TMB showed much higher effect in the microstructure compared to heptane for both Capstone and Glucopon. The polydispersity for the reported sizes was around 0.2 – 0.3 which means a moderately polydisperse distribution type.

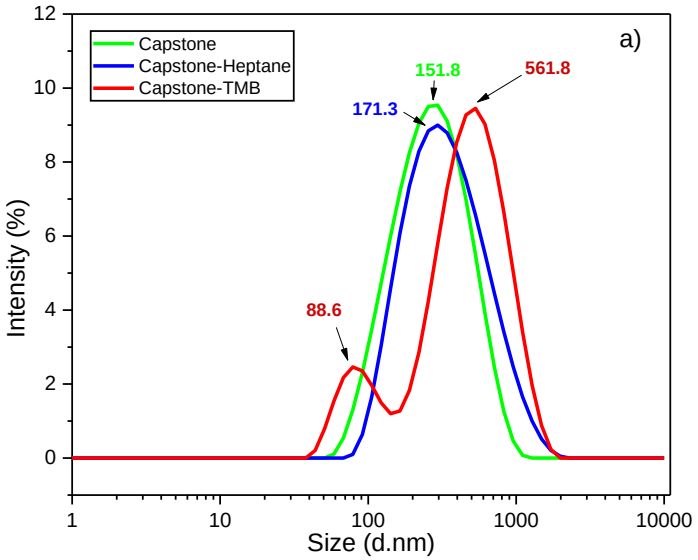

a)

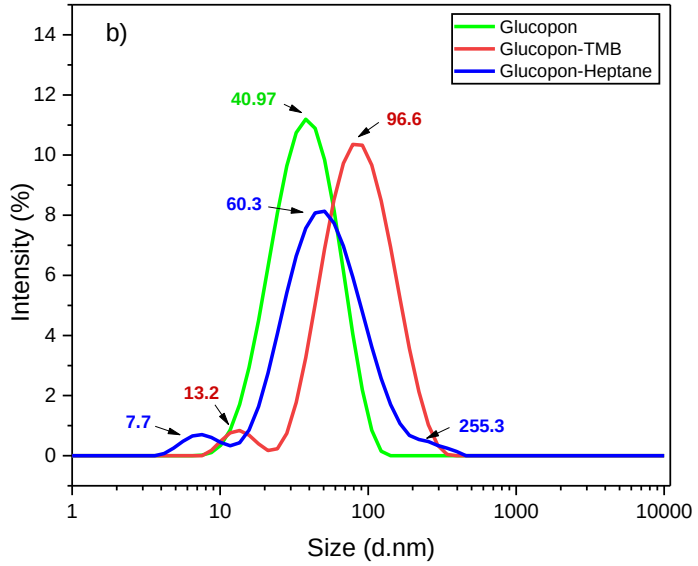

b)

Figure 9. DLS results a) Capstone b) Glucopon with and without fuel exposure.

2.3.3. Interfacial properties

To observe the impact of fuel at the interface surface tension, interfacial tension, and surface excess, CMC has been measured with or without the presence of fuel.

2.3.3.1. Surface tension

Surface tension results were presented in Figure 10 for all three surfactants at initial concentrations higher than their CMC. This includes both the surface tension (SFT) for air/surfactant solution as well as interfacial surface tension (IFT) for fuel/surfactant solution. Comparing the SFT for three single surfactants, Capstone has its greatest ability to lower the surface tension at the air/surfactant solution interface (15.99 mN/m) while Glucopon has the highest (28.45 mN/m). All values were consistent with those reported elsewhere [25], [26].

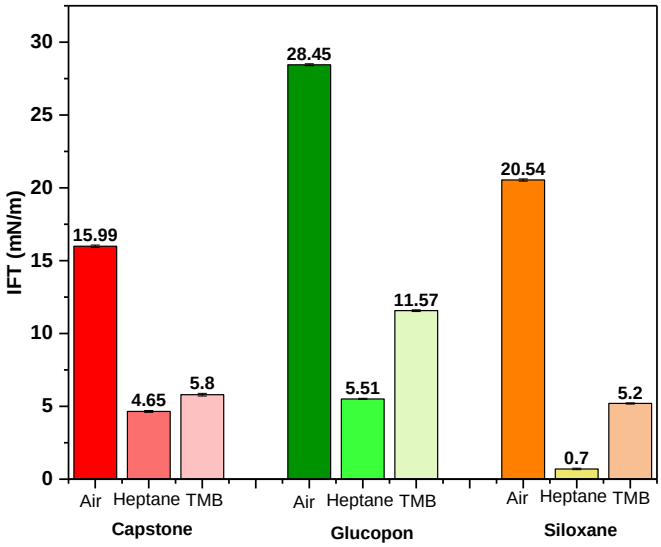

Figure 10. Surface tension (SFT) and Interfacial tension (IFT) values.

The results in Figure 10 demonstrated that IFT value is fuel and surfactant type dependent. Glucopon-TMB IFT value of 11.57 mN/m is higher than Glucopon-heptane IFT value of 5.51 mN/m. In most cases, IFT values are in the range of 4-12 mN/m except for Siloxane-heptane which has a very low IFT of 0.7 mN/m. This indicated that the siloxane surfactant made the heptane and aqueous solution more miscible.

2.3.3.2. CMC

The CMC for the solutions was determined using surface tension data at different surfactant concentrations. Below the CMC, the surface tension increases with a decrease in surfactant level while above the CMC the

surface tension is constant. The surfactant concentration at the intersection of these two lines is the CMC. The CMC value measured for Capstone, Glucopon, and Siloxane surfactant solutions of 0.011, 0.012, and 0.009 wt.% of surfactant, respectively (Figure 11). CMC values were consistent with literature for all the cases [25, 26].

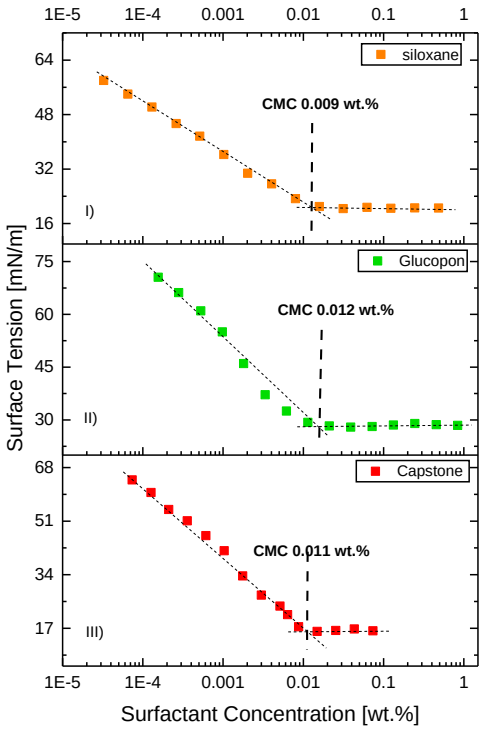

Figure 11. CMC for surfactants i) Siloxane ii) Glucopon iii) Capstone.

2.3.3.3. Impact of fuel on CMC

CMC values for Capstone, Capstone-heptane, and Capstone-TMB are 0.011, 0.011, and 0.006 wt.% respectively (Figure 12a). A similar trend was observed for CMC values for Glucopon, Glucopon-heptane, and Glucopon-TMB which are 0.012, 0.012, and 0.006 wt.% respectively (Figure 12b). Results showed that for both Capstone and Glucopon surfactants, CMC with heptane-surfactant solution was same as air-solution. However, CMC with TMB-surfactant solution was lower than air-solution. This indicated that the TMB interacted with the surfactant solution causing micelle formation at lower concentrations. Hence, decreasing CMC in the presence of TMB.

CMC values for Siloxane, Siloxane-heptane, and Siloxane-TMB are 0.009, 0.06, and 0.009 wt.% respectively (Figure 12c). CMC with TMB-surfactant solution was same as air-solution. However, CMC with heptane-solution was higher than air-solution. This indicated that near CMC region, surfactants travel to the fuel phase rather than forming micelle in the bulk of surfactant solution. Hence, CMC value increased. This indicated the formation of reverse micelle.

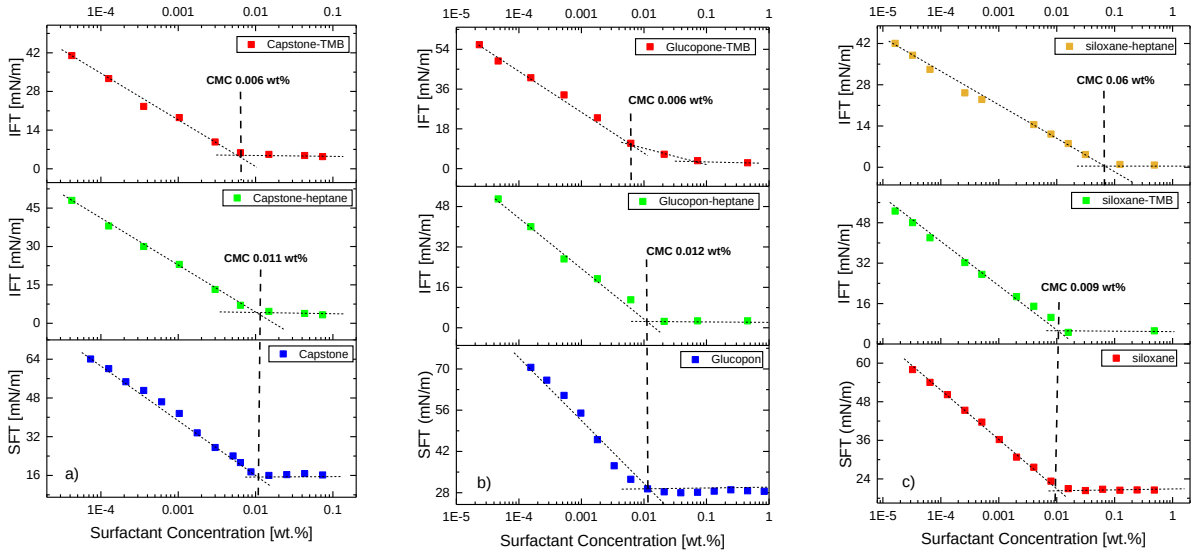

Figure 12. CMC in the presence of fuel a) Capstone b) Glucopon c) Siloxane.

2.3.3.4. Surface excess

Figure 13 showed that surface excess for Capstone-TMB in comparison to Capstone was decreased to 70%, for Glucopon-TMB in comparison to Glucopon decreased to 52%. These results indicated that TMB caused surfactants to go away from the interface and reduced surface excess. For heptane-siloxane in comparison to siloxane surface excess was reduced to 73%, meaning that heptane caused siloxane surfactants to move away from the interface reducing the surface excess. A similar trend for low surface excess was observed for Trisiloxane surfactants in the presence of hydrocarbon fuels [27].

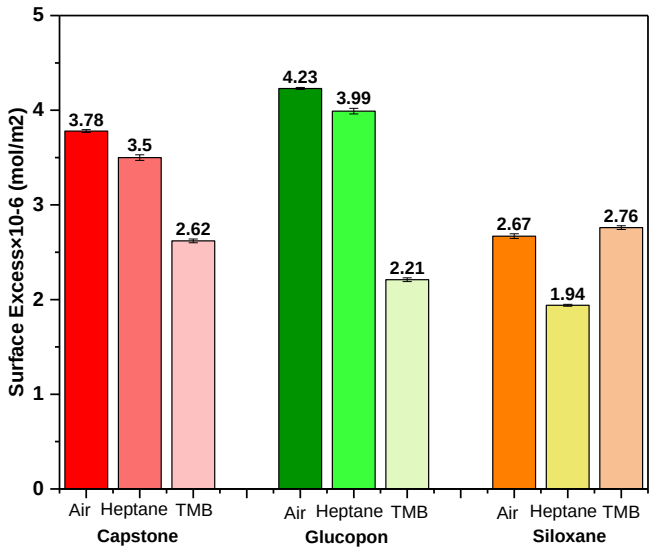

Figure 13. Surface excess with or without fuel exposure.

2.3.4. Impact of surfactants on fuel solubility

UV-Vis spectroscopy measurements were performed to quantify the fuel solubility in the bulk of the surfactant solution. According to previous literature octane, heptane, TMB have 0.000066, 0.0003, and 0.0057 wt.% solubility in water consecutively [11, 12, 17] presented in Table 8. Benzene ring fuel (TMB) has higher water solubility than alkane type fuels.

Table 8. Water solubility of fuel

Fuel	Water Solubility (wt.%)
octane	0.000066
heptane	0.00034
TMB	0.0057

The UV-Vis spectroscopy results revealed that none of the surfactants used in this study increased the solubility of alkane type of fuel (octane, heptane). The absorbance versus wavelength spectrum for Capstone-octane and Capstone-heptane was close to Capstone-baseline (Figure 14a). For Glucopon-octane and Glucopon-heptane was close to Glucopon-baseline (Figure 14b). Therefore, Capstone and Glucopon did not increase the solubility of octane and heptane in water. According to Figure 14(a, b) Capstone-TMB and Glucopon-TMB absorbance versus wavelength peaks were higher than Capstone-baseline and

Glucopon-baseline respectively. Therefore, Capstone and Glucopon surfactant increased the solubility of TMB in water. The concentration of TMB in Capstone and Glucopon solution was found 0.12 wt.% and 0.18 wt.% respectively (Figure 15). According to Figure 14 siloxane did not increase the solubility of octane, heptane, 25%TMB-hepatne. The absorbance for siloxane-TMB was slightly higher than siloxane baseline. However, the solubility of TMB in siloxane solution was 0.0038 wt.% smaller than the solubility of TMB in water.

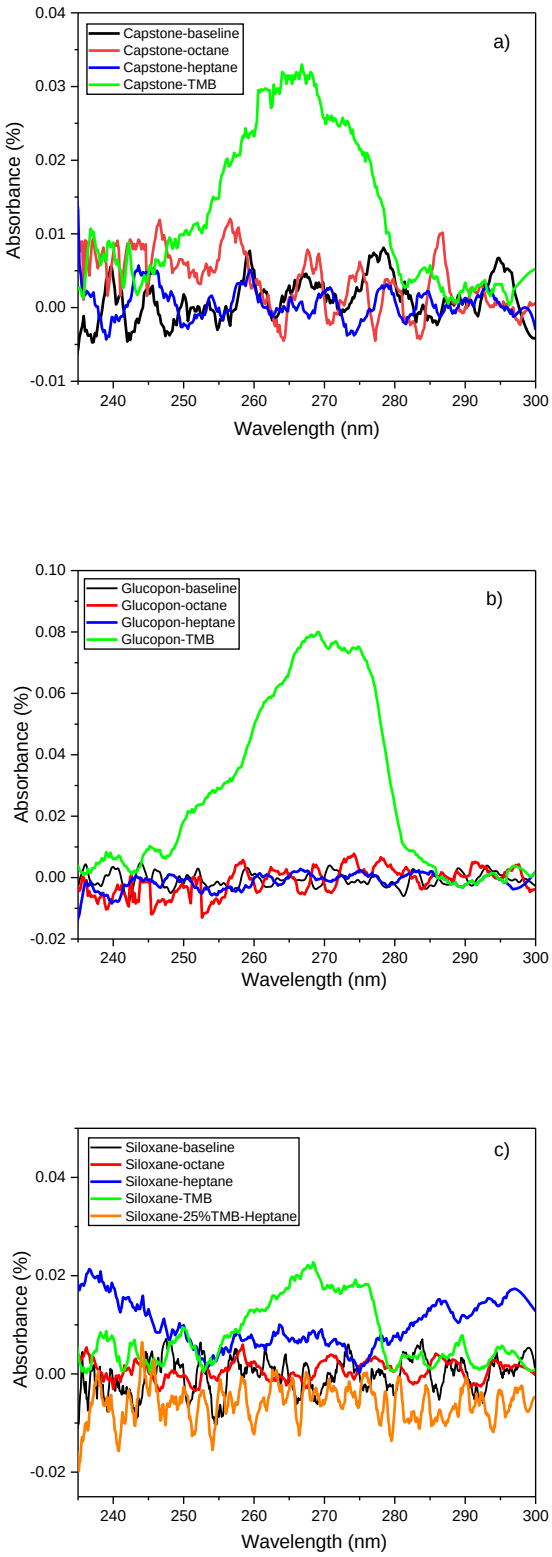

Figure 14. Solubility of fuel into surfactant solution a) Capstone b) Glucopon c) Siloxane.

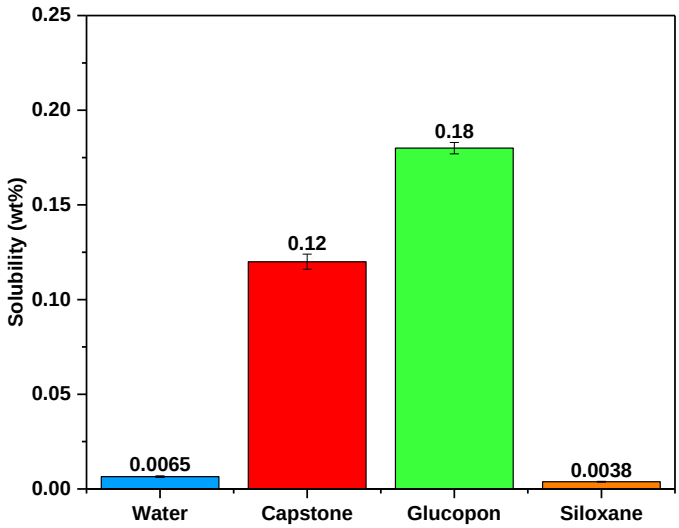

Figure 15. Solubility of TMB in Capstone, Glucopon, and siloxane solution.

UV-Vis spectroscopy could not detect the solubility of 25%TMB-heptane in water. Figure 16 showed that absorbance peak was higher for Glucopon-25%TMB-heptane than Glucopon-baseline. Therefore, 25%TMB-heptane has solubility in Glucopon solution. For Capstone-25%TMB-heptane the absorbance peak was close to Capstone-baseline. Therefore, 25%TMB-heptane was not soluble in Capstone solution in a static liquid-liquid setup. In the liquid-liquid set up stirring was introduced at the bottom phase (as shown in Figure 3) for 15 minutes for Capstone-25% TMB-heptane before sample extraction. After stirring Capstone-25%TMB-heptane showed an absorbance peak higher than Capstone-baseline. Therefore, 25%TMB-heptane has solubility in capstone solution with stirring. However, with and without stirring Glucopon-25%TMB-heptane showed higher absorbance peaks compared to Capstone-25%TMB-heptane. Therefore, 25%TMB-heptane has higher solubility in Glucopon solution compared to Capstone solution.

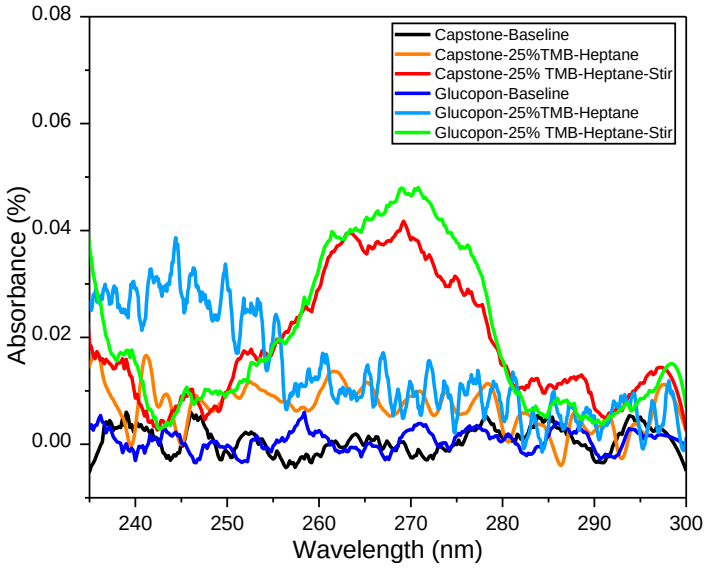

Figure 16. Solubility of 25% TMB-heptane in Capstone and Glucopon surfactant solution with and without stirring.

2.3.5. Ignition test

For ignition tests, foam was generated using DFA as detailed in the experimental section. Three different types of foams and two different types of fuels were used for analysis. Foam properties were observed as well. Ignition time for each type of fuel through different surfactant foam solutions was recorded for analysis purposes.

2.3.5.1. Foam tests

Table 9 highlighted that the expansion ratio for Glucopon was lowest in comparison to Capstone and siloxane. 25% liquid drainage time was lowest for Glucopon. Wetter foam usually drains faster compared to drier foam. Longer drain time has been observed for Capstone due to having smaller bubble diameter compared to Glucopon. Since the mean free paths length would then become higher due to smaller bubble diameter and the solution would have a longer distance to go. However, Siloxane formed comparatively a less wet foam indicated by high expansion ratio compared to Capstone and Glucopon; therefore, a longest drain time [28]. Figure 17 depicts the bubble diameter for three surfactants. Siloxane has the largest and

Capstone has the smallest diameter bubble. The decrease in bubble size was most likely due to a decrease in expansion ratio [29]. The bubble size and expansion ratio were dependent on each other but are not dependent on surfactant molecular structure or surface tension [25].

Table 9. Foam properties

Surfactant	Expansion Ratio (ER)	25% Liquid Drainage [s]
Capstone	7.4 ± 0.3	54.1 ± 2
Glucopon	6 ± 0.07	43.3 ± 1.3
Siloxane	10.5 ± 0.1	65.6 ± 0.5

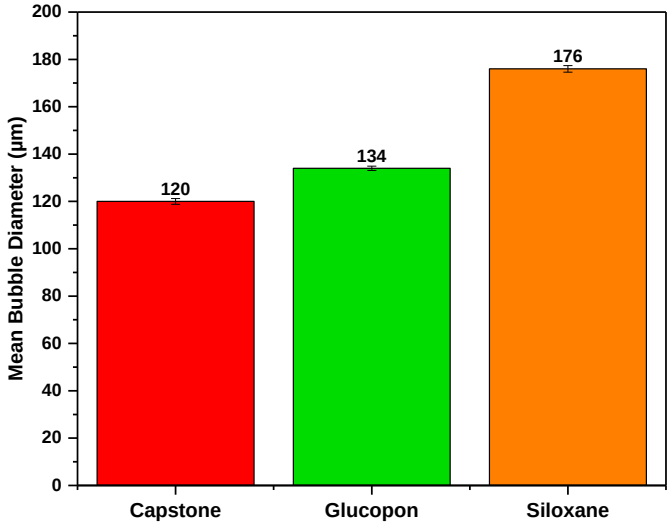

Figure 17. Bubble diameter.

2.3.5.2. Ignition time of fuel

The ignition time for heptane, octane, and 25%TMB-heptane through Capstone, Glucopon, and siloxane foam solution were presented in

Figure 18. 25% TMB-heptane has the lowest and Octane has the highest ignition time for all three-surfactant foam solutions tested. Irrespective of the fuel types, Capstone foam solution has the highest, and siloxane foam solution has the lowest ignition time.

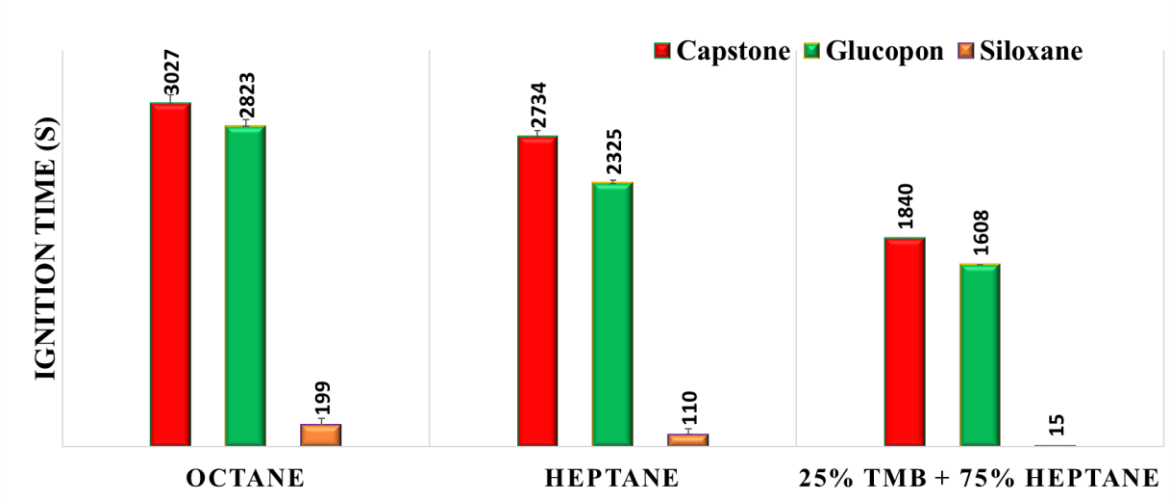

Figure 18. Ignition test results.

2.4. Discussion

The findings from this study show that TMB has affected the microstructure of Capstone and Glucopon due to their higher solubility in surfactant solution. On the other hand, microstructure is unaffected by heptane due to its poor solubility in surfactant solution. The ignition time for fuel mixture 25%TMB-heptane is shorter compared to heptane and octane due to higher solubility in Capstone and Glucopon foam solution.

The solubility of fuel (i.e., the maximum amount of fuel solubilized in surfactant solution) in surfactant solution will have a significant impact on the microstructure. According to SANS and DLS results, heptane did not change the micelle size in the bulk for the three surfactants used in this study significantly. Heptane has 0.0003 wt.% solubility in water which makes them almost insoluble. Fuel concentration measurements (Figure 14) reveal that in a static liquid-liquid setup (Figure 3) Capstone, Glucopon, and siloxane did not increase the solubility of heptane in water. Therefore, due to the poor solubility of heptane in surfactant solutions, no changes in the micelle size or shape have been observed for Capstone, Glucopon, and siloxane. Cryo-TEM, SANS, and DLS reveal that TMB has changed the micelle size for both Capstone and Glucopon.

Figure 15 shows that the presence of Capstone and Glucopon in water has increased TMB solubility and the values are 0.12 and 0.18 wt.% respectively. We have observed the formation of multilayer vesicles, an increase in diameter of vesicles for Capstone (Figure 6), and one-dimensional growth of worm-like micelle of Glucopon (Table 5). Previous literature has shown that hydrocarbon surfactant diffuses to bulk along with the solubilized fuel molecules forming swollen micelle [30]. The data from this research indicates that micelle size increases due to the TMB solubility; however, the location of TMB molecules inside the micelle has not been verified. Further study would require locating the fuel molecules inside the micelle.

The solubility of fuel in surfactant solution will impact the interfacial properties. According to literature, once fuel molecules have higher surface activity, the effectiveness of the surfactants in keeping low IFT decreases, hence interfacial tension increases [31]. Interfacial tension (IFT) measurements (Figure 10) show higher IFT values for Capstone-TMB and Glucopon-TMB compared to Capstone-heptane and Glucopon-heptane respectively. The benzene ring increases the amphiphilicity or surface activity of TMB. Fuel concentration measurements (Figure 15) show that TMB has higher solubility in Capstone and Glucopon solution. The higher solubility of TMB in Capstone and Glucopon solution (Figure 15) causes surfactants to go away from the interface to the bulk and form structure at lower concentrations. Thus, increasing IFT value for Glucopon-TMB and Capstone-TMB, reduces surface excess (Figure 13) and decreases CMC (Figure 12). A comparable decrease in surface excess has also been reported for long chain alkylpolyglucoside surfactants in the presence of benzene ring fuels as second phase [30]. Figure 19 is the representation of the normalized value of surface excess. It is interesting to observe that when surface excess reduction is ~70% or less microstructure seems to be changing in the presence of fuel. Microstructural and interfacial properties indicated that fuel solubility in surfactant solution is critical to fuel transport.

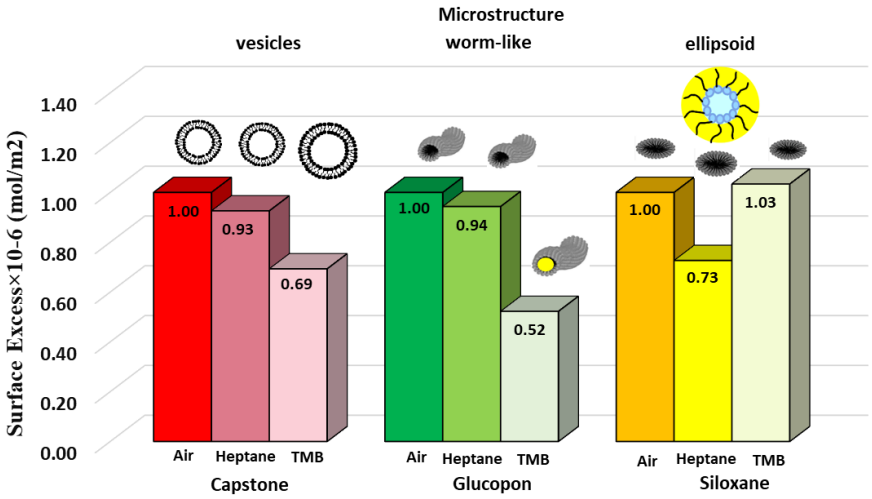

Figure 19. Comparison of interfacial properties at air/solution and fuel/solution interface for Capstone, Glucopon, and siloxane to their microstructural properties.

The fuel solubility in surfactant solution will have an impact on ignition time. From ignition tests we have observed that Capstone has higher ignition time irrespective of fuel type (Figure 18). Due to oleophobic and hydrophobic combination along with lowest surface tension, Capstone is the best performer. Capstone has longer ignition time compared to Glucopon for 25%TMB-heptane. The higher solubility of 25% TMB-heptane in Glucopon solution is the reason for shorter ignition time compared to Capstone solution. Hydrocarbon surfactant can solubilize 25%TMB-heptane fuel molecules more than fluorocarbon surfactant which follows the trend provided by Hinnant et al., [9]. Therefore, higher fuel solubility in surfactant solution causes shorter ignition time. The solubility of this fuel mixture in surfactant solutions increases due to the presence of TMB. In addition, TMB solubility in water increases due to Capstone and Glucopon. Therefore, due to higher solubility of TMB in surfactant solution, observed changes in microstructure, interfacial properties, and ignition time is shorter.

Higher vapor pressure decreases ignition time as well. Both octane and heptane have poor solubility in water (Table 8). None of the surfactants have increased solubility of octane or heptane (Figure 14) in water. Nonetheless, the vapor pressure of heptane is higher than octane (Table 1) and higher vapor pressure decreases the ignition time in this instance. Hence, ignition time is shorter for heptane compared to octane

Figure 18). Although, the vapor pressure for heptane is 49 mm Hg higher than the vapor pressure of 25%TMB-heptane which is 37.9 mm Hg. However, ignition time for 25%TMB-heptane is shorter compared to heptane due to its higher solubility. Therefore, the poor solubility of heptane in Capstone and Glucopon solutions caused longer ignition time compared to 25%TMB-heptane. The fire extinguishment time has increased with increasing vapor pressure and fuel water solubility as shown by Briggs and Webb et al. [32]. In this work, we have shown that surfactant increases solubility of fuel in water. Then higher solubility of fuel decreases ignition time. It would be expected that a lower ignition time would correspond to a higher extinguishment time. Therefore, the trend for ignition test results is similar to the fire extinguishment tests by Biggs and Webb [32].

A low surface excess might be the reason for the poor performance of surfactant foam solution during ignition test. Figure 18 shows that siloxane foam solution has a very low ignition time for all the fuels tested. Heptane and TMB have poor solubility in siloxane surfactant solution (Figure 14). SANS result reveals that siloxane micelle size and shape do not have any effect of heptane or TMB (Table 6). However, surface excess for siloxane is smaller compared to Capstone and Glucopon (Figure 13). A lower surface excess means the number of surfactants at the interface is low which cannot provide enough resistance against fuel transport. A comparatively high expansion ratio (Table *9*Table 9) and larger bubble size (Figure 17) have been observed for siloxane foam solution which means foams are comparatively dry, and a smaller number of surfactants are present throughout the foam solution. Therefore, lower surface excess and higher expansion ratio might be the reason for poor performance of siloxane foam solution during ignition test.

Convection might have some effect on fuel transport. In foams, the solution is continuously draining down the foam due to gravity toward the fuel surface. The motion of the drained surfactant solution at the fuel surface induces convection at this interface. To explore the convection effect, stirring was introduced in the bottom phase of Capstone solution (Figure 3). Figure 16 shows that 25%TMB-heptane gets solubilized by Capstone solution when stirring was done in the bottom phase (Figure 3) which means convection might have an effect on surfactant foam solution draining. Glucopon solution can solubilize 25% TMB-heptane

with and without stirring (Figure 16). Convection effect can be fuel and surfactant-type dependent, and further work is needed to fully understand this effect.

Vesicles formed by Capstone in the bulk might have some effect on the longer ignition time of Capstone compared with Glucopon. Vesicles might be more stable while capturing fuel [33] and not allowing fuel to be released in the gas phase compared to worm-like micelles of Glucopon. However, further studies will be required to confirm the impact of micelle shape on fuel transport.

2.5. Conclusions

The analysis of fuel impact on single surfactants followed common trends. However, microstructural visualization of single surfactants provides direct evidence of the impact of fuel. Moreover, factors affecting microstructure and implication of this factor in ignition time.

Capstone forms vesicles at the nanoscale. The diameter and sometimes membrane layer thickness of the vesicles increase in the presence of TMB. Glucopon forms worm-like micelles, and one-dimensional growth occurs in the presence of TMB. Due to the higher solubility of TMB in Capstone and Glucopon solution, microstructural changes occur. Heptane does not impact Capstone and Glucopon microstructure. Due to the poor solubility of nonpolar fuel like heptane in Capstone and Glucopon solution microstructure is unaffected. Siloxane creates ellipsoidal micelles, and TMB or heptane does not impact the bulk microstructure rather siloxane forms reverse micelle in heptane. In addition, interfacial tension increases, surface excess, and CMC reduces due to the higher solubility of polar fuel like TMB in Capstone and Glucopon solution. Microstructural and interfacial properties show that fuel solubility in surfactant solution is an important factor during fuel transport.

Ignition time is shorter when microstructure and interfacial properties have shown an impact of fuel solubility. The higher solubility of 25%TMB-75%heptane in Capstone and Glucopon solution causes lower ignition time compared to heptane. However, heptane has a shorter ignition time than octane due to its higher vapor pressure. Moreover, siloxane has the lowest ignition time due to its's low surface excess compared to Capstone and Glucopon solution. Therefore, ignition test results show that higher solubility of

fuel in surfactant solution and higher vapor pressure, low surface excess impact ignition time. Overall, this study highlights the significance of both surface excess and fuel solubility in surfactant solution as important properties when developing a novel surfactant.

References

[1] R. Ananth, K. M. Hinnant, S. L. Giles, J. P. Farley, and A. W. Snow, "Environmentally Friendly Surfactants for Foams with Low Fuel Permeability Needed for Effective Pool Fire Suppression," NAVAL RESEARCH LAB WASHINGTON DC, 2020.

[2] N. Jiang, Y. Sheng, C. Li, and S. Lu, "Surface activity, foam properties and aggregation behavior of mixtures of short-chain fluorocarbon and hydrocarbon surfactants," *Journal of Molecular Liquids*, vol. 268, pp. 249-255, 2018.

[3] X. Li, Y. Gao, C. E. Boott, M. A. Winnik, and I. Manners, "Non-covalent synthesis of supermicelles with complex architectures using spatially confined hydrogen-bonding interactions," *Nature Communications*, vol. 6, no. 1, p. 8127, 2015.

[4] C. Hill *et al.*, "Surface and bulk properties of surfactants used in fire-fighting," *Journal of colloid and interface science*, vol. 530, pp. 686-694, 2018.

[5] D. Langevin, "On the rupture of thin films made from aqueous surfactant solutions," *Advances in colloid and interface science*, vol. 275, p. 102075, 2020.

[6] P. Stevenson, "Inter-bubble gas diffusion in liquid foam," *Current Opinion in Colloid & Interface Science*, vol. 15, no. 5, pp. 374-381, 2010.

[7] J.-F. Berret, P. Herve, O. Aguerre-Chariol, and J. Oberdisse, "Colloidal complexes obtained from charged block copolymers and surfactants: A comparison between small-angle neutron scattering, Cryo-TEM, and simulations," *The Journal of Physical Chemistry B*, vol. 107, no. 32, pp. 8111-8118, 2003.

[8] Y. Fan and Y. Wang, "Applications of small-angle X-ray scattering/small-angle neutron scattering and cryogenic transmission electron microscopy to understand self-assembly of surfactants," *Current Opinion in Colloid & Interface Science*, vol. 42, pp. 1-16, 2019.

[9] K. M. Hinnant, S. L. Giles, and R. Ananth, "Measuring fuel transport through fluorocarbon and fluorine-free firefighting foams," *Fire Safety Journal*, vol. 91, pp. 653-661, 2017, doi: 10.1016/j.firesaf.2017.03.077.

[10] A. W. Snow, S. Giles, K. Hinnant, J. Farley, and R. Ananth, "Fuel for Firefighting Foam Evaluations: Gasoline vs Heptane," NAVAL RESEARCH LAB WASHINGTON DC WASHINGTON United States, 2019.

[11] "National Center for Biotechnology Information (2024). PubChem Compound Summary for CID 8900, Heptane. Retrieved February 27, 2024 from." [Online]. Available: https://pubchem.ncbi.nlm.nih.gov/compound/Heptane.

[12] "National Center for Biotechnology Information (2024). PubChem Compound Summary for CID 356, Octane. Retrieved February 27, 2024 from." [Online]. Available: https://pubchem.ncbi.nlm.nih.gov/compound/Octane.

[13] "National Center for Biotechnology Information (2024). PubChem Compound Summary for CID 7247, 1,2,4-Trimethylbenzene. Retrieved February 27, 2024 from." [Online]. Available: https://pubchem.ncbi.nlm.nih.gov/compound/1_2_4-Trimethylbenzene.

[14] A. W. Snow, S. Giles, K. M. Hinnant, J. P. Farley, and R. Ananth, "Quantification of Fluorine Content in AFFF Concentrates," NAVAL RESEARCH LAB WASHINGTON DC WASHINGTON United States, 2017.

[15] J. Eastoe and J. Dalton, "Dynamic surface tension and adsorption mechanisms of surfactants at the air–water interface," *Advances in colloid and interface science*, vol. 85, no. 2-3, pp. 103-144, 2000.

[16] T. Bastow, W. H. Durnie, A. Jefferson, and J. Pang, "Ultraviolet spectroscopy for the analysis of oil-in-water effluent using isopropanol as co-solvent," *Applied spectroscopy*, vol. 51, no. 3, pp. 318-322, 1997.

[17] "<1,2,4-Trimethylbenzene _ C9H12 - PubChem.pdf>."

[18] J. N. Israelachvili, D. J. Mitchell, and B. W. Ninham, "Theory of self-assembly of hydrocarbon amphiphiles into micelles and bilayers," *Journal of the Chemical Society, Faraday Transactions 2: Molecular and Chemical Physics*, vol. 72, pp. 1525-1568, 1976.

[19] M. Salim, H. Minamikawa, A. Sugimura, and R. Hashim, "Amphiphilic designer nano-carriers for controlled release: from drug delivery to diagnostics," *MedChemComm,* vol. 5, no. 11, pp. 1602-1618, 2014.
[20] R. A. Khalil and A. Z. Al-hakam, "Theoretical estimation of the critical packing parameter of amphiphilic self-assembled aggregates," *Applied surface science,* vol. 318, pp. 85-89, 2014.
[21] G. L. Mosley, C. D. Yamanishi, and D. T. Kamei, "Mathematical modeling of vesicle drug delivery systems 1: vesicle formation and stability along with drug loading and release," *Journal of laboratory automation,* vol. 18, no. 1, pp. 34-45, 2013.
[22] M. D. Hanwell, D. E. Curtis, D. C. Lonie, T. Vandermeersch, E. Zurek, and G. R. Hutchison, "Avogadro: an advanced semantic chemical editor, visualization, and analysis platform," *Journal of cheminformatics,* vol. 4, no. 1, pp. 1-17, 2012.
[23] X. Yu *et al.*, "Foaming behavior of fluorocarbon surfactant used in fire-fighting: The importance of viscosity and self-assembly structure," *Journal of Molecular Liquids,* vol. 327, p. 114811, 2021.
[24] T. Sato *et al.*, "Oil-induced structural change of wormlike micelles in sugar surfactant systems," *Journal of dispersion science and technology,* vol. 27, no. 5, pp. 611-616, 2006.
[25] K. Hinnant, "Characterizing Trends Between Surfactant Structure, Fuel Transport through a Foam Layer, and Foam Fire Extinction Performance for Firefighting Foams Containing Novel Environmentally-Friendly Surfactants," The George Washington University, 2021.
[26] M. W. Sulek and T. Wasilewski, "Influence of critical micelle concentration (CMC) on tribological properties of aqueous solutions of alkyl polyglucosides," *Tribology transactions,* vol. 52, no. 1, pp. 12-20, 2008.
[27] T. Svitova, R. Hill, Y. Smirnova, A. Stuermer, and G. Yakubov, "Wetting and interfacial transitions in dilute solutions of trisiloxane surfactants," *Langmuir,* vol. 14, no. 18, pp. 5023-5031, 1998.
[28] K. M. Hinnant *et al.*, "Extinction Performance Summary of Commercial Fluorine-free Firefighting Foams over a 28 ft2 Pool Fire Detailed by MIL-PRF-24385," NAVAL RESEARCH LAB WASHINGTON DC WASHINGTON United States, 2020.
[29] K. Koczo and G. Racz, "Foaming properties of surfactant solutions," *Colloids and surfaces,* vol. 56, pp. 59-82, 1991.
[30] D. Balzer and H. Luders, *Nonionic surfactants: alkyl polyglucosides*. CRC press, 2000.
[31] E.-M. Kutschmann, G. Findenegg, D. Nickel, and W. Von Rybinski, "Interfacial tension of alkylglucosides in different APG/oil/water systems," *Colloid and Polymer Science,* vol. 273, pp. 565-571, 1995.
[32] A. Briggs and J. Webb, "Gasoline fires and foams," *Fire technology,* vol. 24, pp. 48-58, 1988.
[33] D. Gu *et al.*, "An aqueous emulsion route to synthesize mesoporous carbon vesicles and their nanocomposites," *Advanced Materials,* vol. 22, no. 7, pp. 833-837, 2010.

Appendix A. Supplementary information

A.1. Packing parameter

The volume and length of the surfactant structure have been obtained from Avogadro software. Effective area at the interface has been obtained from tensiometer results. All the values are tabulated below in Table S1 for packing factor calculation.

Table S1. Packing factor calculation

surfactant	Volume of tail (v)	Area per molecule (a_o)	length of tail (l)	packing factor $p = v/(a_o*l)$
	nm^3	nm^2	nm	
Capstone	0.056	0.439	0.809	1/2
Glucopon	0.067	0.392	1.333	1/2
Siloxane	0.045	0.621	0.488	1
(n = 6 to 9)	0.051	0.621	0.501	1

A.2. Small Angle neutron Scattering (SANS)

SANS data were fitted to form factors describing either a sphere model, ellipsoidal model, or lamellar model using the fitting program Sas View, an iterative, least-squares fitting process. Known model parameters were set to constant values (e.g., scattering length densities) and unknown fit parameters were set allowing the program to refine them to obtain an optimized fit. A structure factor S(Q), which described inter-particle interactions within the system (attractive, repulsive), was introduced when combined with an appropriate form factor P(Q).

Capstone

The scattering profile (Figure S1) for Capstone 1157 formed lamellar structure has been fitted with the model “lamellar structure paracrystal” which is the representation of large multilamellar vesicles. The peak at higher q region indicates structure factor (length, thickness of lamellar), here length is infinity. This model calculates the scattering from a stack of repeating lamellar structures. The stacks of lamellae (infinite

in lateral dimension) are treated as a paracrystal to account for the repeating spacing. The repeat distance is further characterized by a Gaussian polydispersity.

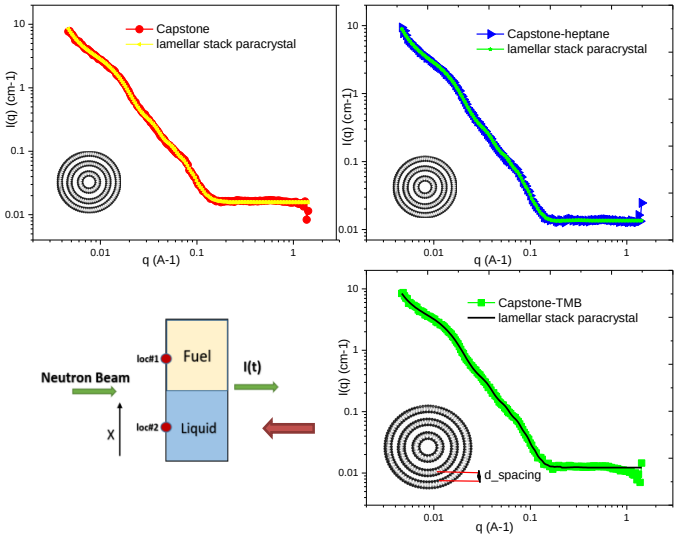

Figure S1. SANS Scattering profile for Capstone.

Glucopon

The scattering profile (Figure S2) from SANS has been fitted to the model “flexible cylinder elliptical” is representation of worm-like micelle.

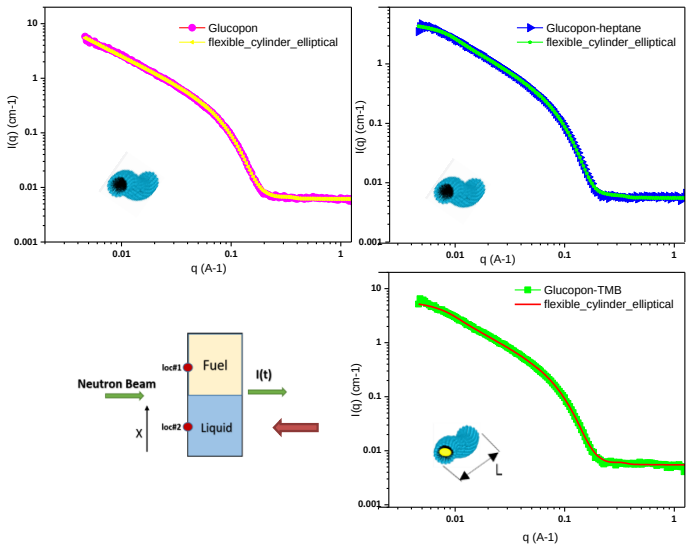

Figure S2. SANS Scattering profile for Glucopon.

This model calculates the form factor for a flexible cylinder with an elliptical cross section and a uniform scattering length density. The non-negligible diameter of the cylinder is included by accounting for excluded volume interactions within the walk of a single cylinder. The form factor is normalized by the particle volume such that:

$$P(q) = \frac{\text{scale}(F^2)}{V} + \text{background}$$

where the averaging is over all possible orientations of the flexible cylinder. The 2D scattering intensity is the same as 1D, regardless of the orientation of the q vector which is defined as

$$\boxed{q = \sqrt{q_x^2 + q_y^2}}$$

The chain of contour length, L, (the total length) can be described as a chain of some number of locally stiff segments of length l_p, the persistence length (the length along the cylinder over which the flexible cylinder can be considered a rigid rod). The Kuhn length ($b = 2 * l_p$,) is also used to describe the stiffness of a chain.

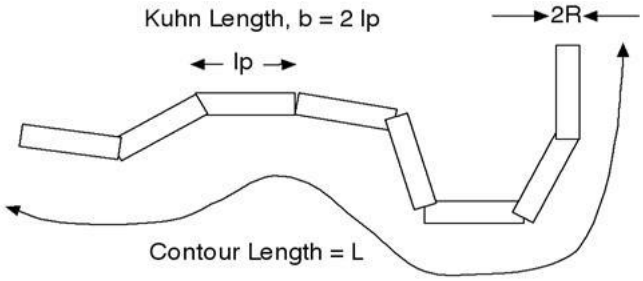

Siloxane

The scattering profile (Figure S3) from SANS has been fitted to the model "triaxial ellipsoidal" which is representation of ellipsoid shape micelle.

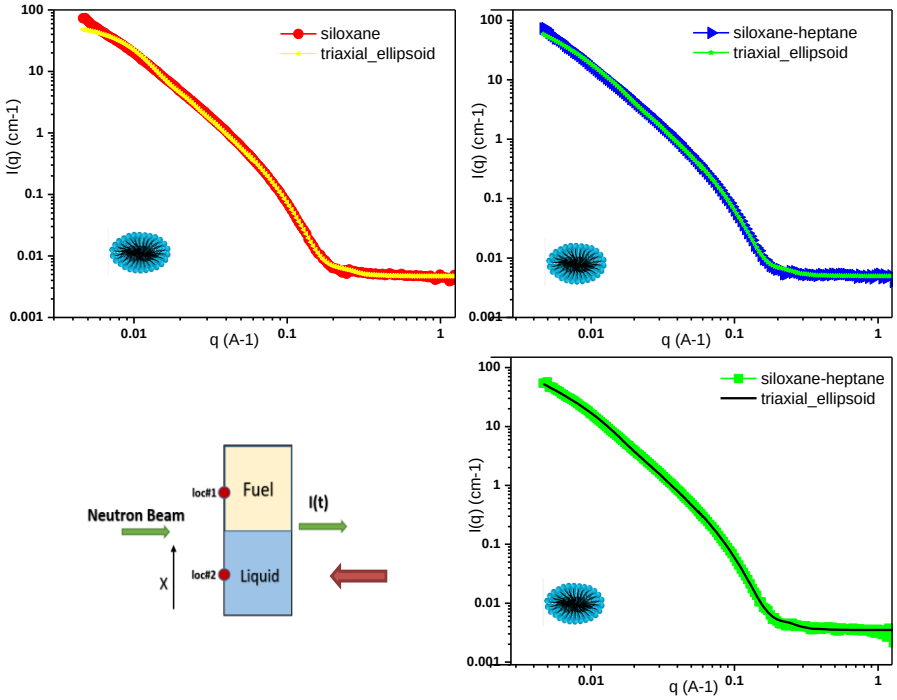

Figure S3. SANS Scattering profile for Siloxane (bottom phase)

Ellipsoid of uniform scattering length density with three independent axes. Given an ellipsoid.

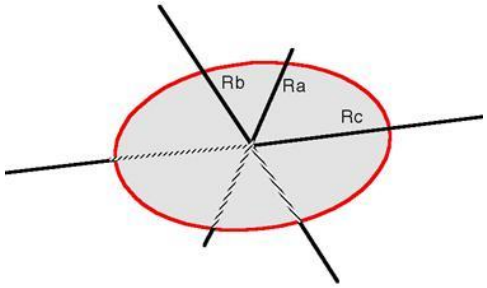

$$\frac{X^2}{R_a^2}+\frac{Y^2}{R_b^2}+\frac{Z^2}{R_c^2}=1$$

the scattering for randomly oriented particles is defined by the average over all orientations Ω of:

$$P(q)=\text{scale}\,(\Delta p)^2\frac{V}{4\pi}\int_{\Omega}\Phi^2\,(qr)d\Omega+\text{background}$$

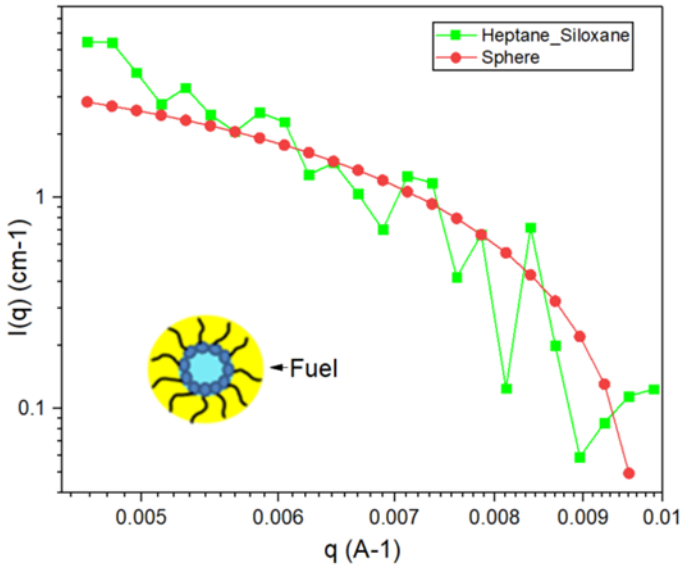

Figure S4. SANS Scattering profile for Siloxane (top phase)

The scattering profile (Figure S4) for the top phase for siloxane has been fitted using simple power law.

This model calculates a simple power law with a flat background.

$$I(q) = \text{scale} \cdot q^{-\text{power}} + \text{background}$$

References

1. http://www.sasview.org/

CHAPTER 3

Understanding the interaction between fuel and single surfactants of firefighting foam

Rezawana Islam[1], Rui Qiao[2], and Brian Y. Lattimer[2]

[1]Materials Science and Engineering, Virginia Tech

[2]Mechanical Engineering, Virginia Tech

Abstract

Traditional firefighting foams contain fluorinated surfactants which have negative environmental and health impacts. To develop a safer alternative to traditional firefighting foam, it is important to investigate the existing AFFF foam formulation and identify the factors influencing the firefighting performance of surfactants. Fuel transport through surfactant foam solution has been identified as a dominant mechanism for poor fire extinguishing performance. It has been hypothesized that presence of micelles will affect fuel transport. Experiments were conducted with and without the presence of micelles by varying surfactant concentration. Two different types of single surfactants (Glucopon and Capstone) and three different types of fuels (TMB, heptane, and 25%TMB-heptane) were included in the study to explore the impact of surfactant type and fuel type on fuel transport. Isothermal titration calorimetry (ITC) was used to study the thermodynamics of the interaction between fuel and surfactant. UV-Vis spectroscopy has been used to measure fuel transport in surfactant solution. This work shows that increasing surfactant concentration from below to above the critical micelle concentration (CMC) the interactions between fuel and single surfactants become thermodynamically more favorable and more fuel is transported into the surfactant solution. This was attributed to micelles serving as a mechanism to transport fuel from the fuel-surfactant interface and into the bulk solution. Moreover, the interaction between fuel and surfactant becomes thermodynamically more favored with increasing polarity of fuel; hence, fuel transport enhances.

3.1. Introduction

Surfactants are the key components of Aqueous Film-Forming Foams (AFFF), which is a type of firefighting foam used to extinguish flammable large hydrocarbon liquid fires. It has applications in fire departments for fire extinguishing, in military, transportation, and fuel storage applications [1-3]. AFFF contains fluorocarbon surfactants, hydrocarbon surfactants, additives, and water. Fluorocarbon surfactants in AFFF formulations effectively reduce surface tension and provide good firefighting performance. However, fluorinated surfactants have raised concerns about environmental persistence and toxicity. Replacement firefighting foams should meet environmental regulations and provide similar fire extinguishment performance compared with AFFF.

Researchers have developed environmentally friendly alternatives for current AFFF [4]. However, fluorine-free alternatives cannot perform as efficiently as current fluorinated AFFF [4, 5]. Foam collapse due to fuel transport through the foam solution has been identified as the reason for this poor performance [6]. Therefore, it is critical to understand the interaction between fuel and surfactants of firefighting foam. Surfactant concentration plays a significant role in foam preparation and maintaining firefighting performance. At low surfactant concentrations below critical micelle concentration (CMC), monomers exist in the foam solution. However, as the concentration of surfactants in a solution increases to the CMC or above, solutions tend to aggregate and form micelles [7]. When firefighting foam is exposed to fuel, fuel solubilization by surfactants/micelles allows the hydrophobic fuel to disperse and remain in the aqueous solution. Studies have shown that with increasing surfactant concentration in water, fuel solubilization occurs and the fuel solubility increases considerably [8]. Shah et al. [9] measured rates of solubilization of toluene into SDS solutions and found that solubilization rates were independent of time but increased with surfactant concentration until a limiting value was reached at high concentrations. Fuel solubilization enhances with increasing surfactant concentration mentioned by Ward et. al [10] that below CMC no rates were measurable until the total surfactant concentration was greater than that of the CMC.

As shown in Figure 20, two alternative pathways for fuel solubilization into micelles have been proposed: a) nonpolar fuel with poor solubility is taken by the micelle at the interface (Figure 20a) b) polar fuel with higher solubility dissolved in aqueous phase and captured by surfactant micelle (Figure 20b) [10-14]. Carroll et al. [12] showed that the rate of nonpolar fuel solubilization is proportional to the nonionic surfactant concentration above the CMC. Youn et. al. [15] showed that the solubility of the polycyclic aromatic hydrocarbons above the CMC increases linearly and rapidly with increasing perfluorinated surfactant concentration.

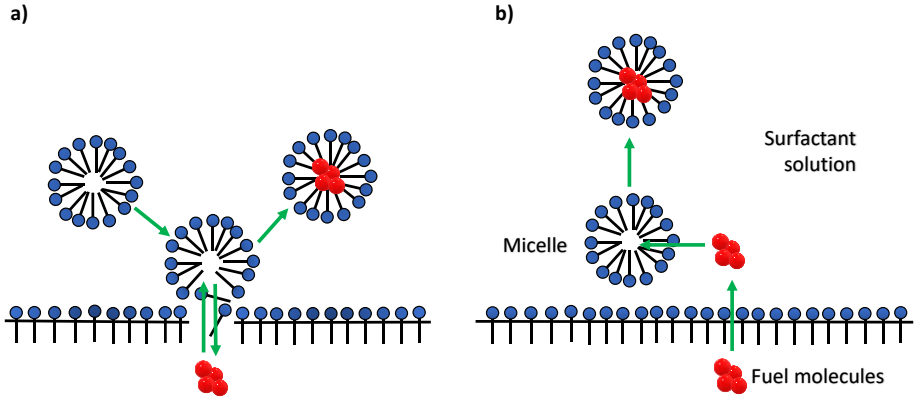

Figure 20. Fuel solubilization mechanism a) nonpolar fuel b) polar fuel.

In the past years, fuel solubilization has been studied extensively using a drop-on-fiber [9, 11-13, 16] method to understand the kinetics of solubilization process with changing surfactant concentration. However, there is a lack of data that demonstrates solubilization using a direct method and explains the thermodynamics of the process which will help to understand the role of micelle during fuel transport. Isothermal titration calorimetry (ITC) is a direct method that can be used to quantify the thermodynamics of the interaction between fuel and a single surfactant.

ITC is a powerful analytical technique used in chemistry and biochemistry. It measures the heat absorbed or released during a chemical reaction or binding event which is directly related to the change in enthalpy (ΔH) of the process. ITC enables the determination of thermodynamic binding parameters (free energy, enthalpy, and entropy) and binding stoichiometry in a single experiment by fitting the binding isotherm to a suitable binding model in complex systems such as colloidal mixtures [17-20]. Its ability to directly

measure heat changes makes it an effective tool for understanding the thermodynamics of molecular interactions.

An experimental study was performed to examine the effect of surfactant concentration on fuel transport on the surfactant solution. By changing surfactant concentrations, the role of micelles was investigated. Experiments were also conducted using various fuels to explore the impact of fuel types on fuel transport into the surfactant bulk solution. The values of affinity, Gibbs energy, enthalpy, entropy of interaction of liquid fuel with water, and surfactant solutions were quantified and used to explain the interaction between fuels and surfactants.

3.2. Experimental

A series of experiments were conducted exposing aqueous surfactant mixtures to different fuels. Through this research, we have investigated the thermodynamics of the interaction between fuel and surfactant using ITC. UV-vis spectroscopy has been performed to quantify the fuel transport into surfactant solution.

3.2.1. Materials

The interaction between fuels and surfactant solutions have been studied. These were selected to represent the fuels used in standardized testing and surfactants representative of those used in AFFF.

The three fuels included in the study were n-heptane with high purity (99%) purchased from LAB ALLEY, TX; 1,2,4 trimethylbenzene (TMB) with high purity <= 100% purchased from Sigma-Aldrich, St. Louis, MO; and 25%TMB-heptane mixture was prepared in a laboratory at Virginia Tech. Gasoline is the most commonly used fuel for evaluating firefighting foam performance using the MilSpec standard method for firefighting [21]. A mixture of fuel composed of 25% TMB and 75% heptane was used as a simple surrogate for gasoline. Due to the presence of an aromatic component (TMB), the suppression time for this fuel mixture is very close to the suppression time for gasoline [21]. Most other methods use heptane as fuel for fire suppression tests [21]. Pure TMB was included due to its higher water solubility. The chemical structures and select physical properties of the fuels [22, 23] are provided in Table 10.

Two different types of surfactants used in the study were Capstone 1157 and Glucopon 600 CS UP purchased from Sigma-Aldrich, St. Louis, MO; Capstone and Glucopon are representative of the types of surfactants used in firefighting foams and are the two components used in a Reference AFFF developed elsewhere [24]. Their chemical structure and select properties are given in Table 11. Measurements were done at CMC, 2 times below, and 5 times higher than the CMC concentrations for surfactants. The 5 times the CMC concentration was chosen since it is similar to the surfactant concentration in Reference AFFF [25]. CMC presented in Table 11 were based on surfactant concentration. The physical properties are taken from the Safety data sheet for these.

Table 10. Physical properties of fuels.

Fuel	Chemical formula	Structure	Water Solubility (mg/L)
1,2,4 Tri-methylbenzene (TMB)	C_9H_{12}	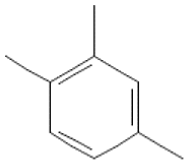	57
Heptane	C_7H_{16}	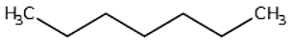	3.4

Table 11. Surfactant Properties [5, 26].

Name	Chemical Structure	Molecular Weight (g/mol)	CMC (wt.%)	Tail Type	Head Type
Capstone 1157	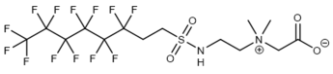	570	0.011	Fluorocarbon	Zwitterionic
Glucopon 600 CS UP	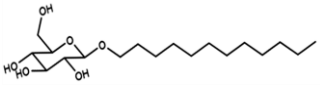	386	0.012	Hydrocarbon	Nonionic

3.2.2. Methods

Isothermal titration calorimetry (ITC)

An isothermal titration calorimeter (Nano-ITC) from TA Instruments was used to measure the thermodynamics of the fuel and single surfactant solution interaction. The nano calorimeter was equipped with a reference and a sample cell, 4 ml removable stainless-steel titration/perfusion ampoule (reaction vessel) with a circlip cap and stirring facilities, and a precision syringe pump for efficient titrant delivery.

All titrations were carried out at 25 °C using a 250 μL syringe. The sample cell was filled with 3 mL surfactant solution, while the reference cell was always filled with 3mL of distilled water. The titration experiments were performed by 12 injections each of 20 μL of fuel over a 20 s period and injection interval was 300 s. A calibration was performed in a dynamic corrected mode before experiments. All the measurements were performed three times to confirm repeatability.

Nano analyze software (provided by TA instruments, New castle, DE) was used to fit the raw heat data collected from ITC. The raw experimental data were presented as heat flow versus time, a positive heat flow indicated an exothermic peak, and a negative heat flow indicated an endothermic peak. The first peak includes the heat flow due to interaction with sample cell other than fuel and surfactant solution interaction; therefore, the first data point from heat flow versus time plot was not considered for analysis. The area of each peak is integrated and plotted versus the molar ratio of ligand to protein. The resulting isotherm fitted to a binding model from which the binding enthalpy ($\Delta H, \mathrm{kJ/mol}$) was calculated and was the integrated area (heat released or absorbed) per mole of ligand bound. From the inflection point of the area versus molar ratio curve fit reaction stoichiometry (n), and binding affinity K_a (M^{-1}) was determined. From the obtained enthalpy, (ΔH) and binding affinity, K_a Gibbs free energy ($\Delta G, \mathrm{kJ/mol}$) and entropy ($T\Delta S, \mathrm{kJ/mol}$)) can be calculated using the following equations [27, 28]:

$$\Delta G = -RT\ln K_a \quad (1)$$

$$\Delta G = \Delta H - T\Delta S \quad (2)$$

where, R is the gas constant, T is absolute temperature (298.15 K).

Binding affinity, K_a is a measure of the strength of the binding interaction between a single molecule to its binding partner. The larger the binding affinity, the greater the attraction between the molecules, in this work, affinity between fuel and surfactant solution has been measured. In addition, the meaning of the thermodynamic parameter's sign is as follows: ΔG negative means forward reaction is favorable (reactants go to products); ΔG positive indicates reverse reaction is favorable (products to reactants). ΔH negative means exothermic reaction (favors getting negative ΔG). ΔH positive indicates endothermic reaction (favors positive ΔG) (add heat for reactions). ΔS negative indicates decrease in entropy going from reactants to products (favors positive ΔG). ΔS positive means increasing entropy due to reactants turn into products (favors getting negative ΔG).

UV Vis spectroscopy

The transport of fuel into the surfactant solution was quantified through a diffusion experiment with liquid fuel over a layer of surfactant solution. The fuel and surfactant solution two-phase system were prepared in a 20 mL glass vial. After pouring the surfactant solution (~ 15 ml) in the glass vial, a syringe was inserted to avoid any contamination on the needle. Then a fuel layer (~ 15 ml) was added at the top of the surfactant solution. The top of the vial was covered to avoid any evaporation. To observe the effect of changing surfactant concentrations on fuel solubilization, a wait time of 15 minutes before extracting the sample was used to allow for the fuel and surfactant solution to reach equilibrium at room temperature (Figure 21).

UV-Vis measurements were done to quantify the fuel concentration in the bulk using a Hitachi U4100 UV-VIS-NIR spectroscopy. To prepare the standard curve the absorbance spectra for known concentrations of fuel in surfactant solution were measured as discussed in section 2.2.2. For analysis, a sample was extracted from the two-layer interaction sample of surfactant solution (bottom phase) and fuel (top phase) as shown in Figure 21, and transferred into the UV-transparent disposable cuvette with dimensions 12.5 × 12.5 × 45 mm. The absorbance attained was placed into the standard curve (absorbance versus fuel concentration) to

quantify the concentration of fuel in surfactant solution. The absorption peak from 230 – 300 nm was used for all the analysis. All the measurements were done three times to check the reproducibility.

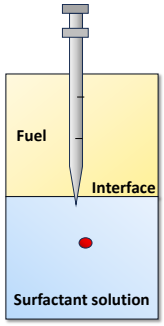

Figure 21. Experimental setup.

3.3. Results

3.3.1. Fuel Transport

To observe the effect of surfactant concentration on fuel transport UV-Vis Spectroscopy has been used. Fuel concentration measurements have been performed at different surfactant concentrations below, at, and above CMC.

Heptane

Figure 22 showed measured heptane concentration 2x below, at CMC, and 5x above CMC. CMC values for Glucopon and Capstone were 0.012 and 0.011 wt.% respectively based surfactant concentration (see section 2.3.3.2). Below and at the CMC concentration there is no fuel detected in Glucopon solution. Above the CMC concentration, the concentration of heptane fuel molecules was quantified indicating heptane was transported into the Glucopon solution due to addition of micelles in the bulk solution. Similarly, heptane concentration was measured into the Capstone solution above 5x CMC concentration implying heptane was transported.

TMB

Figure 22 contains data for TMB concentrations in Glucopon surfactant solutions below, at, and above CMC concentration of Glucopon. Below CMC concentration, measured TMB concentration in Glucopon solution was ~ 0.04 wt.%, higher than the solubility of TMB in water (0.0057 wt.% or 57 mg/L) (Table 10).

At and above CMC concentration, TMB concentrations were measured 0.06 and 0.18 wt.% respectively. This indicated that fuel solubilization concentration increased with increasing surfactant concentration.

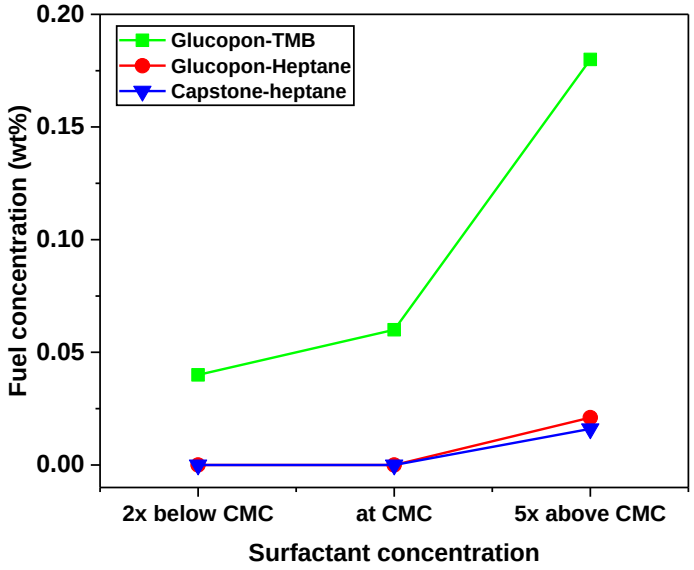

Figure 22. TMB and heptane concentration measurements in Glucopon below, at, and 5x CMC concentration for 15 minutes.

Figure 23 represents TMB, 25%TMB-heptane, and heptane concentration in Capstone and Glucopon solution at 5x CMC concentration. Samples were extracted after waiting for 15 minutes and 3 mm away from the interface. The concentration measured for TMB was highest in both Capstone and Glucopon solution and lowest for heptane. 25%TMB-heptane concentration measured was higher than heptane for Capstone and Glucopon solution. Moreover, fuel transport was higher through Glucopon solution compared to Capstone solution irrespective of fuel types as indicated by the fuel concentration measurement.

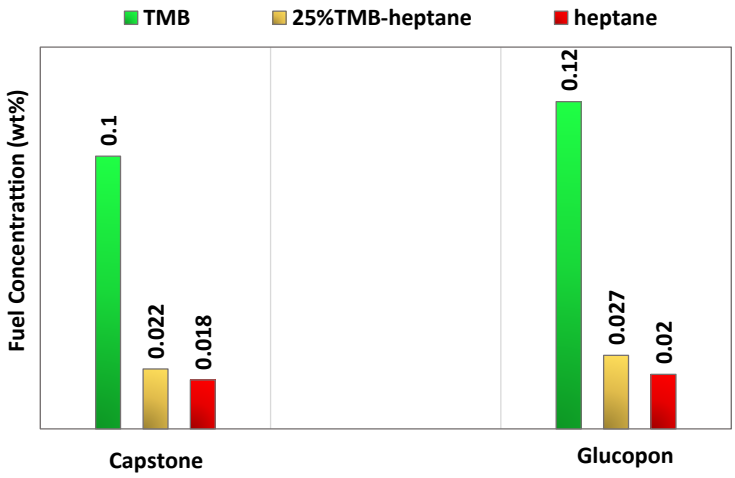

Figure 23. TMB, 25%TMB-heptane, and heptane concentration in a) Capstone and b) Glucopon solution at 5x CMC for 15 minutes 3 mm distance.

3.3.2. Microstructural characterization

To observe the effect of surfactant concentration on the micelle size with and without fuel exposure, Dynamic light scattering (DLS) measurements were performed (Figure 24). Below CMC concentration, the structure size in the bulk of the solution had a single size distribution. Fuel exposure did not affect the structures size significantly for Glucopon and Capstone indicating no fuel transport. At CMC concentration, two different size distributions were observed for Capstone indicating micelle formation of two different sizes. For both Capstone and Glucopon, micelle size increased due to TMB effect indicating fuel transport occurred, however, did not increase for heptane. Above 5x CMC concentration, fuel transport occurred indicated by the increment in the micelle size for Glucopon and Capstone due to both TMB and heptane exposure. For Glucopon, multiple size distributions were more prominent due to fuel exposure indicating micelles were segregating into two different sizes while accommodating fuel molecules. For Capstone, multiple size distribution was more visible due to the TMB effect.

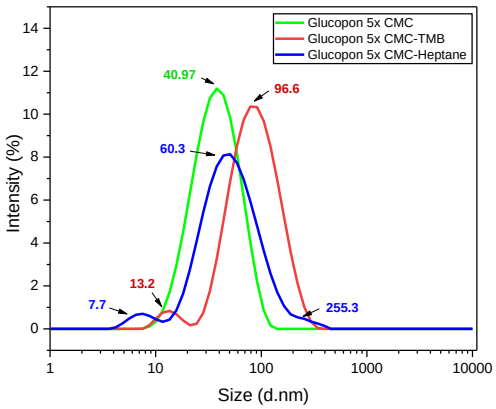

a) Glucopon 5x CMC

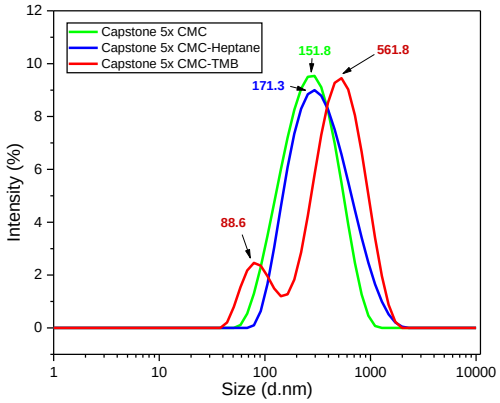

b) Capstone 5x CMC

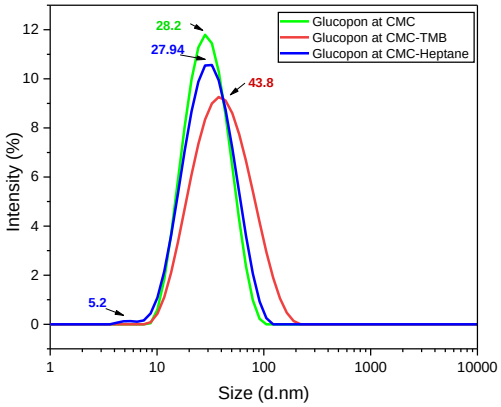

c) Glucopon at CMC

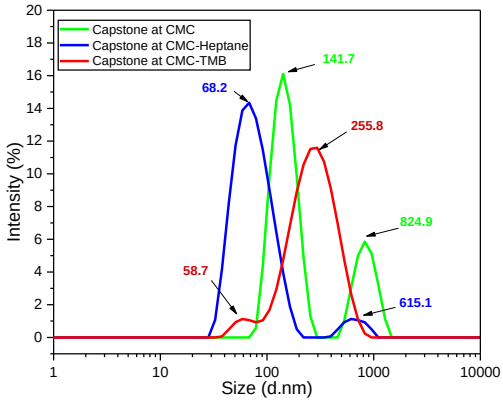

d) Capstone at CMC

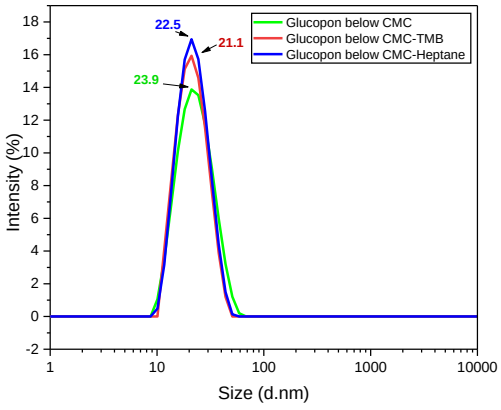

e) Glucopon below CMC

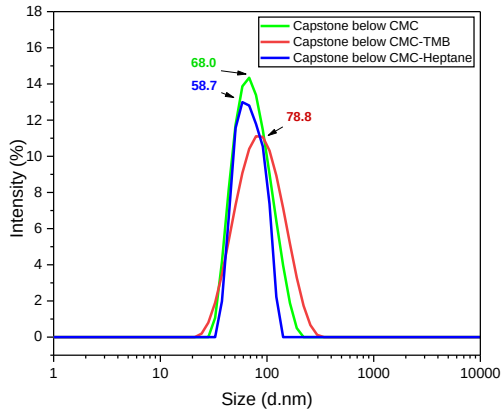

f) Capstone below CMC

Figure 24. DLS results below, at, and above CMC concentrations of surfactants with and without fuel exposure a) Glucopon b) Capstone.

3.3.3. Thermodynamic characterization

A series of experiments were performed using the ITC to quantify the thermodynamic parameters associated with the interaction of TMB, heptane, and 25%TMB-heptane with water and aqueous surfactant solutions. The heat flow versus time plots were presented below for each interaction. The values of enthalpy, entropy, Gibbs free energy, and affinity were calculated.

3.3.3.1. Heptane

According to the heat flow versus time plot, the water-heptane interaction was exothermic (Figure 25). The exothermic peaks were attributed to an increased ordering of hydrogen bonds in water near the interface in the presence of heptane molecules as a second phase [29] as shown in Figure 28a. The peak magnitude decreased with subsequent injections indicating that the majority of this reordering occurred upon the first few injections, likely at the surface. As seen in Figure 27, the overall process of the fuel addition resulted in a negative enthalpy change of -3.3 kJ/mol and negative entropy change (Figure *27*). This resulted in a positive Gibbs free energy indicating that the interaction between water and heptane molecules was not spontaneous / favorable.

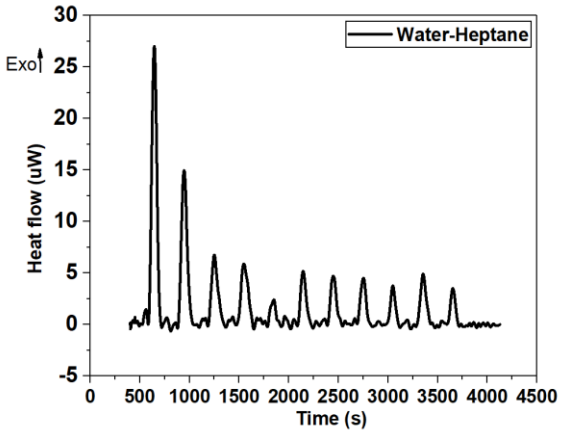

Figure 25. ITC thermogram (Heat flow versus time) after titration of heptane into sample cell with water.

The heat flow associated with adding heptane to solutions with different concentrations of Glucopon is provided in Figure 26. As seen in Figure 26a, Glucopon 2x below the CMC concentration resulted in positive exothermic heat flow peaks similar to that observed for heptane added to water. This resulted in a negative enthalpy (-2.46 kJ/mol) and negative entropy (increased order within the system), see Figure 27.

The results indicate that there was little interaction of heptane with the low concentration of surfactants and the heptane-water interaction was dominating the system as provided in Figure 28a. The Gibbs free energy was positive (Figure 27) indicating that this process was not favorable.

Increasing the Glucopon concentration to the CMC level resulted in a different system behavior. As shown in Figure 26b, the heat flow peaks were downward indicating an endothermic interaction between heptane and the solution with Glucopon at the CMC concentration. This resulted in a positive enthalpy change of 1.23 kJ/mol (Figure 27), which indicates the heptane molecules undergo hydrophobic interaction with the Glucopon solution as represented in Figure 28b. This is consistent with what has been reported in other studies where positive enthalpies were obtained by hydrocarbon surfactants for the solubilization of non-polar octane molecules [27]. The peaks in the heat flow have a higher endothermic magnitude at the initial injections and then decrease with subsequent injections. This indicates that the surfactants at the surface become depleted through the transport process. Entropy increased (Figure 27) which further supports the breaking of bonds at the surface as well as bonds between the water in the bulk to make room for the solubilized fuel. The Gibbs free energy was determined to be negative indicating that the CMC concentration of Glucopon was sufficient to make the interactions between fuel and surfactant solution favorable.

Further increasing the Glucopon concentration to 5X the CMC resulted endothermic interaction in similar behavior compared with the Glucopon at the CMC. As seem in Figure 26c, the heat flow is endothermic at a relatively constant value for all injections. The magnitude is similar to that measured for the Glucopon at the CMC during the first initial peaks. Similar to the Glucopon at the CMC both the enthalpy and entropy changes are positive indicating the transport processes described above were also occurring at this concentration (Figure 28b). However, since the peaks did not decrease this indicates there was no depletion of surfactant at the surface which may be due to surfactants in the bulk replenishing the surface. Compared with the Glucopon at the CMC, the Glucopon with 5x CMC had a higher affinity (Table 12) and more

negative Gibbs free energy, both of which indicate that increasing the concentration makes the fuel transport process more favorable.

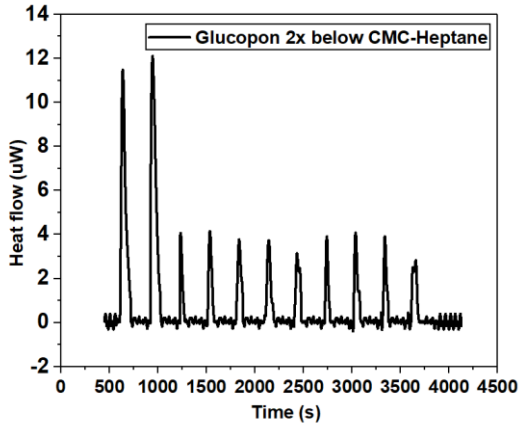

a)

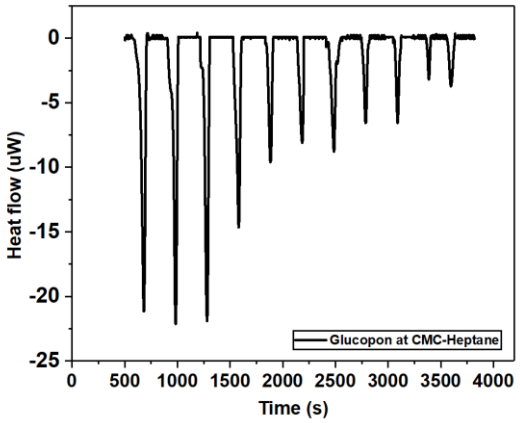

b)

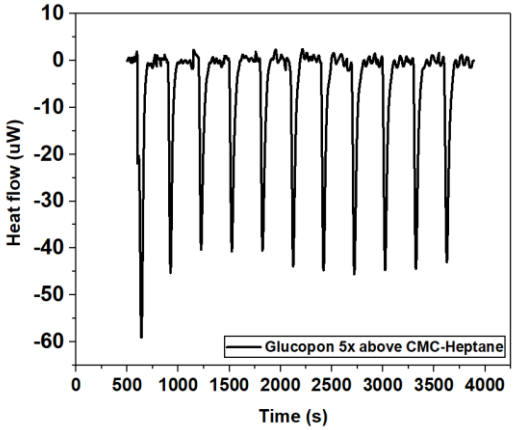

c)

Figure 26. ITC thermogram (Heat flow versus time) after titration of heptane into Glucopon solution a) 2x below CMC b) at CMC c) 5x above CMC.

Table 12. Affinity value for Water-heptane, Glucopon-heptane below, at, and above CMC concentrations.

Sample	**Affinity, Ka (M^{-1})**
Water- Heptane	1.15E+03
Glucopon 2x below CMC- Heptane	7.52E+03
Glucopon at CMC-Heptane	2.19E+04
Glucopon 5x above CMC- Heptane	5.02E+05

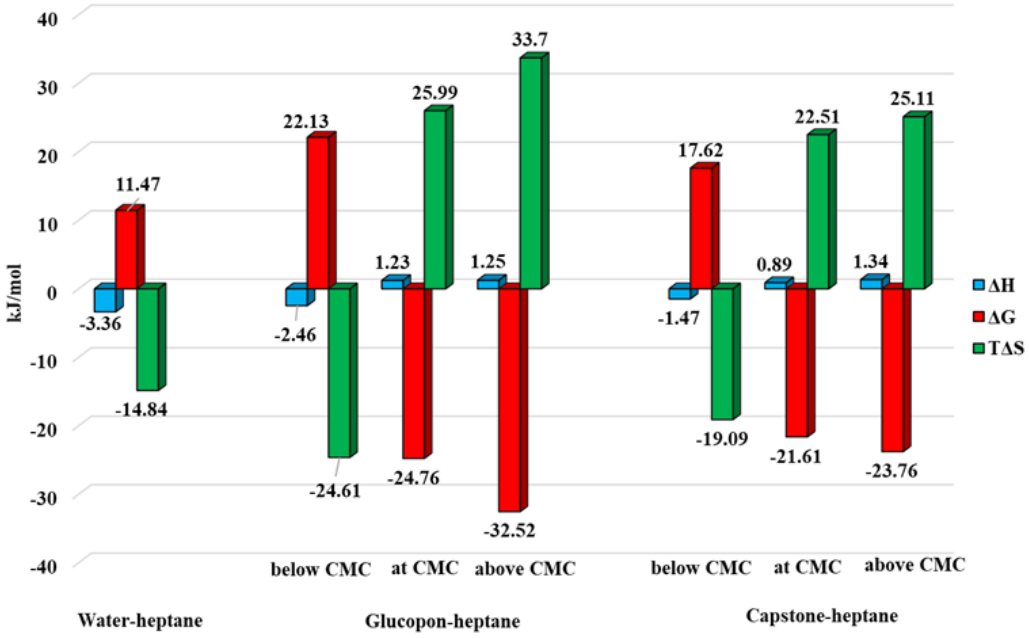

Figure 27. Thermodynamic parameters enthalpy, Gibbs free energy, and entropy for heptane.

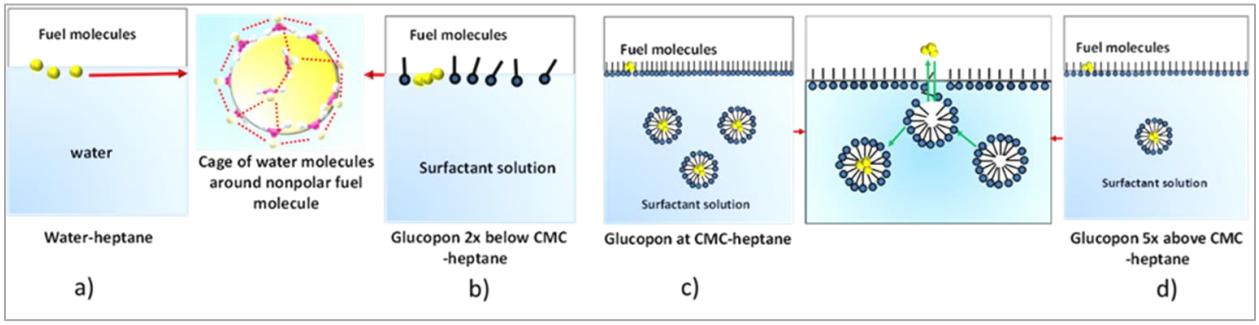

Figure 28. Fuel solubilization mechanism a) water-heptane b) Glucopon 2x below CMC c) Glucopon at CMC, and d) Glucopon 5x above CMC.

The heat flow due to injecting heptane to the solution at different concentrations of Capstone surfactant provided in Figure 29. As seen in Figure 29a Capstone below CMC concentration resulted in positive exothermic peaks similar to water and heptane interaction. The enthalpy was negative value of -1.47 kJ/mol and negative entropy -19.09 kJ/mol (Figure 27). Due to the low surfactant concentration, it was likely that heptane was interacting with water resulting in an increased ordering of hydrogen bonds in water near the interface in the presence of heptane molecules. In addition, Gibbs free energy was positive (Figure 27) indicating a non-favorable reaction like water-heptane.

Increasing the Capstone concentration at the CMC point (Figure 29b) resulted in endothermic interaction between heptane and Capstone molecules indicated by the downward heat flow peaks. The heptane molecules undergo hydrophobic interaction with the Capstone solution and the enthalpy was 0.89 kJ/mol (Figure 27). The heptane solubilization process in Capstone surfactant solution was similar to that observed for heptane and Glucopon. Due to the solubilization of non-polar heptane molecules positive enthalpies were obtained. Entropy increased (Figure 27) due to solubilization of heptane molecules as they exit the aqueous phase and were captured by the micelle. Gibbs free energy (Figure 27) became negative at CMC concentration making the interaction between fuel and surfactant solution spontaneous. The reduction in the magnitude of the heat flow peaks with subsequent injections indicated less interaction between Capstone and fuel molecules due to depletion of surfactants at the surface.

Further increasing the surfactant concentration to 5x CMC resulted in endothermic interaction indicated by the downward heat flow peaks, as seen in Figure 29c. The interaction between heptane and 5x CMC concentration of Capstone resulted in positive enthalpy of 1.34 kJ/mol (Figure 27) and entropy was large compared to at CMC concentration. For all injections, the heat flow was endothermic at a relatively constant value. The heat flow magnitude is similar to that measured for the Capstone at the CMC during the first initial peaks. Both the enthalpy and entropy changes were positive indicating the process is same as CMC level concentration; however, the values were higher compared to at CMC concentration indicating more fuel solubilization. Due to surfactants in the bulk replenishing the surface, the heat flow peaks did not

decrease with subsequent injections. Compared with the Capstone at the CMC, the Capstone with 5x CMC had a higher affinity (Table 13). The fuel transport process was more favorable at 5x CMC compared to at the CMC indicated by a more negative Gibbs free energy.

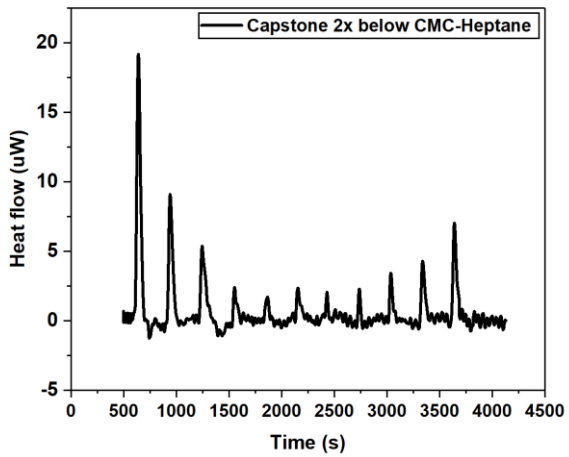

a)

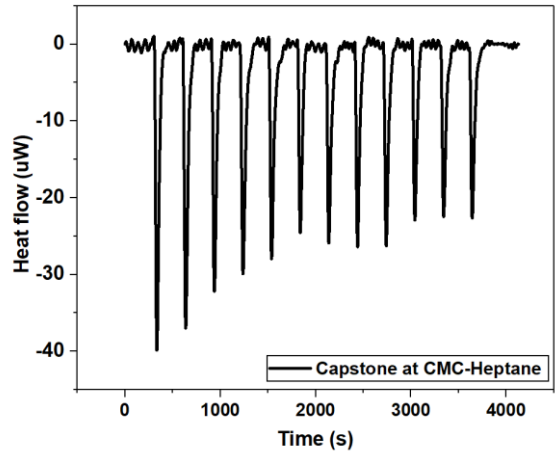

b)

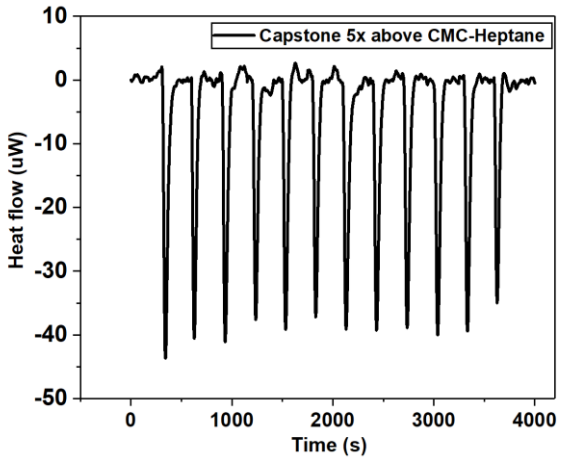

c)

Figure 29. ITC thermogram (Heat flow versus time) after titration of heptane into Capstone solution a) below CMC b) at CMC c) 5x CMC.

Table 13. Affinity value for Water-heptane, Capstone-heptane below, at, and above CMC concentrations.

Sample	**Affinity, Ka (M^{-1})**
Water-heptane	1.15E+03
Capstone 2x below CMC- Heptane	1.22E+03
Capstone at CMC- Heptane	6.13E+03
Capstone 5x above CMC- Heptane	1.46E+04

3.3.3.2. TMB

The heat flow due to injecting TMB to the water provided in Figure 30. The water-TMB interaction was endothermic (Figure 30a) indicated by the downward heat flow peaks. The interaction between TMB and water resulted in an enthalpy of 2.836 kJ/mol which was similar to the enthalpy of interaction of benzene (another aromatic fuel) with water (2.08 ± 0.04 kJ/mol) [31]. As indicated from Table (Table 10), TMB is more soluble in water compared with heptane. As a result, TMB was transported in the water and moved apart the water molecules breaking the van der Waals hydrogen bonds. This resulted in both an increase in enthalpy and increase in entropy due to more hydrogen bonding sites being available. A negative Gibbs free energy for TMB and water indicated this interaction was favorable [30].

The heat flow associated with injecting TMB to Capstone solution was provided in Figure 30b. the interaction between Capstone and TMB was exothermic indicated by the upward heat flow peaks and enthalpy was a negative value of -0.155 kJ/mol. Most likely, TMB preferred to stay close to the polar part or head of the surfactant inside the Capstone vesicles (Figure 35a) causing the exothermic peak. The heat flow associated with each peak was decreasing with continuing injections. TMB has higher water solubility and surfactants were occupied solubilizing them; therefore, over time the amount of surfactants replenishing the surface reduced. Surface started getting saturated with fuel and heat flow reduced. The capstone-TMB resulted in an entropy value that was smaller than that measured for water-TMB. Barry et al. [31] mentioned that more polar molecules solubilizing in structures results in a more ordered state by restricting molecular movement. Therefore, a decrease in entropy could be expected for Capstone-TMB due to more ordered state. Capstone-TMB affinity was close to the Water-TMB affinity (Table 14) indicating the binding

interaction between Capstone and TMB molecules was not much different from water and TMB molecules. The Gibbs free energy was more negative compared to water-TMB indicating presence of Capstone creates more favorable fuel transport.

The heat flow associated with adding TMB to Glucopon solution is provided in Figure 30c. The upward heat flow peaks indicated exothermic interaction between TMB and Glucopon. A negative enthalpy of -0.27 kJ/mol was obtained for Glucopon-TMB. Similar to Capstone, TMB molecules interact with head (polar part) of the Glucopon surfactant and stay inside the wormlike micelles (Figure 35b) of Glucopon causing exothermic interaction. The heat flow generated for Glucopon-TMB was larger compared to Capstone-TMB. This indicated more interaction and solubilization of TMB in the Glucopon solution compared to Capstone. The heat flow for each peak was decreasing with injection similar to the process that occurred with Capstone and TMB. A more negative Gibbs free energy was measured compared to Capstone-TMB indicating a more spontaneous reaction (Figure 31). The entropy value and affinity were increasing compared to water-TMB and Capstone-TMB (Table 14) indicating a more disordered state in Glucopon solution and more bonding of Glucopon surfactant with TMB molecules.

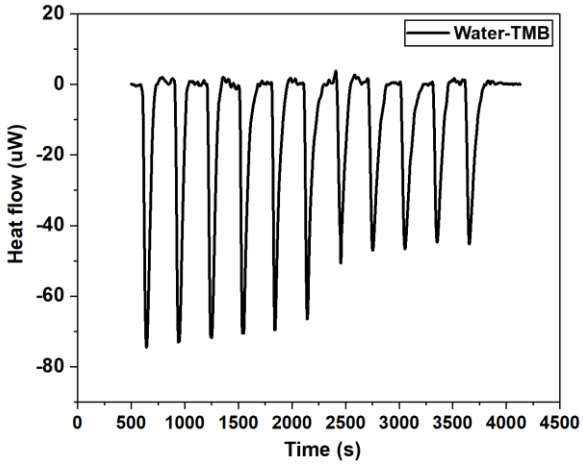

a)

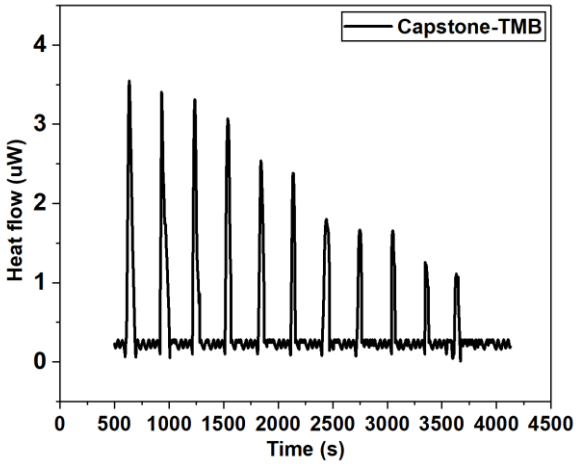

b)

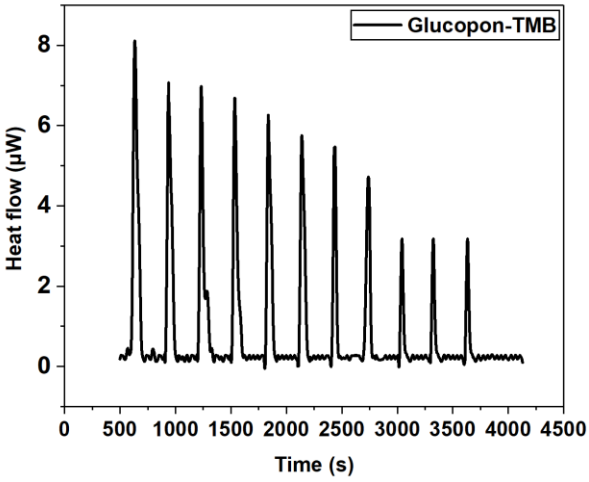

c)

Figure 30. ITC thermogram (Heat flow versus time) after titration of TMB into a) sample cell with water b) Capstone 5x CMC solution c) Glucopon 5x CMC solution.

Table 14. Affinity value for water-TMB, Capstone- TMB and Glucopon- TMB.

Sample	Affinity, Ka (M^{-1})
Water-TMB	1.00E+03
Capstone-TMB	2.00E+03
Glucopon-TMB	1.01E+04

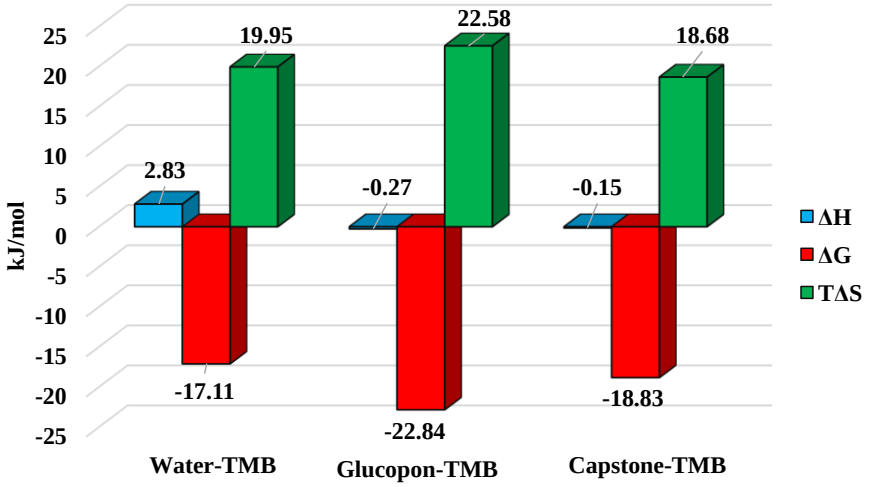

Figure 31. Thermodynamic parameters enthalpy, Gibbs free energy, and entropy for TMB.

3.3.3.3. 25%TMB-Heptane

The heat flow associated with injecting 25%TMB-heptane to the water provided in Figure 32. The ITC heat flow had attributes of both the TMB-water and heptane-water behaviors. Both exothermic and endothermic interactions were observed (Figure 32a) indicated by the upward and downward heat flow peaks for Water-25%TMB-Heptane. These resulted in a negative and positive enthalpy of -0.27 and 0.22 kJ/mol (Figure 33)**.** The endothermic peak was first indicating the TMB was transported into the bulk and separated water hydrogen bonds to make room. Following this was an exothermic peak due to the water and heptane bonding near the surface. The positive Gibbs free energy indicated that interaction between water and 25%TMB-heptane molecules was not spontaneous for both cases (Figure 33). The affinity values were on the order of magnitude of two (Figure 33) for both cases indicating low attractions between water and

surfactant molecules. Eventually, the positive Gibbs free energy and negative entropy indicated that the interaction between water and 25%TMB-heptane was not favorable.

The heat flow associated with adding 25%TMB-heptane to Glucopon solution is provided in Figure 32b. As indicated by the downward heat flow peaks the interaction between fuel mixture and Glucopon solution was endothermic and resulted in a positive enthalpy of 0.88 kJ/mol (Figure 33). 25%TMB-heptane transport process was similar as described for Glucopon and heptane indicated by the positive enthalpy and positive entropy. The affinity value was higher (Table 15) indicating more attractions between fuel and Glucopon molecules. A negative Gibbs free energy (Figure 34) indicated that the reaction was favorable, unlike water-25%TMB-heptane.

The heat flow related to 25%TMB-heptane in Capstone solution is provided in Figure 32c. The interaction between fuel mixture and Capstone was endothermic indicated by the downward heat flow peaks. The transport process of 25%TMB-heptane in Capstone solution was similar to what observed for Capstone and heptane indicated by the positive enthalpy of 0.32 kJ/mol and positive entropy (Figure 33). The entropy (Figure 33) value was smaller compared to Glucopon-25%TMB-heptane, most likely TMB molecular movement was limited in fuel mixture causing more ordering. Moreover, the affinity value was (Table 15) low between fuel mixture and Capstone solution. However, a negative Gibbs free energy (Figure 33) indicated that the reaction was spontaneous between the fuel mixture and Capstone solution.

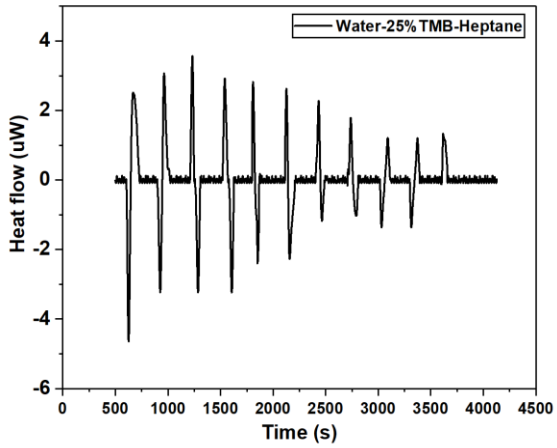

a)

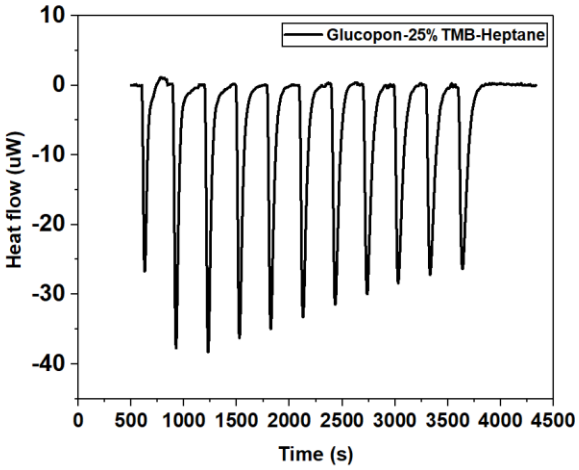

b)

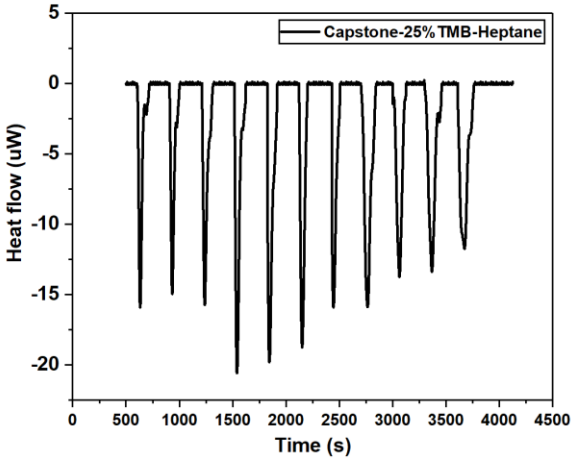

c)

Figure 32. ITC thermogram (Heat flow versus time) after titration of 25% TMB-heptane into a) sample cell with water b) Glucopon 5x CMC solution c) Capstone 5x CMC solution.

Table 15. Affinity value for water-25%TMB-heptane, Capstone-25%TMB-heptane and Glucopon-25%TMB-heptane.

Sample	Affinity, Ka (M^{-1})
Water-25%TMB-heptane	1.00E+02
	1.52E+02
Glucopon-25%TMB-heptane	1.00E+07
Capstone-25%TMB-heptane	4.98E+03

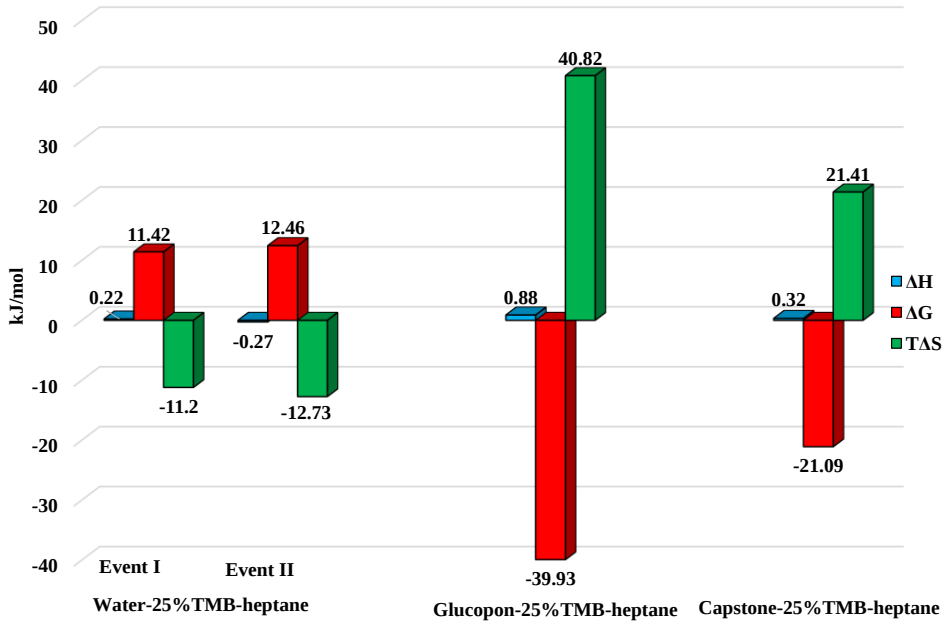

Figure 33. Thermodynamic parameters enthalpy, Gibbs free energy, and entropy for 25% TMB-heptane.

3.4. Discussion

Through this work, the interaction between surfactants (Capstone, and Glucopon) and fuels (heptane, TMB, and 25%TMB-heptane) has been observed. This study reveals that fuel transport occurs at and above CMC concentrations when the interactions between fuel and surfactant solutions are thermodynamically more favored. Moreover, fuel transport enhances for more polar fuel due to thermodynamically more favored interaction between fuel and surfactant solution.

Micelles work as medium for fuel transport from the fuel-surfactant interface to the bulk of the solution. As seen in Figure 34, at CMC concentration fuel and surfactant interactions are spontaneous indicated by

the negative Gibbs free energy for both Glucopon and Capstone. The surfactants and heptane molecules undergo hydrophobic interactions (Figure *27*) indicating the breaking of bonds at the interface allowing the solubilization of fuel by the surfactants and transported into the bulk with micelles. As a result, we see an increment in micelle size due to heptane exposure (Figure 34). At a concentration 5x higher than CMC (Figure 34), more negative Gibbs free energy indicating more fuel solubilization; since with increasing surfactant concentration, more surfactant micelles are available to transport fuel molecules into the bulk resulting in a larger increment in the micelle size. In addition, heptane transport concentration is measurable in this instance. Below CMC concentration due to not having any micelles no fuel transport occurred. The interaction between heptane fuel molecules and surfactants was not spontaneous indicated by positive Gibbs free energy (Figure 34). This is further evident by the microstructural observation in the bulk where the size of the agglomerated surfactant structures in the bulk due to heptane exposure is similar to no exposure condition indicating no fuel transport (Figure 24 e, f). In addition, no heptane concentration was detected in the bulk of the solution (Figure 34).

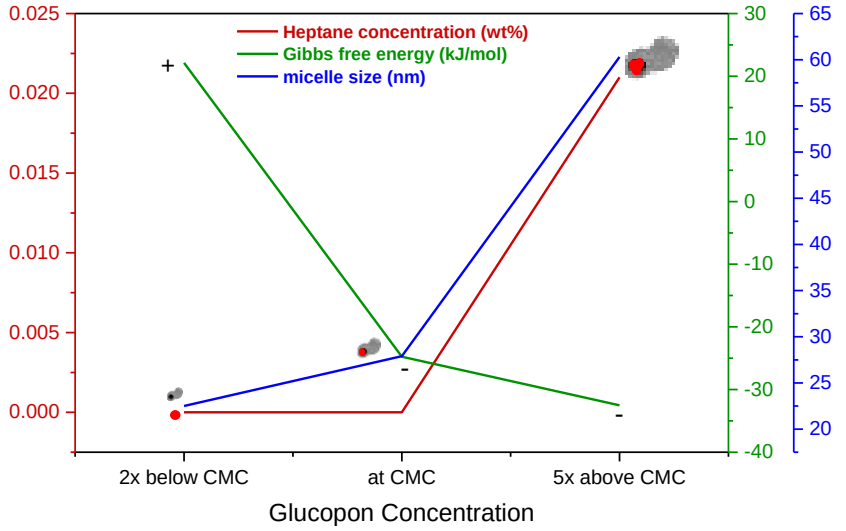

a)

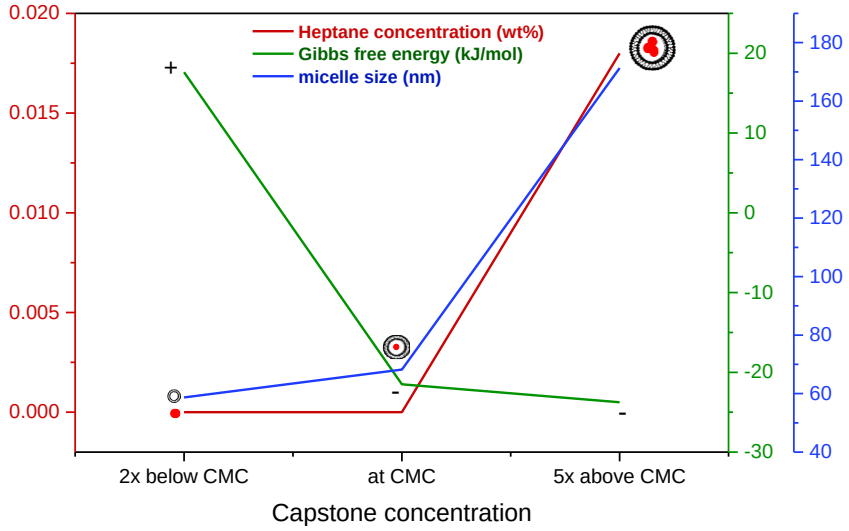

b)

Figure 34. Gibbs free energy versus fuel concentration and micelle size with heptane exposure 2x below, at and 5x above CMC concentration for a) Glucopon b) Capstone.

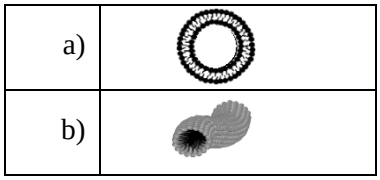

Figure 35. a) Single lamellar vesicle formed by Capstone b) Wormlike micelles formed by Glucopon [32].

Thermodynamically more favored interaction between fuel and surfactant enhances fuel transport. Comparing the fuels, the exothermic interaction between TMB and Capstone or Glucopon solution (Figure 31) is thermodynamically more favored compared to the endothermic interaction with heptane and 25%TMB-heptane (Figure 27, Figure 33). Non polar fuel heptane has poor solubility in water (Table 10), and requires a micelle-mediated pathway to get solubilized (Figure 20a). Favorable entropy leads to weaker bond formation between heptane and surfactant solution. Therefore, the solubility of heptane molecules is enhanced by Glucopon and Capstone surfactant at 5x CMC concentration (Figure 22). However, the solubility of polar fuel TMB is enhanced more by Glucopon and Capstone surfactant compared to heptane (Figure 23) indicating more fuel transport. Due to more water solubility (Table 10), TMB directly goes to the bulk and stronger bond forms with surfactants through favorable enthalpy (Figure 31) and enhances fuel transport. Due to presence of TMB, the transport of 25%TMB-heptane is enhanced in surfactant solution compared to heptane indicated by the higher positive entropy and more negative Gibbs free energy (Figure 27, Figure 33).

For the surfactants, fuel transport is higher for Glucopon compared to Capstone. The interaction between Glucopon and fuels (Glucopon-TMB, Glucopon-heptane) has a higher positive entropy indicating higher solubilization compared to Capstone (Capstone-TMB, Capstone-heptane) (Figure 27, Figure 31). TMB molecules are less restricted by the worm-like micelles (Figure 35b) [32] formed by Glucopon compared to vesicles formed by Capstone (Figure 35a) [32] as indicated by the higher entropy changes for Glucopon-TMB compared to Capstone-TMB (Figure 31). On the other hand, a smaller value of entropy changes for Capstone-heptane indicates that the complex shape of Capstone bilayer vesicles [32] has low diffusivity for heptane. Therefore, the fuel transport concentration is lower for Capstone. Other than the shape, Capstone and Glucopon have different head types, which might be another factor for their performance difference during fuel transport. Therefore, further studies will be required to confirm which factor has the bigger impact against fuel transport, head types or micelle shape or vesicles.

3.5. Conclusions

This study on fuel and single surfactants interaction provides understanding of the role of surfactant micelle during fuel solubilization and the implications of fuel types on fuel transport.

Below CMC concentration, the interaction between fuel and surfactant solutions is not thermodynamically favored. Since there is no micelle present in the solution resulting in no fuel transport. Fuel transport occurs at and above CMC concentration of Capstone and Glucopon surfactants when the interactions are thermodynamically favored resulting in a change in micelle size. Fuel and surfactant interactions are thermodynamically more favored at 5x CMC compared to at CMC concentration indicating with increasing surfactant concentration more micelles are available enhancing fuel transport. Micelles grow more in size due to fuel transport. Fuel interaction with surfactant solutions is thermodynamically more favorable for polar fuel TMB compared to 25%TMB-heptane followed by heptane indicating more TMB transport. Compared to Capstone, Glucopon interaction with fuels is thermodynamically more favorable and solubilizes more fuel molecules indicating more fuel transport.

References

[1] C. Baduel, J. F. Mueller, A. Rotander, J. Corfield, and M. J. Gomez-Ramos, "Discovery of novel per- and polyfluoroalkyl substances (PFASs) at a fire fighting training ground and preliminary investigation of their fate and mobility," *Chemosphere,* vol. 185, pp. 1030-1038, Oct 2017, doi: 10.1016/j.chemosphere.2017.06.096.

[2] B. J. Place and J. A. Field, "Identification of novel fluorochemicals in aqueous film-forming foams used by the US military," *Environ Sci Technol,* vol. 46, no. 13, pp. 7120-7, Jul 3 2012, doi: 10.1021/es301465n.

[3] W. J. Backe, T. C. Day, and J. A. Field, "Zwitterionic, cationic, and anionic fluorinated chemicals in aqueous film forming foam formulations and groundwater from U.S. military bases by nonaqueous large-volume injection HPLC-MS/MS," *Environ Sci Technol,* vol. 47, no. 10, pp. 5226-34, May 21 2013, doi: 10.1021/es3034999.

[4] R. Ananth, A. W. Snow, K. M. Hinnant, S. L. Giles, and J. P. Farley, "Synergisms between siloxane-polyoxyethylene and alkyl polyglycoside surfactants in foam stability and pool fire extinction," *Colloids and Surfaces A: Physicochemical and Engineering Aspects,* vol. 579, p. 123686, 2019.

[5] K. Hinnant, "Characterizing Trends Between Surfactant Structure, Fuel Transport through a Foam Layer, and Foam Fire Extinction Performance for Firefighting Foams Containing Novel Environmentally-Friendly Surfactants," The George Washington University, 2021.

[6] K. M. Hinnant, S. L. Giles, and R. Ananth, "Measuring fuel transport through fluorocarbon and fluorine-free firefighting foams," *Fire Safety Journal,* vol. 91, pp. 653-661, 2017, doi: 10.1016/j.firesaf.2017.03.077.

[7] X. Cui, S. Mao, M. Liu, H. Yuan, and Y. Du, "Mechanism of surfactant micelle formation," *Langmuir,* vol. 24, no. 19, pp. 10771-10775, 2008.

[8] D. A. Edwards, R. G. Luthy, and Z. Liu, "Solubilization of polycyclic aromatic hydrocarbons in micellar nonionic surfactant solutions," *Environmental Science & Technology,* vol. 25, no. 1, pp. 127-133, 1991.

[9] R. Shah and P. Neogi, "Interfacial resistance in solubilization kinetics," *Journal of colloid and interface science,* vol. 253, no. 2, pp. 443-454, 2002.

[10] A. J. Ward, "The Kinetics of Oil Solubilisation in Aqueous Surfactant Solutions," in *Proceedings of the Royal Irish Academy. Section B: Biological, Geological, and Chemical Science*, 1989: JSTOR, pp. 375-382.

[11] P. Todorov, P. Kralchevsky, N. Denkov, G. Broze, and A. Mehreteab, "Kinetics of solubilization of n-decane and benzene by micellar solutions of sodium dodecyl sulfate," *Journal of colloid and interface science,* vol. 245, no. 2, pp. 371-382, 2002.

[12] B. J. Carroll, "The kinetics of solubilization of nonpolar oils by nonionic surfactant solutions," *Journal of Colloid and Interface Science,* vol. 79, no. 1, pp. 126-135, 1981.

[13] B. Carroll, B. O'ROURKE, and A. Ward, "The kinetics of solubilization of single component non-polar oils by a non-ionic surfactant," *Journal of Pharmacy and Pharmacology,* vol. 34, no. 5, pp. 287-292, 1982.

[14] S. Ariyaprakai and S. R. Dungan, "Contribution of molecular pathways in the micellar solubilization of monodisperse emulsion droplets," *Langmuir,* vol. 24, no. 7, pp. 3061-3069, 2008.

[15] Y.-J. An and S.-W. Jeong, "Interactions of perfluorinated surfactant with polycyclic aromatic hydrocarbons: critical micelle concentration and solubility enhancement measurements," *Journal of colloid and interface science,* vol. 242, no. 2, pp. 419-424, 2001.

[16] A. C. Donegan and A. J. Ward, "Solubilization kinetics of n-alkanes by a non-ionic surfactant," *Journal of pharmacy and pharmacology,* vol. 39, no. 1, pp. 45-47, 1987.

[17] K. Bouchemal, "New challenges for pharmaceutical formulations and drug delivery systems characterization using isothermal titration calorimetry," *Drug discovery today,* vol. 13, no. 21-22, pp. 960-972, 2008.

[18] R. J. Falconer, B. Schuur, and A. K. Mittermaier, "Applications of isothermal titration calorimetry in pure and applied research from 2016 to 2020," *Journal of Molecular Recognition*, vol. 34, no. 10, p. e2901, 2021.
[19] W. Loh, C. Brinatti, and K. C. Tam, "Use of isothermal titration calorimetry to study surfactant aggregation in colloidal systems," *Biochimica et Biophysica Acta (BBA)-General Subjects*, vol. 1860, no. 5, pp. 999-1016, 2016.
[20] J. W. Chang, A. Armaou, and R. M. Rioux, "Continuous Injection Isothermal Titration Calorimetry for In Situ Evaluation of Thermodynamic Binding Properties of Ligand–Receptor Binding Models," *The Journal of Physical Chemistry B*, vol. 125, no. 29, pp. 8075-8087, 2021.
[21] A. W. Snow, S. Giles, K. Hinnant, J. Farley, and R. Ananth, "Fuel for Firefighting Foam Evaluations: Gasoline vs Heptane," NAVAL RESEARCH LAB WASHINGTON DC WASHINGTON United States, 2019.
[22] "National Center for Biotechnology Information (2024). PubChem Compound Summary for CID 8900, Heptane. Retrieved February 27, 2024 from." [Online]. Available: https://pubchem.ncbi.nlm.nih.gov/compound/Heptane.
[23] "National Center for Biotechnology Information (2024). PubChem Compound Summary for CID 7247, 1,2,4-Trimethylbenzene. Retrieved February 27, 2024 from." [Online]. Available: https://pubchem.ncbi.nlm.nih.gov/compound/1_2_4-Trimethylbenzene.
[24] K. M. Hinnant, S. L. Giles, A. W. Snow, J. P. Farley, J. W. Fleming, and R. Ananth, "An analytically defined fire-suppressing foam formulation for evaluation of fluorosurfactant replacement," *Journal of surfactants and detergents*, vol. 21, no. 5, pp. 711-722, 2018.
[25] A. W. Snow, S. Giles, K. M. Hinnant, J. P. Farley, and R. Ananth, "Quantification of Fluorine Content in AFFF Concentrates," NAVAL RESEARCH LAB WASHINGTON DC WASHINGTON United States, 2017.
[26] M. W. Sulek and T. Wasilewski, "Influence of critical micelle concentration (CMC) on tribological properties of aqueous solutions of alkyl polyglucosides," *Tribology transactions*, vol. 52, no. 1, pp. 12-20, 2008.
[27] H. Zhang, B. Zeeb, H. Salminen, and J. Weiss, "Isothermal titration calorimetric analysis on solubilization of an octane oil-in-water emulsion in surfactant micelles and surfactant–anionic polymer complexes," *Journal of colloid and interface science*, vol. 438, pp. 7-13, 2015.
[28] A. I. Rodriguez-Perez, C. Rodriguez-Tenreiro, C. Alvarez-Lorenzo, P. Taboada, A. Concheiro, and J. J. Torres-Labandeira, "Sertaconazole/hydroxypropyl-β-cyclodextrin complexation: Isothermal titration calorimetry and solubility approaches," *Journal of pharmaceutical sciences*, vol. 95, no. 8, pp. 1751-1762, 2006.
[29] D. B. Alger, "Erroneous explanations for the limited water solubility of organic liquids," *Journal of Chemical Education*, vol. 71, no. 4, p. 281, 1994.
[30] J. Lakra *et al.*, "Mixed micellization of gemini and cationic surfactants: physicochemical properties and solubilization of polycyclic aromatic hydrocarbons," *Colloids and Surfaces A: Physicochemical and Engineering Aspects*, vol. 451, pp. 56-65, 2014.
[31] B. Barry and D. E. Eini, "Solubilization of hydrocortisone, dexamethasone, testosterone and progesterone by long-chain polyoxyethylene surfactants," *Journal of Pharmacy and Pharmacology*, vol. 28, no. 3, pp. 210-218, 1976.
[32] R. I. Islam, "Understanding the impact of fuel on surfactant microstructure of firefighting foam," Unpublished Work, 2023.

Chapter 4

Understanding the effect of convection on fuel transport of firefighting foam

Rezawana Islam[1], and Brian Y. Lattimer[2]

[1]Materials Science and Engineering, Virginia Tech

[2]Mechanical Engineering, Virginia Tech

Abstract

Aqueous Film-Forming Foam (AFFF) is being phased out or restricted in many places due to concerns about its environmental and health impacts. AFFF is a type of firefighting foam that contains a fluorinated surfactant which is highly persistent in the environment. To develop a safer alternative to current firefighting foam, it is important to understand the factors influencing the firefighting performance of surfactants. Fuel transport through foam has been considered as a dominant mechanism for foam collapse. Therefore, a two-phase system of fuels (TMB, heptane and 25%TMB-heptane) and surfactant solutions were studied for two different types of surfactants (Capstone and Glucopon) that have applications in firefighting foam. UV-Vis spectroscopy was used to measure the fuel transport in surfactant solution. Ignition test was conducted to observe the ignition time of fuel molecules through surfactant foam solution. This work shows that convection enhances fuel transport. Moreover, fuel transport occurring through surfactant solutions under kinetically more favored conditions results in shorter ignition time.

4.1. Introduction

Aqueous Film Forming Foam (AFFF) is the most efficient firefighting foam available to suppress flammable liquid fires, consists of fluorochemical surfactant, hydrocarbon surfactant, additives, and water [1]. AFFF is commonly used in fire extinguishing that includes fuels like gasoline, diesel, and jet fuels and has applications in fire departments for fire extinguishing, in military, transportation, and fuel storage [2-4]. Currently, AFFF has been phased out due to environmental concerns related to fluorochemical surfactants used in its formulation which are persistent in the environment and have been associated with

potential health risks. Therefore, the foam industry introduced fluorine-free firefighting foams that contain non-fluorinated surfactants in the solution [5]. However, existing fluorine-free alternatives to AFFF are unable to perform at the same level as AFFF [6]. Therefore, it is imperative to understand the factors affecting the firefighting performance of AFFF. Fuel transport through the foam surfactant solution has been identified as being a dominant reason for foam collapse [7]. The fuel transport steps through surfactant foam solution are thought of as four different steps (i) fuel solubility into the surfactant foam solution, (ii) vaporization through the gas bubble, (iii) diffusion of fuel in the lamellae, and (iv) re-dissolving in the solution around the bubble. During this process, surfactant foam solution keeps draining down at the foam-fuel interface [8]. However, the parameters controlling fuel transport phenomena are not fully understood.

When firefighting foam is exposed to liquid fuel, surfactant micelles solubilize hydrophobic compounds, and thus enhance the water solubility of fuel molecules [9]. There are two parallel pathways available for the solubilization of fuel molecules into the aqueous micellar phase: it can transfer as an individual molecule through the water (pathway 1), or it can be carried by micelles from the interface to the bulk aqueous solution (pathway 2) [9-14]. The fuel molecule transfer through the aqueous solution occurs via a convective or diffusive processes [9]. Alejandro et al [15] showed in their study that the onset of convection causes an increase in the rate of oil solubilization with nonionic surfactants. In addition, they showed that resistance to mass transfer diminishes as surfactant concentration is increased due to spontaneously generated natural convection that arises near the oil-water interfaces owing to the density change produced by solubilized oil in micelles near the surface. Benzene exhibits significant solubility in water but is less dense than the water, convective effect might happen as benzene is solubilized due to buoyancy and the density of the aqueous solution near the benzene droplet diminishes [15]. It has been proposed that the diffusional transport is enhanced by convection. This type of natural convection enhances fuel solubilization.

During a firefighting event, foam is spread over the fuel pool fire. The foam solution is continuously draining down due to gravity toward the fuel surface as represented in Figure 36. The motion of the drained

surfactant solution at the fuel surface creates a mixing, this induces convection at the interface. This type of convection might affect or enhance fuel transport. There are two types of convections can be expected during fuel transport; firstly, natural convection, occurs during fuel solubilization by surfactant/micelle due to density difference of fuel and aqueous solution; secondly, forced convection that occurs at the foam-fuel interface due to the motion of the drained solution. Therefore, forced convection might have a significant role to play during fuel transport. Previous studies on firefighting foam mentioned surfactants solubilizing fuel molecules and enhancing fuel solubility [7]. Then, the liquid drained out of the foam forming an aqueous film on the surface of liquid fuel relying on the very low surface tension of the liquid containing fluorocarbon surfactant [16]. However, none of the previous works have discussed convection occurring at the foam-fuel surface that is affecting fuel transport. In addition, time taken for transport of fuel molecules in surfactant solution has not been evaluated for firefighting foam. This provides insights into how quickly or slowly fuel transport occurs in surfactant solution; hence delivers kinetic information of fuel transport.

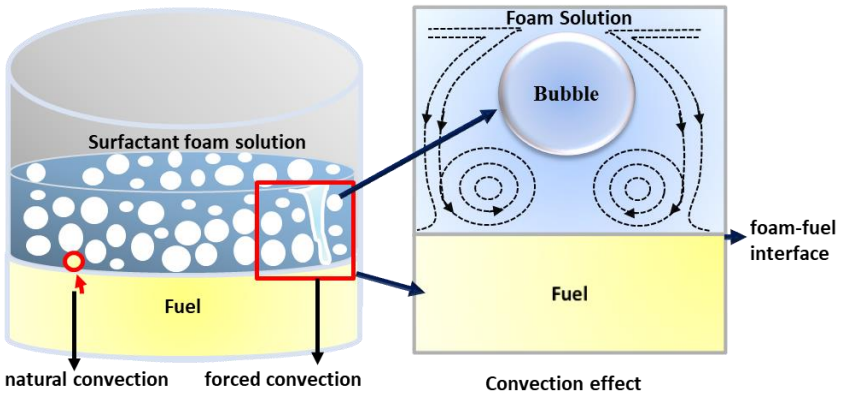

Figure 36. Illustration of convection effect at the foam-fuel interface.

In this work, we have assessed the effect of convection on fuel transport. A two-phase system of surfactant solution (bottom phase) and fuel (top phase) with and without stirring in the bottom phase was studied. To create the experimental conditions of convection at the foam-fuel interface, stirring was done in the bottom phase. Experiments without stirring were referred as natural convection and with stirring were referred as forced convection. In addition, fuel concentration has been quantified at different times and distances away from the interface. This allows us to understand the effect of convection on fuel transport. In addition, ignition test outcomes are included to understand the effect of fuel transport kinetics on ignition time.

4.2. Experimental Details

A series of experiments were conducted exposing aqueous surfactant solutions to different fuels. UV-vis spectroscopy has been performed to quantify the spatial and temporal fuel transport into surfactant solution.

4.2.1. Materials

To study the convection effect, three types of fuels (heptane, TMB, and 25%TMB-heptane) and two types of surfactants (Capstone, Glucopon) have been used. Capstone and Glucopon surfactants have been used in Reference AFFF [1]. Heptane has commonly being used as a fuel for fire suppression tests [17]. At room temperature ignition of TMB was challenging due to its high flash point. Therefore, a mixture of 25% TMB + heptane was used as a simulant for gasoline to evaluate ignition time. Since, Gasoline is the most commonly used fuel for evaluating firefighting foam performance using the MilSpec standard method for firefighting foams [17].

The physical properties for surfactants given in Table 16. Measurements were done at 5 times higher than the CMC concentrations for surfactants which is similar to the surfactant concentration in Reference AFFF [18]. CMC presented in Table 16 were based on surfactant concentration. Table 17 represents the physical properties of fuels. The physical properties are taken from the Safety data sheet [19, 20].

Table 16. Surfactant Properties [21, 22].

Name	Chemical Structure	Molecular Weight (g/mol)	CMC (wt.%)	Tail Type	Head Type
Capstone 1157	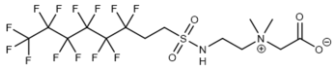	570	0.011	Fluorocarbon	Zwitterionic
Glucopon 600 CS UP	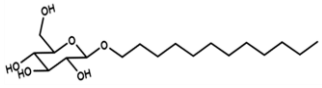	386	0.012	Hydrocarbon	Nonionic

Table 17. Physical properties of fuel.

Fuel	Chemical formula	Structure	Water Solubility (mg/L)
1,2,4 Tri-methylbenzene (TMB)	C_9H_{12}	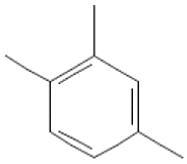	57
Heptane	C_7H_{16}	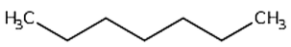	3.4

4.2.2. Methods

UV Vis spectroscopy

The transport of fuel into the surfactant solution was evaluated through a diffusion experiment. A layer of liquid fuel over a layer of surfactant solution was poured in a 20 mL glass vial to prepare a two-phase system. After pouring the surfactant solution (~15 ml) in the glass vial, a syringe was inserted. Then a fuel layer was added at the top of the surfactant solution to avoid any contamination on the needle. The top of the vial was covered to avoid any evaporation. All the measurements were done at 5x CMC concentrations of surfactants. To observe the effect of time and distance on fuel solubilization, wait times of 1 min, 15 min, 30 min, and 60 min were used before sample extraction for analysis. Samples were extracted from 3 mm, 7 mm, 10 mm, and 15 mm away from the interface (Figure 37). All these experiments were done with and without stirring. Stirring was introduced at the bottom phase of the surfactant solution at 60 rpm without disturpting the interface.

UV-Vis measurements were done to quantify the fuel concentration in the bulk using a Hitachi U4100 UV-VIS-NIR spectroscopy. To prepare the standard curve the absorbance spectra for known concentrations of fuel in surfactant solution were measured (as mentioned in section 2.2.2). For analysis, sample was extracted from a two-layer interaction sample of surfactant solution (bottom phase) as shown in Figure 37, and transferred into the cuvette The absorbance attained was placed into the standard curve (absorbance versus Fuel concentrations) to quantify the concentration of fuel in surfactant solution. The absorption peak

from 230 – 300 nm was used for all the analysis. All the measurements were repeated three times to check the reproducibility.

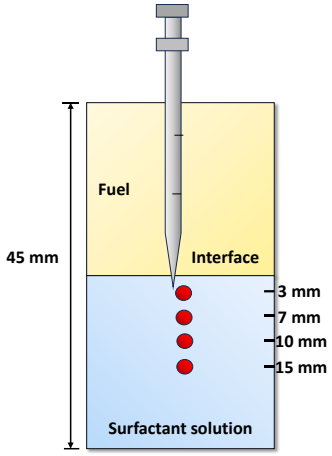

Figure 37. Experimental setup.

Ignition test

To observe the ignition time of fuel vapors transported through a layer of foam, an ignition test was conducted. The ignition test setup is illustrated in Figure 38. For ignition tests, foam was generated using a Dynamic Foam Analyzer (DFA) (as mentioned in section 2.2.2). All the foams were generated at 5 times the CMC based on surfactant concentration for ignition tests. A 15 mm thick layer of foam was poured into a 75 mm diameter, 25 mm deep glass dish. Using a syringe, 25 mL of fuel was injected across the foam. The foam height was maintained close to the top of the dish. Finally, a pilot flame igniter was positioned at the top of the foam and located at the center of the pan. Using a high-resolution video camera, the changes in foam during the experiments were captured and ignition time for the fuel vapor above the foam was recorded. Ignition time measurements were repeated three times to confirm the repeatability.

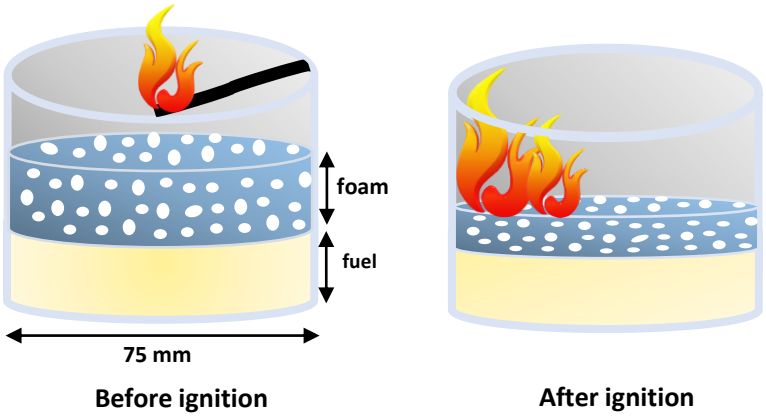

Figure 38. Ignition test set up.

4.3. Results

4.3.1. Fuel Transport

To observe the effect of surfactant concentration, and effect of convection on fuel transport UV-Vis Spectroscopy has been used. Fuel concentration measurements have been performed at different surfactant concentrations below, at, and above CMC with and without stirring. The fuel concentration and transport time have been measured at four different time intervals and four different distances away from the interface for different fuels.

4.3.1.1. Heptane

Glucopon

Figure 39 showed heptane concentrations at different times and distances in Glucopon solution. At 1 min heptane concentration was not detected for natural and forced convection samples, indicating no fuel solubilization occurred. For natural convection, heptane concentration was detected only close to the interface at 3 mm away from the interface. While for forced convection, at 15 minutes heptane concentration was observed at 3 mm, 7 mm and 10 mm away from the interface indicating higher fuel level throughout the distances. At 60 minutes, a larger gradient over the distances compared with Glucopon-TMB. In addition, no heptane concentration was measured at 15 mm away from the interface in any case. Heptane concentrations at different times and distances revealed that convection escalated the heptane solubilization in the bulk of the Glucopon solution.

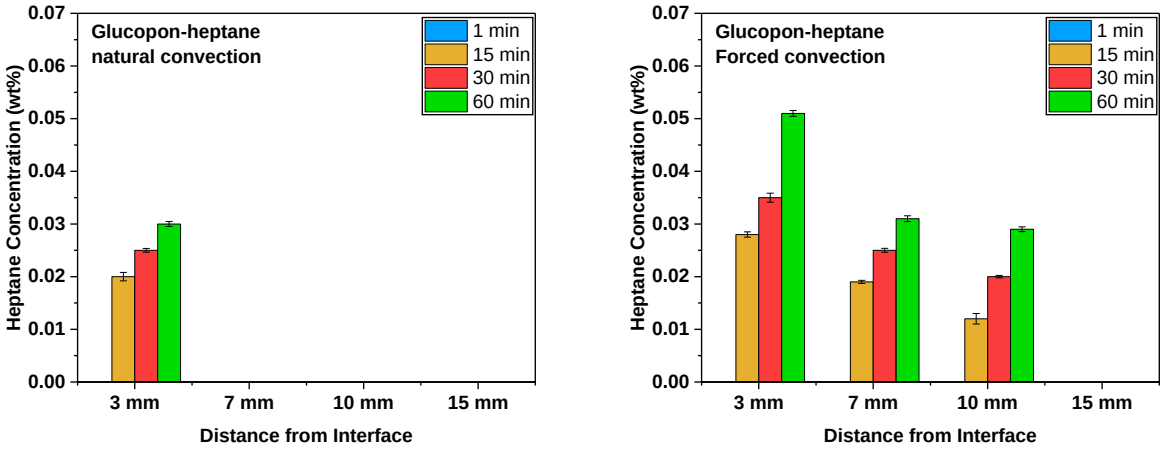

a) b)

Figure 39. Heptane concentration measurement in Glucopon solution at four different distances away from the interface and times for a) natural and b) forced convection.

Capstone

Fuel concentration measurements at different times and distances in Capstone solution (Figure 40) showed a similar trend to Glucopon. At 1 min no heptane concentration was detected for natural and forced convection samples, indicating no fuel solubilization occurred. For natural convection, heptane concentration was detected only close to the interface distance which is 3 mm. For forced convection, at 15 minutes heptane concentration was quantified at 3 mm and 7 mm away from the interface indicating more fuel transport throughout the distances. After 60 minutes, a more heptane concentration over the distances compared with 30 minutes. At 15 mm away from the interface no heptane concentration was observed for any distances and times. Heptane concentration measurement at different times and distances showed that convection increased the heptane solubilization in the bulk of the Capstone solution.

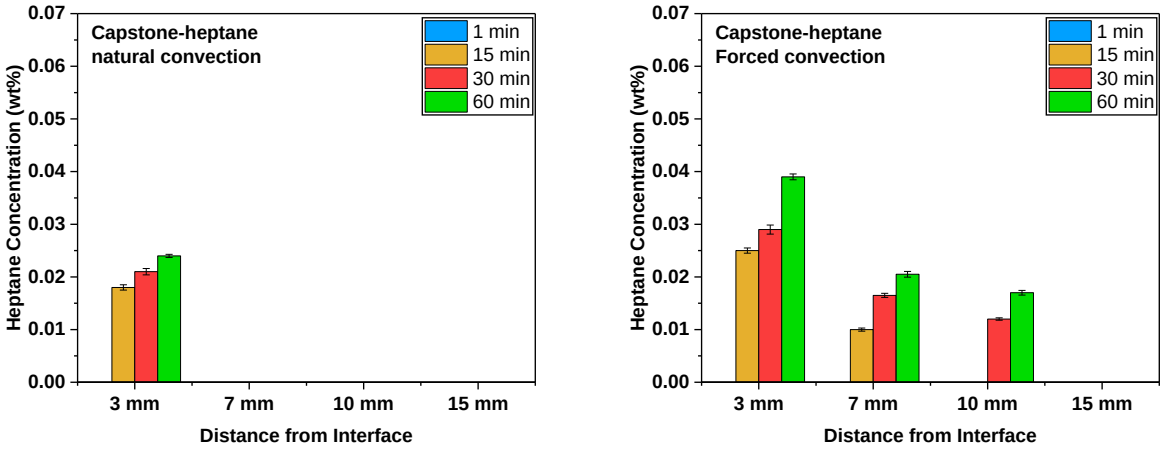

a) b)

Figure 40. Heptane concentration measurement in Capstone solution at four different distances away from the interface and times for a) natural and b) forced convection.

4.3.1.2. TMB

Glucopon

Figure 41 represented data for TMB concentrations in Glucopon surfactant solutions at different times and locations from the interface. For natural convection, the 1 min sample for 3 mm to 15 mm distances away from the interface TMB concentration decreased from 0.04 to 0.01 wt.%. It appeared that for natural convection, the fuel concentration near the interface (3 mm away) reaches a solubility limit and then did not increase significantly with time from 1 minute to 60 minutes while the fuel concentrations further away from the interface increased but never quite reached the concentration at 3 mm. Due to forced convection, at 60 minutes TMB concentration was significantly higher compared to 1, 15, and 30 minutes for all the distances. For TMB concentration, less of a gradient was observed across the distances away from the interface 3 mm to 15 mm meaning that TMB can transport fast across the distances. However, due to forced convection TMB concentration was increasing with time for each distance unlike natural convection. Therefore, forced convection increased TMB solubilization concentration.

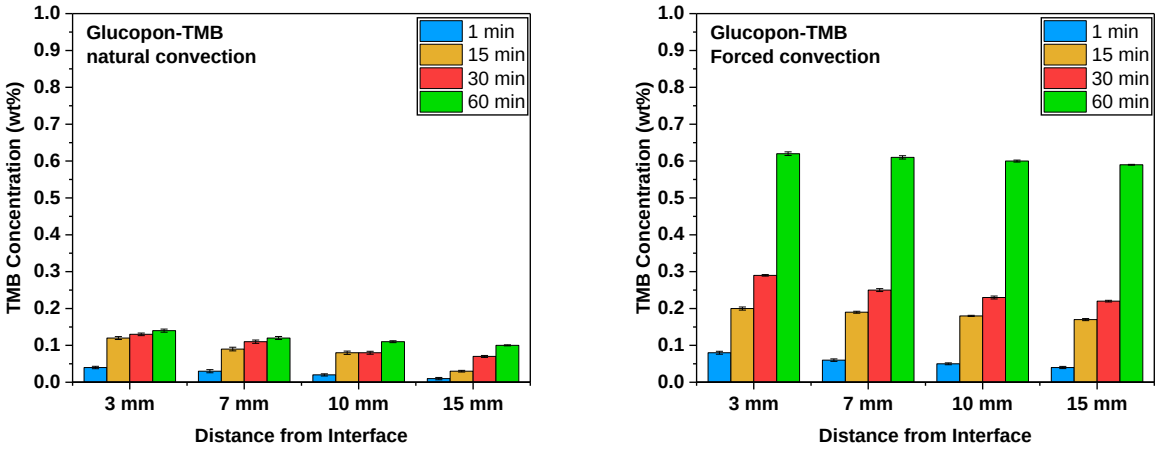

a) b)

Figure 41. TMB concentration measurement in Glucopon solution for a) natural and b) forced convection at four different distances away from the interface and times.

Capstone

Figure 42 contains data for TMB concentrations in Capstone surfactant solutions at different times and locations from the interface. For natural convection, the 1 min sample for 3 mm to 10 mm distances away from the interface TMB concentration decreased from 0.025 to 0.009 wt.%. For natural convection, the fuel concentration near the interface (3 mm) did not change significantly with time from 15 minutes to 60 minutes while the fuel concentrations further away from the interface (10 mm) somewhat increased. Due to forced convection, at 60 minutes TMB concentration was significantly higher compared to 1, 15, and 30 minutes for all the distances. For 3 mm and 10 mm distances TMB concentration was increased significantly with time from 1 to 60 minutes. Therefore, forced convection increased TMB solubilization concentration.

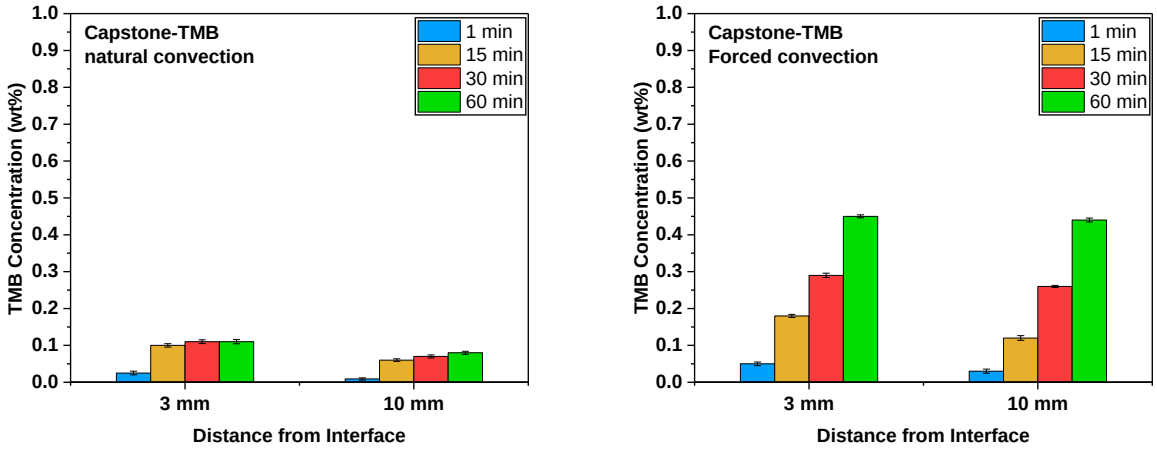

a) b)

Figure 42. TMB concentration measurement in Capstone solution for a) natural and b) forced convection at different distances away from the interface and times.

4.3.1.3. 25%TMB/Heptane

Glucopon

25%TMB-Heptane concentrations in Glucopon surfactant solutions at different times and locations from the interface were presented in Figure 43. For natural convection, at 15 min sample from 3 mm to 15 mm distances away from the interface fuel concentration decreased from 0.027 to 0.009 wt.%. After 30 minutes fuel concentration did not change significantly with time for all the distances. For forced convection, at 60 minutes fuel concentration was higher compared to 15, and 30 minutes for all the distances. For fuel concentration, less of a gradient was observed across the distances away from the interface 3 mm to 15 mm. Forced convection showed higher fuel concentrations at all the cases compared with natural convection.

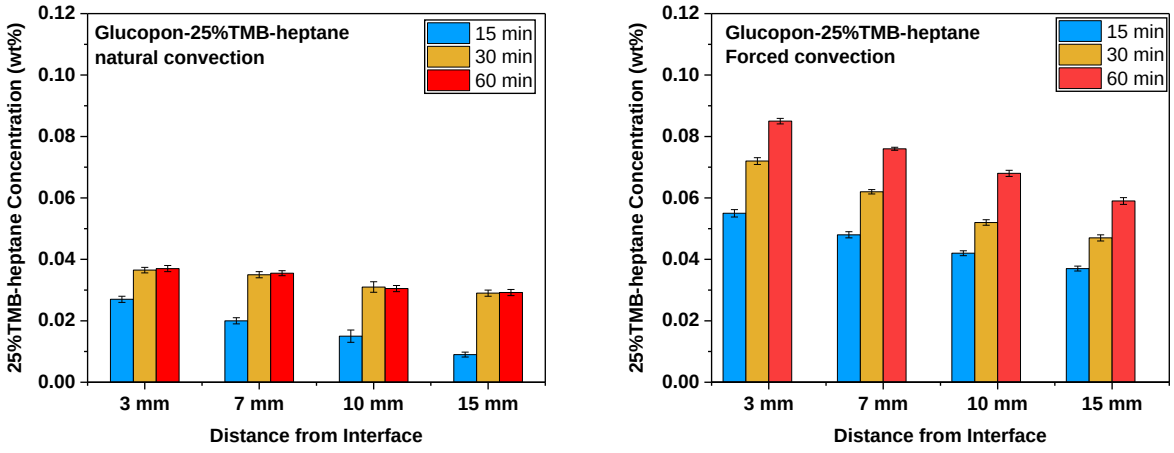

a) b)

Figure 43. 25%TMB-Heptane concentration measurement in Glucopon solution at four different distances away from the interface and times for a) natural and b) forced convection.

Capstone

25%TMB-Heptane concentrations in Capstone surfactant solutions at different times and locations from the interface were shown in Figure 44. For natural convection, at 15 min fuel concentration was detected at 3 mm and at 7 mm away from the interface and measured concentrations were 0.018 wt.% and 0.016 wt.%. At 60 minutes fuel concentration was detected for all the distances and decreased from 0.03 to 0.019 wt.% from 3 mm to 15 mm away distances. For forced convection, less of a gradient was observed across the distances away from the interface. Forced convection showed higher fuel concentrations in all the cases compared with natural convection.

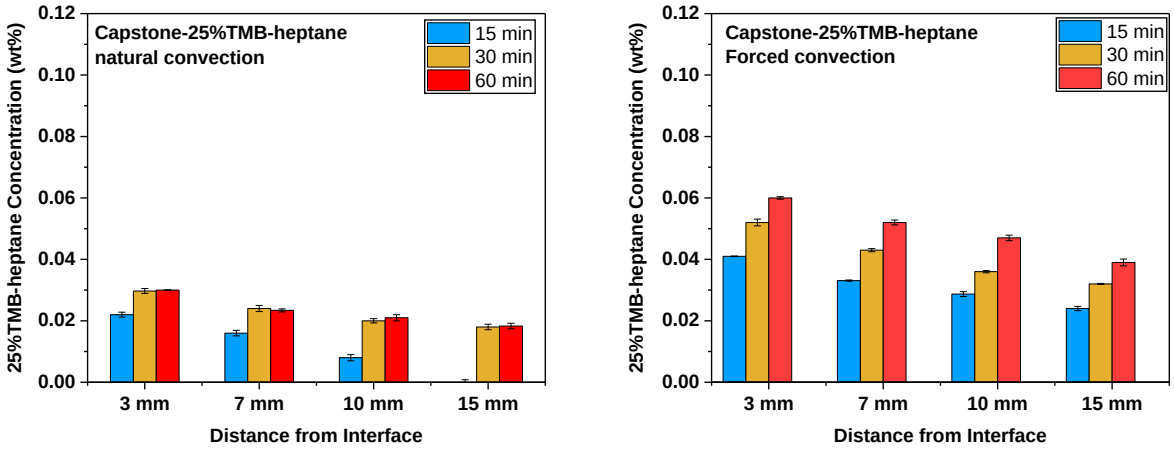

a) b)

Figure 44. 25%TMB-Heptane concentration measurement in Capstone solution at four different distances away from the interface and times for a) natural and b) forced convection.

4.3.2. Ignition test

For ignition tests, foam was generated using a Dynamic foam analyzer (DFA). Two different types of foams and two different types of fuels were used for analysis. Ignition time for each type of fuel through different surfactant foam solutions was recorded for analysis purposes. The ignition time for heptane and 25%TMB-heptane through Capstone, and Glucopon foam solution were presented in Figure 45. The ignition time for 25% TMB-heptane was lower than heptane for two-surfactant foam solutions tested. Irrespective of the fuel types, Capstone foam solution has higher ignition time compared to Glucopon foam solution.

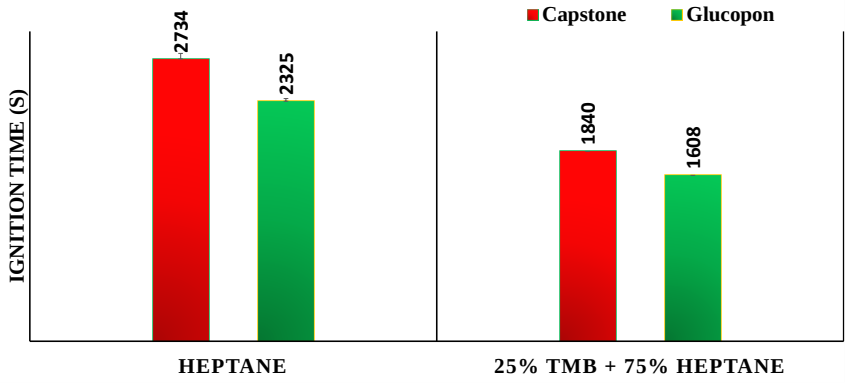

Figure 45. Ignition test result.

4.4. Discussion

Through this work, the effect of convection on fuel transport has been observed. This study reveals that due to forced convection the extent of fuel solubilization increases. Moreover, when fuel transport through surfactant solutions is kinetically more favored a shorter ignition time has been observed.

Convection effect enhances fuel transport. Due to natural convection, TMB concentration reaches a solubility limit with time; concentration did not change significantly (Figure 41, Figure 42); hence a saturated bulk phase is formed indicating limited fuel transport. However, due to forced convection, TMB concentration increases with time significantly (Figure 41, Figure 42) indicating more fuel transport. A similar trend to TMB has been observed for 25%TMB-heptane (Figure 43, Figure 44). Due to forced convection, near the interface heptane concentration is increasing compared to natural convection (Figure 39, Figure 40). Without forced convection heptane concentration is not detectable further away from the interface of Glucopon and Capstone solution (Figure 39, Figure 40) even after 60 minutes indicating fuel transport to the bulk do not occur without forced convection. Therefore, forced convection enhances TMB, 25%TMB-heptane, and heptane transport through surfactant solutions.

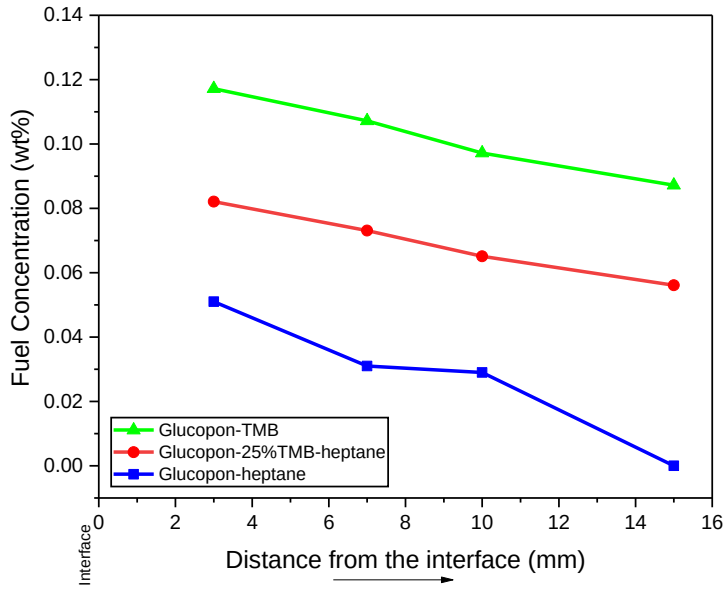

a)

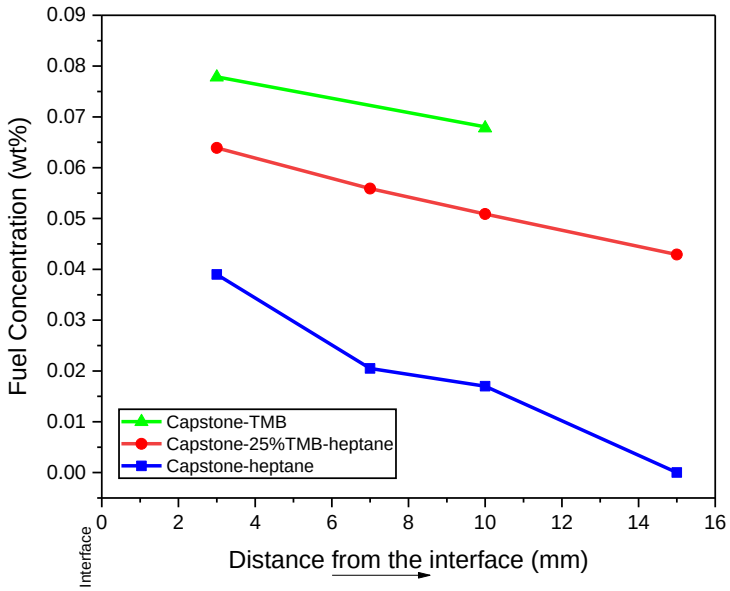

b)

Figure 46. Values for fuel concentration change across the distance for forced convection at 60 min in a) Glucopon b) Capstone solution.

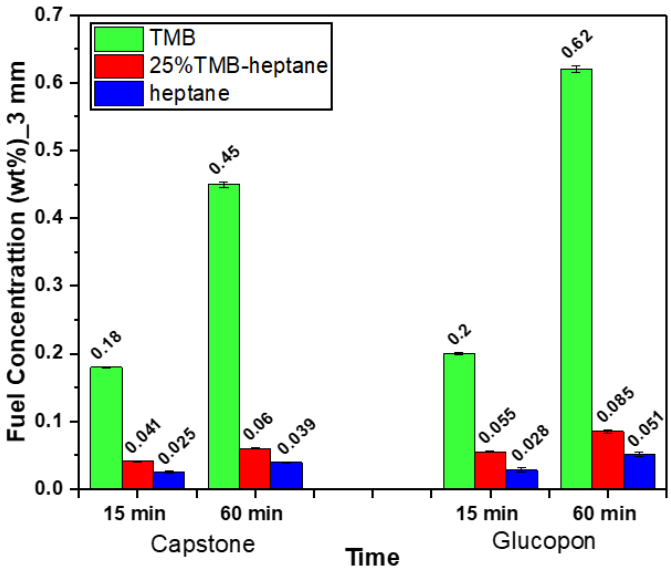

Figure 47. Fuel concentration versus time at 3 mm distance from the interface for forced convection in Capstone and Glucopon solution.

Kinetically more favored cases of fuel transport results in shorter ignition time. For the fuels, TMB molecule is solubilizing fast as lower concentration changes across the distances (Figure 46a) has been observed. This is further evident by the higher concentration measured (at 15 min 3 mm distance) for TMB (0.2 wt.%) compared to the concentration of 25%TMB-heptane and heptane (Figure 47). Due to higher polarity, TMB solubilization time was reduced across the distances, similar observation has been made by Rajesh et. al. [23]. Due to the presence of TMB, the concentration measured for 25%TMB-heptane is 0.055 wt.% (at 15 min 3 mm distance) higher than the concentration of heptane which is 0.028 wt.%. Its concentration change across the distance is less pronounced than heptane and follows a linear slope indicating that transport time is faster than heptane. Nonpolar fuel heptane has longer transport time indicated by the nonlinear change of concentrations across the distances (Figure 46a). This indicates the slower interactions of heptane fuel molecule with surfactant solution. A similar trend has been observed for Capstone (Figure 46b). Therefore, ignition time for heptane is longer than 25%TMB-heptane through Glucopon or Capstone solution (Figure 45).

For the surfactants, fuel transport time is faster for Glucopon compared to Capstone. The fuel concentrations measured in Glucopon solution at 15 min and 60 min have been consistently higher compared to the fuel concentrations measured in Capstone solution irrespective of fuel types (Figure 47). This indicates that fuel transport time through Glucopon solution is comparatively shorter than Capstone; hence fuel transport kinetics are faster and ignition time is shorter (Figure 45).

4.5. Conclusions

This study on two phase liquid-liquid system provides an understanding on the effect of convection on fuel transport of firefighting foam. Moreover, fuel concentration measurements show the effect of fuel transport kinetics on ignition time.

Due to natural convection, TMB, and 25%TMB-heptane concentrations get saturated over time indicating limited fuel transport through bulk phase; for heptane, concentration is only detectable near the interface indicating no fuel transport further away. However, due to forced convection, TMB, and 25%TMB-heptane transport increase with time and heptane transport escalates to the bulk. Therefore, forced convection enhances fuel transport through surfactant foam solution. Moreover, a shorter ignition time has been observed when fuel transport through surfactant solutions is kinetically more favored. TMB transport time is faster due to higher polarity. Due to the presence of TMB, 25%TMB-heptane has faster transport time; hence shorter ignition time compared to heptane. Fuel transport kinetic is faster through Glucopon surfactant solution compared to Capstone, hence shorter ignition time.

References

[1] K. M. Hinnant, S. L. Giles, A. W. Snow, J. P. Farley, J. W. Fleming, and R. Ananth, "An analytically defined fire-suppressing foam formulation for evaluation of fluorosurfactant replacement," *Journal of surfactants and detergents,* vol. 21, no. 5, pp. 711-722, 2018.

[2] C. Baduel, J. F. Mueller, A. Rotander, J. Corfield, and M. J. Gomez-Ramos, "Discovery of novel per- and polyfluoroalkyl substances (PFASs) at a fire fighting training ground and preliminary investigation of their fate and mobility," *Chemosphere,* vol. 185, pp. 1030-1038, Oct 2017, doi: 10.1016/j.chemosphere.2017.06.096.

[3] B. J. Place and J. A. Field, "Identification of novel fluorochemicals in aqueous film-forming foams used by the US military," *Environ Sci Technol,* vol. 46, no. 13, pp. 7120-7, Jul 3 2012, doi: 10.1021/es301465n.

[4] W. J. Backe, T. C. Day, and J. A. Field, "Zwitterionic, cationic, and anionic fluorinated chemicals in aqueous film forming foam formulations and groundwater from U.S. military bases by nonaqueous large-volume injection HPLC-MS/MS," *Environ Sci Technol,* vol. 47, no. 10, pp. 5226-34, May 21 2013, doi: 10.1021/es3034999.

[5] R. Ananth, A. W. Snow, K. M. Hinnant, S. L. Giles, and J. P. Farley, "Synergisms between siloxane-polyoxyethylene and alkyl polyglycoside surfactants in foam stability and pool fire extinction," *Colloids and Surfaces A: Physicochemical and Engineering Aspects,* vol. 579, p. 123686, 2019.

[6] R. Ananth, K. M. Hinnant, S. L. Giles, J. P. Farley, and A. W. Snow, "Environmentally Friendly Surfactants for Foams with Low Fuel Permeability Needed for Effective Pool Fire Suppression," NAVAL RESEARCH LAB WASHINGTON DC, 2020.

[7] K. M. Hinnant, S. L. Giles, and R. Ananth, "Measuring fuel transport through fluorocarbon and fluorine-free firefighting foams," *Fire Safety Journal,* vol. 91, pp. 653-661, 2017, doi: 10.1016/j.firesaf.2017.03.077.

[8] R. I. Islam, "Understanding the impact of fuel on surfactant microstructure of firefighting foam," Unpublished Work, 2023.

[9] S. R. Dungan, B. H. Tai, and N. I. Gerhardt, "Transport mechanisms in the micellar solubilization of alkanes in oil-in-water emulsions," *Colloids and Surfaces A: Physicochemical and Engineering Aspects,* vol. 216, no. 1-3, pp. 149-166, 2003.

[10] P. Todorov, P. Kralchevsky, N. Denkov, G. Broze, and A. Mehreteab, "Kinetics of solubilization of n-decane and benzene by micellar solutions of sodium dodecyl sulfate," *Journal of colloid and interface science,* vol. 245, no. 2, pp. 371-382, 2002.

[11] B. J. Carroll, "The kinetics of solubilization of nonpolar oils by nonionic surfactant solutions," *Journal of Colloid and Interface Science,* vol. 79, no. 1, pp. 126-135, 1981.

[12] B. Carroll, B. O'ROURKE, and A. Ward, "The kinetics of solubilization of single component non-polar oils by a non-ionic surfactant," *Journal of Pharmacy and Pharmacology,* vol. 34, no. 5, pp. 287-292, 1982.

[13] S. Ariyaprakai and S. R. Dungan, "Contribution of molecular pathways in the micellar solubilization of monodisperse emulsion droplets," *Langmuir,* vol. 24, no. 7, pp. 3061-3069, 2008.

[14] A. J. Ward, "The Kinetics of Oil Solubilisation in Aqueous Surfactant Solutions," in *Proceedings of the Royal Irish Academy. Section B: Biological, Geological, and Chemical Science*, 1989: JSTOR, pp. 375-382.

[15] A. A. Peña and C. A. Miller, "Solubilization rates of oils in surfactant solutions and their relationship to mass transport in emulsions," *Advances in colloid and interface science,* vol. 123, pp. 241-257, 2006.

[16] Y. Sheng, N. Jiang, S. Lu, Q. Wang, Y. Zhao, and X. Liu, "Study of environmental-friendly firefighting foam based on the mixture of hydrocarbon and silicone surfactants," *Fire Technology,* vol. 56, no. 3, pp. 1059-1075, 2020.

[17] A. W. Snow, S. Giles, K. Hinnant, J. Farley, and R. Ananth, "Fuel for Firefighting Foam Evaluations: Gasoline vs Heptane," NAVAL RESEARCH LAB WASHINGTON DC WASHINGTON United States, 2019.
[18] A. W. Snow, S. Giles, K. M. Hinnant, J. P. Farley, and R. Ananth, "Quantification of Fluorine Content in AFFF Concentrates," NAVAL RESEARCH LAB WASHINGTON DC WASHINGTON United States, 2017.
[19] "National Center for Biotechnology Information (2024). PubChem Compound Summary for CID 8900, Heptane. Retrieved February 27, 2024 from." [Online]. Available: https://pubchem.ncbi.nlm.nih.gov/compound/Heptane.
[20] "National Center for Biotechnology Information (2024). PubChem Compound Summary for CID 7247, 1,2,4-Trimethylbenzene. Retrieved February 27, 2024 from." [Online]. Available: https://pubchem.ncbi.nlm.nih.gov/compound/1_2_4-Trimethylbenzene.
[21] K. Hinnant, "Characterizing Trends Between Surfactant Structure, Fuel Transport through a Foam Layer, and Foam Fire Extinction Performance for Firefighting Foams Containing Novel Environmentally-Friendly Surfactants," The George Washington University, 2021.
[22] M. W. Sulek and T. Wasilewski, "Influence of critical micelle concentration (CMC) on tribological properties of aqueous solutions of alkyl polyglucosides," *Tribology transactions*, vol. 52, no. 1, pp. 12-20, 2008.
[23] R. Shah and P. Neogi, "Interfacial resistance in solubilization kinetics," *Journal of colloid and interface science*, vol. 253, no. 2, pp. 443-454, 2002.

Appendix B. Supplementary Information

UV-Vis Spectroscopy

As seen in Figure 48a, the absorbance spectra for known concentrations of TMB in Glucopon solution was measured to prepare the standard curve in Figure 48b. TMB was added to Glucopon solution in known concentrations of 0.4, 0.8, and 1.2 wt.%. A stirring plate and a magnetic stirring bar were used for approximately 15 minutes for mixing. Afterwards, waited for 15 minutes for sample equilibration and transferred it to the cuvette for analysis. The absorption peak from 300 – 230 nm was used for the analysis. The absorbances of all the standard samples were recorded keeping Glucopon solution as the baseline. For Glucopon-TMB analysis, sample was extracted from a two-layer interaction sample of Glucopon solution (bottom phase) and TMB (top phase). The absorbance attained at 267 nm placed into the standard curve (absorbance versus Fuel concentrations Figure 48b) to quantify the concentration of TMB in water. Heptane was added to Glucopon solution in known concentrations of 0.04, 0.08, and 0.12 wt.%. Glucopon solution and heptane were mixed for at least 15 minutes. After transferring the samples to cuvette, the absorbance was captured (Figure 48c). For Glucopon-heptane analysis, sample was extracted from a two-layer interaction sample of Glucopon solution (bottom phase) and heptane (top phase). The absorbance attained at 242 nm placed into the standard curve (absorbance versus Fuel concentrations Figure 48d) to quantify the concentration of TMB in water. Similarly, 25%TMB-heptane was added to Glucopon solution in known concentrations of 0.04, 0.08, and 0.12 wt.%. Glucopon solution and 25%TMB-heptane were mixed for at least 15 minutes. After transferring the samples to cuvette, the absorbance was captured (Figure 48e). For Glucopon-25%TMB-heptane analysis, sample was extracted from a two-layer interaction sample of Glucopon solution (bottom phase) and 25%TMB-heptane (top phase). The absorbance attained at 267 nm placed into the standard curve (absorbance versus fuel concentrations Figure 48f) to quantify the concentration of 25%TMB-heptane in water.

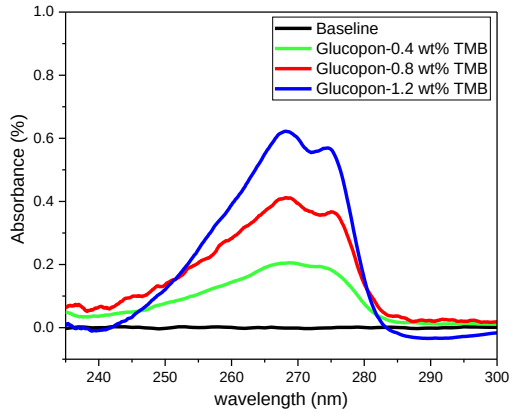

a)

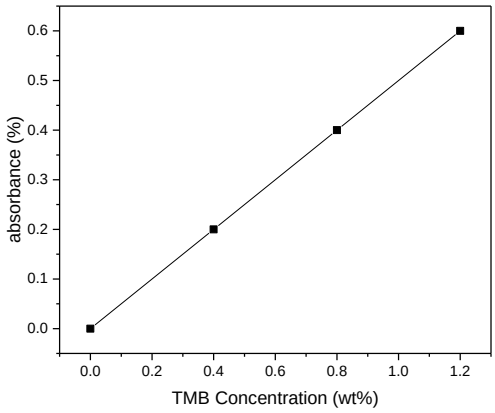

b)

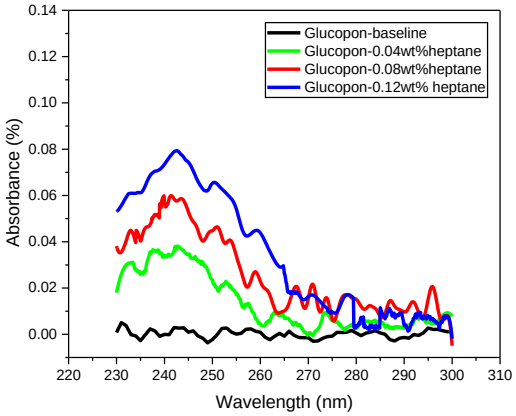

c)

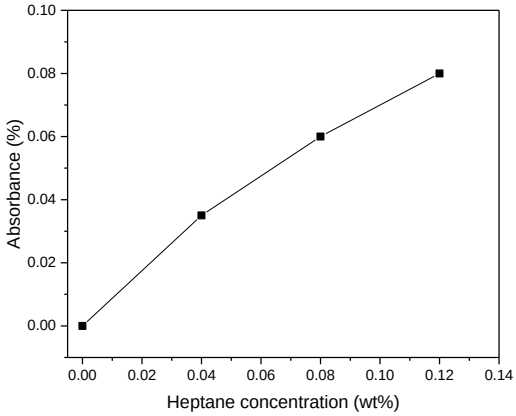

d)

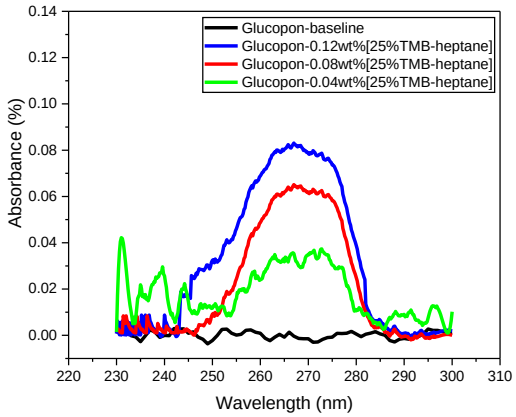

e)

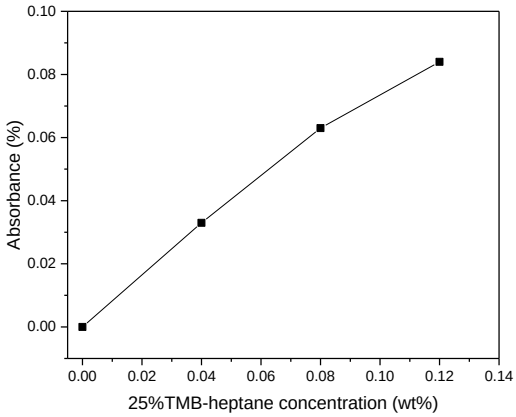

f)

Figure 48. Absorbance versus wavelength plots and standard graph for fuel concentration measurment in Glucopon solution a) & b) TMB; c) & d)heptane; e) & f) 25%TMB-heptane.

CHAPTER 5

Conclusion

5.1. Summary

The overall aim of this work is to understand the factors affecting fuel transport of the firefighting foams. To achieve this goal, a two-phase liquid-liquid system has been investigated to observe the microstructural, interfacial properties of surfactant with and without fuel exposure, fuel transport has been quantified. Moreover, the role of surfactant micelle and effect of convection on fuel transport have been observed.

The focus of Chapter 2 was to identify the effect of liquid fuel on surfactant microstructure, interfacial properties. Specifically, the key research questions guiding this work were: i) is liquid fuel affecting microstructure and interfacial properties of surfactant? ii) What are the factors affecting microstructure and interfacial properties? iii) finding out the implications of these factors on ignition time. To find the answer, various experiments were conducted with three different surfactants (Capstone, Glucopon, and siloxane), and four different fuels (TMB, heptane, octane, and 25%TMB-heptane). Due to higher solubility, TMB affected surfactant microstructure and interfacial properties. Due to poor solubility, heptane did not impact the surfactant microstructure and interfacial properties and ignition time was longer. Due to higher solubility shorter ignition time was observed for 25%TMB-heptane. Moreover, due to higher vapor pressure shorter ignition time was observed for heptane compared to octane.

Chapter 3 was aimed at understanding the thermodynamics of the interaction between liquid fuel and single surfactant. The key research questions for this study were as follows: i) role of the micelle during fuel transport ii) effect of fuel type on fuel transport. To answer these questions, Capstone and Glucopon as surfactants and TMB, heptane, 25%TMB-heptane as fuels were studied. Initially this research was conducted with varying surfactant concentration to observe the effect of micelle. At 5x CMC concentration experiments were done to explore the effect of fuel types on fuel transport. Fuel transport occurred at and above CMC concentration of surfactants when the interactions are thermodynamically favored. Glucopon interaction with fuels was thermodynamically more favorable compared to Capstone indicating more fuel

transport. Due to more polarity, fuel transport is higher for TMB compared to 25%TMB-heptane followed by heptane.

Chapter 4 was aimed at understanding the effect of convection on fuel transport. The key research questions for this study were as follows: i) effect of convection during fuel transport iii) understand the effect of fuel transport kinetics on ignition time. To answer these questions, Capstone and Glucopon as surfactants and TMB, heptane, 25%TMB-heptane as fuels were studied. Experiments were conducted in a two-phase fuel-surfactant solution system with and without stirring to observe the effect of convection. At different times and distances experiments were conducted to understand the fuel transport kinetic. Due to convection fuel transport enhanced. Fuel transport kinetic was faster for Glucopon, and the ignition time was shorter. Due to the presence of TMB, fuel transport kinetic was faster 25%TMB-heptane compared to heptane, and the ignition time was shorter.

5.2. Conclusions

The following conclusions were made through the course of the research process:

- Liquid fuel transport impact surfactant microstructure due to higher solubility in surfactant solution and higher solubility in surfactant solution decreases ignition time. The higher solubility of 25%TMB-heptane in Capstone and Glucopon solution causes lower ignition time compared to heptane. Ignition time is shorter when microstructure and interfacial properties have shown an impact of fuel solubility. Moreover, higher vapor pressure causes shorter ignition time. Heptane has a shorter ignition time than octane due to its higher vapor pressure.
- Micelles serve as a medium to transport fuel from the fuel-surfactant interface into the bulk solution. No fuel transport occurred during below CMC concentration due to not having any micelles and with increasing surfactant concentrations number of micelles enhances (above CMC concentration) and more fuel transport occurred.
- The interaction between polar fuel and surfactant is thermodynamically more favored and fuel transport is higher. Polar fuel TMB interacts with surfactant solutions in thermodynamically more favorable

conditions compared to 25%TMB-heptane followed by heptane; hence fuel transport is higher for TMB.

- Forced convection enhances fuel transport. Without forced convection heptane concentration is only detectable near the interface indicating no fuel transport further away. Forced convection enhances heptane transport to the bulk and increases transport of TMB, and 25%TMB-heptane with time. Due to natural convection, TMB, and 25%TMB-heptane concentrations get saturated over time indicating limited fuel transport through bulk surfactant solution.
- When fuel transport through surfactant solutions is kinetically more favored a shorter ignition time has been observed. TMB transport time is faster due to higher polarity. Due to the presence of TMB, 25%TMB-heptane has faster transport time; hence shorter ignition time compared to heptane.
- Fuel transport kinetic is faster through Glucopon surfactant solution compared to Capstone, hence shorter ignition time.

5.3. Future Work

This work helped to understand factors affecting fuel transport of firefighting foams. However, each of the chapters has its own limitations and openings to improve the established evidence by added research efforts. Some of the limitations and future research paths are provided below:

In Chapter 2, data indicates that micelle size increases due to the TMB solubility; however, the location of TMB molecules inside the micelle has not been verified. Further study would require locating the fuel molecules inside the micelle. To confirm the location of fuel molecules inside the vesicles, Electron energy loss spectroscopy (EELS) measurement along with Cryo-TEM can be performed. EELS will provide information on the composition of the structure at different locations. This method will provide information about the elements and concentrations present at different locations.

In Chapter 3, it has been shown that vesicles formed by Capstone, capturing fuel, and not allowing fuel to be released in the gas phase; restricting fuel transport more compared to worm-like micelles of Glucopon. In Chapter 4, it has been found that fuel transport kinetics is faster through Glucopon solution compared to Capstone. Other than the shape, Capstone and Glucopon have different head types, which might be another factor for their performance difference. Therefore, further studies will be required to confirm which factor has the bigger impact against fuel transport, head types or micelle shape or vesicles.

5.4. Publications

Each Chapter in this dissertation will be considered for journal publication. The publication titles and status are listed below:

Chapter	Title	Status
2	Understanding the impact of fuel on surfactant microstructure of firefighting foam	In Review
3	Understanding the interaction between fuel and single surfactants of firefighting foam	To be submitted
4	Understanding the effect of convection on fuel transport of firefighting foam	To be submitted

Other literary/intellectual involvements related to this dissertation work include:

Additional publication:

- Islam, R., and Lattimer, B. (2023) “Evaluation of the Adsorption of Polyfluoroalkyl Substances from Firefighting Foams onto Plastic Surfaces.” (In Review)

Co-authored publication:

- Brown, James R., Margaret D. Madsen, Ayşenur Ateş, **Rezawana Islam**, Seokgyun Ham, Benjamin Agbo, Kamyar Karimi Nikoo et al. "Revealing foam stability for cationic and zwitterionic triethylsilyl-containing surfactants." Physics of Fluids 35, no. 7 (2023).

Accepted Research Proposals:

- Identification of Critical Properties and Features of Surfactant Solutions for Firefighting Foams, Spallation Neutron Source (SNS), Oak Ridge National Laboratory, May 27-May 30, 2022, Instrument: BL-6 EQ-SANS, Instrument Scientist: Gergely, Nagy

- Identification of Critical Properties and Features of Surfactant Solutions for Firefighting Foams, Center for Nanophase Materials Sciences (CNMS), Oak Ridge National Laboratory, Dec 21-Dec 22, 2022, Instrument: STEM, Instrument Scientist: Williams, Alexis

- Identification of Critical Properties and Features of Surfactant Solutions for Firefighting Foams, Center for Nanophase Materials Sciences (CNMS), Oak Ridge National Laboratory, Start Date: Aug 1st, 2023, Instrument: STEM, Instrument Scientist: Williams, Alexis

Appendix C

Evaluating the Adsorption of Polyfluoroalkyl Substances from Firefighting Foams onto Plastic Surfaces

Rezawana Islam[1] and Brian Y. Lattimer[2]

[1]Materials Science and Engineering, Virginia Tech

[2]Mechanical Engineering, Virginia Tech

Submitted to Fire and Materials Journal

Abstract

Aqueous film forming foam (AFFF) used for liquid fuel firefighting contains polyfluoroalkyl substances (PFAS) that has been identified as environmentally persistent and bioaccumulative resulting in a phase out of AFFF. As a result, hardware such as pipes, fittings, and tanks that have contained AFFF need to be remediated to remove PFAS compounds to reduce future contamination. To support this, it is important to understand fluorine bonding of PFAS in AFFF to different polymer surfaces and the potential for removing these compounds from the surface. An experimental study was conducted to quantify the effects of long-term exposure of AFFF derived PFAS to different polymers. Fourier-transform infrared spectroscopy (FTIR) and Raman spectroscopy were used to measure the presence of fluorine, bonding, and its concentration. The data indicates that the PFAS compounds on the surface are dependent on exposure duration and polymer type. Ultrasonic cleaning of these different surfaces showed that not all fluorine would be removed by this process and the reduction was also dependent on the polymer type and exposure duration.

C.1. Introduction

A variety of industries have used per and polyfluoroalkyl substances (PFAS) for many applications due to their unique properties. These manmade chemicals contain both hydrophobic and hydrophilic characteristics which made them attractive to include in aqueous film forming foams (AFFF) for

firefighting as well as oil or water-repellent products [1]. AFFF has been in use by fire departments for fire extinguishing, fire-fighter drills and equipment analysis due to it being the most effective agent at suppressing large hydrocarbon fuel fires [2-4]. Due to AFFF being an aqueous solution, AFFF released into the environment can migrate into soil, water, and animals [1, 3, 5-7], which has resulted in increased regulation on its use.

Fluorinated substances are comprised of one or more C atoms substituting all the H atoms by F atoms, forming the perfluoroalkyl moiety $-C_nF_{2n+1}-$ also referred to as PFAS. The global regulatory community is explicitly concerned about long-chain perfluoroalkyl sulfonic acids ($-C_nF_{2n+1}$ SO_3H, n ≥ 6, PFSAs) and perfluoroalkyl carboxylic acids ($-C_nF_{2n+1}$COOH, n ≥ 7, PFCAs) and their subsequent anions, which are more bioaccumulative in comparison to their short-chain equivalents [8, 9]. Bioaccumulation potential, toxicity, persistence, and pervasive existence in the environment are the reasons for the rising concern of the two long-chain PFAS, perfluorooctanoic acid (PFOA) and perfluoro octane sulfonic acid (PFOS). These two types of PFAS have been most widely stated in studies [5], and have been phased out of currently used AFFF for the shorter chain PFAS.

Numerous grades of zwitterionic, cationic, and anionic PFAS were detected in AFFF formulations utilized by the U.S. military [4]. Mostly PFAS exist in their anionic forms in the environment are highly resistant to conventional cleaning processes [10], and their terminal transformation is very difficult due to the strong carbon-fluorine bonds (C–F) that exist within the compounds. Literature depicts that PFAS generally adsorb to soils through hydrophobic interactions primarily with organic carbon and circumstantially by electrostatic attraction dependent on the charge of the ionic head group [1]. Furthermore, the perfluorocarbon moieties in PFAS are hydrophobic, lipophobic, and oleophobic, making many PFAS efficient surfactants or surface protectors.

Studies have investigated the adsorption of PFAS on solid materials. The highest concentrations of PFAS were found in composite wood building materials dominated by perfluoroalkyl carboxylic acids with 5-8 carbons in the chain (up to 32.9 μg kg^{-1}) and textile materials 77.61 μg kg^{-1} [11]. Raphael et al.[12] showed

that PFAS are applied in building materials and fabrics, unreacted nonpolymeric PFAS might enter the environment by evaporation. PFAS of diverse chain lengths (in the range of C4–C14) were detected in 53% of the analyzed samples, awning materials and coating samples were amongst the highest.

Scott et al. [13] examined the interactions of PFAS and microplastics as in controlled lab conditions as well as after exposing plastics to field conditions in a lake for 1 to 3 months. Microplastics included in the study were low density polyethylene (LDPE), polypropylene (PP), and polyethylene terephthalate (PET). Following immersion of plastics in PFAS for 1 month, a methanol extraction was used to remove PFAS from the surface for analysis using liquid chromatography. The study showed that incubation in the lake conditions caused an increase in adsorption of PFAS onto the plastic surface, which was attributed to the accumulation of inorganic and organic matter onto the plastic surface from the field incubation. For field incubated plastics, the trend in adsorption by plastic type was PP<PET<LDPE; however, the variation in the results indicated the difference may be marginally statistically significant. Plastics not incubated in the field were found to have a different trend with LDPE<PP<PET, though PP and PET were determined to have statistically similar adsorption. Other studies have also shown the relative adsorption of PFAS onto plastic surfaces in laboratory conditions as well as the impact of environmental aging on adsorption of PFAS [14-17]. In a study on sorption of PFAS on laboratory ware, polypropylene was measured to adsorb more PFAS compared with polystyrene, polycarbonate, and glass [18]. With exception of Ref. [14], these studies used pure chemical substances and not AFFF foam concentrate in their studies. AFFF concentrate is a mixture of fluorinated surfactants, hydrocarbon surfactants and other additives which may impact the adsorption onto the surface.

The most common solid phase PFAS destruction technology available is incineration which can convert ~20-45% of the fluorine to hydrogen fluoride gas and emit gaseous fluorocarbon to the surrounding. Additionally, this process needs a high temperature (1000^{o}C) which is not very economical. On the other hand, ultrasonication is a very promising procedure for complete PFAS mineralization at ambient temperature. The mechanism behind this, ultrasound wave propagates in an aqueous solution creating

shockwaves, eventually creating enough temperature and pressure to pyrolyze PFAS [19]. Moreover, ultrasonication delivers high safety, better cleanliness, economical, and most importantly, not causing secondary pollution [20].

The focus of this research was to explore the adsorption of PFAS in AFFF onto polymer surfaces and the potential for removing it. Three different polymer samples were included in the study to determine the impact of material type on AFFF adsorption. Accelerated aging was used to explore the long-term effects (up to 3 years) of AFFF exposure to the PFAS surface adsorption. FTIR spectroscopy and Raman Spectra were used to quantify the level of compounds adsorbed onto the surface with a focus on fluorinated compounds. The effects of removal of the fluorinated compounds from the polymer surfaces using ultrasonic cleaning was also quantified.

C.2. Experimental methods

C.2.1. Materials and Preparation

The polymer materials included in the study were ultra-high molecular weight polyethylene (PE), polypropylene (PP), and nylon (Ny) cast samples. Sample composition was quantified through Xrd analysis and presented in Table 18. These materials were selected because they are common materials used in AFFF hardware systems. In addition, nylon was included because it generally has less chemical resistance compared with polypropylene and polyethylene. Polymer samples were 25 mm x 25 mm and 4 mm thick. The AFFF firefighting foam used in this study was C606-MS-C 6% AFFF (Aqueous Film-Forming Foam).

Table 18: Sample Composition

Sample Type	Composition	Percentage
Polyethylene	$C_{13}H_{10}$	53.00%
	C_{60}	20.00%
	$C_{20}H_{34}$	27.00%
Polypropylene	$C_{19}H_{24}$	99.90%
Nylon	$C_3H_6O_3$	98.50%
	$H_4N_2O_3$	1.50%

Polymer samples were prepared and tested as baseline (unexposed), short term exposure to AFFF concentrate (2 days), long term exposure to AFFF concentrate using accelerated aging (representing 1 – 3 years of exposure). Baseline samples were rinsed with distilled water and dried. For the short-term exposure, samples were soaked in AFFF concentrate within a glass container at room temperature for 2 days, removed, and allowed to dry in laboratory conditions for 2 days.

Long term exposure of the samples was achieved through accelerated aging of the sample within an environmental chamber at 60±0.3°C. As shown in Figure 49, samples were located in glass beakers filled with AFFF concentrate and placed into a metal tray. Dehydration of the concentrate was prevented by placing 20 mm of distilled water in the bottom of the tray and covering the tray with a lid. Samples were removed from the conditioning chamber after 23, 45 and 68 days corresponding to a room temperature exposure of 1 year, 2 years, and 3 years respectively. After exposure, samples were removed from the AFFF and dried for 2 days at laboratory conditions.

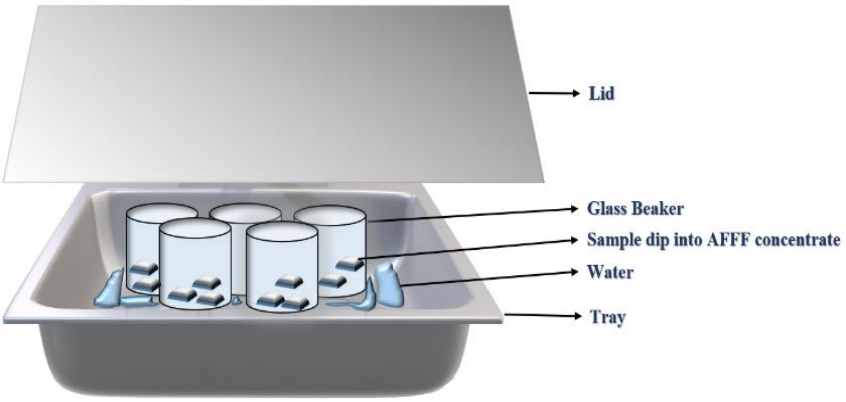

Figure 49: Accelerated aging sample in AFFF concentrate.

Select samples were cleaned through ultrasonic cleaning. For ultrasonic cleaning, a Branson M1800 ultrasonic cleaner was used to perform the cleaning of the AFFF exposed samples. Ultrasonic cleaning was conducted with a frequency of 40 kHz for 30 minutes at room temperature.

C.2.2. Characterization

Samples were analyzed with different methods to quantify the amount of fluorine present on the surface of the polymers. These tests were conducted on the baseline, exposed samples, and cleaned samples to compare the effects of exposure and cleaning on the fluorine at the surface. Measurements were performed with both FTIR and Raman spectroscopy. These are two noninvasive, nondestructive, and complementary vibrational spectroscopy techniques. IR can identify R−O−H vibrations, characteristic for alcohols as well as carbonyl groups in a material. On the other hand, Raman spectroscopy can identify only C−C, C−H, and CH_2 vibrations of these molecules in the same material [21].

FTIR spectroscopy was conducted using a Varian 670-IR with mid-IR integrated sphere manufactured by Pike Technologies. Measurements were conducted at room temperature to detect the fluorine presence on polymer surface. The spectra were obtained in the range 600–4000 cm^{-1} with 16 accumulated cycles.

Raman spectroscopy was performed using a XploRA PLUS Raman microscope manufactured by Horiba. A 532-nm laser source and 600 full-range gratings were used in the measurements. The flat surface of the rectangular-shaped polymer sample was fixed onto the sample holder for data recording. The spectra

presented are the average of spectra measured over a 1000 x1000 micron area. Raman spectroscopy was carried out to identify the presence of C-F bond as well as quantify the fluorine concentration developed on polymer surface.

C.3. Results

The results from the measurements made using the FTIR and Raman spectroscopy are provided in this section for samples having different exposures to AFFF as well as cleaned samples. Both methods provide insight on the amount of fluorine contained on the sample surface.

C.3.1 FTIR

FTIR technique was applied to investigate the presence of fluorinated compound on the polymer surface. The FTIR spectra were detailed for the baseline, fluorinated, and ultrasonicated cleaned polyethylene (PE), polypropylene (PP) and nylon (Ny) samples. The infrared spectra for the samples were measured over a range of 600–4000 cm^{-1}.

C.3.1.1 Polyethylene

The infrared spectra for fluorinated PE samples are presented in Figure 50a with peak assignment description given in Table 19. Spectra of baseline sample and AFFF exposed samples differ from each other significantly. The obtained spectra for baseline contained bands originating from asymmetrical and symmetrical vibrations of C–H at 2846 and 2913 cm^{-1}, CH_2 bending at 1469 cm^{-1}, CH_2 rocking 717 cm^{-1} [22]. The specific vibrations bands of the perfluorinated chains at occur at a frequency range of 1030 – 1242 cm^{-1} for all the AFFF exposed samples (PE concentrated, PE Accld 1 yr, PE Accld 2 yr, and PE Accld 3 yr). The band at 1103 cm^{-1} is characterized by the transmittance (%) for C-F bond [23]. Other bands that show variation from baseline samples to the AFFF exposed samples include the C=C stretching at 1644 cm^{-1} and O–H stretching peaks at 3354 cm^{-1} [24]. Table 19 lists the peak positions and their corresponding assignment to vibrational bands for the peaks and bond associated to AFFF exposed samples.

Results for ultrasonic cleaning of samples is provided in Figure 50b. Samples with long term exposure still have a peak present in the range of 1030–1242 cm^{-1} corresponding to the fluorinated bond. However, no peak was measured in the fluorinated bond range for the sample with a short term AFFF exposure.

Table 19: FTIR peak assignment and description for polyethylene samples.

Sample Name	**Peak Position, Wavenumber (cm^{-1})**						
PE Baseline	717	No Peak	1469	No Peak	2846	2913	No Peak
PE Concentrate		1190		1644			3354
PE Accld 1 yr							
PE Accld 2 yr							
PE Accld 3 yr							
Bond Type	CH_2 rocking	C-F stretching	CH_2 scissoring	C=C stretching	C-H stretching	C-H stretching	O-H stretching

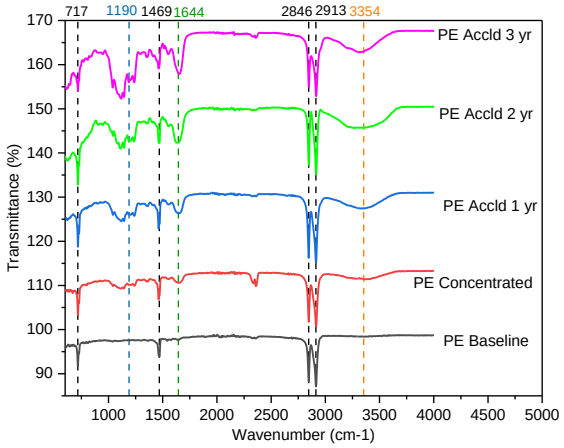

a)

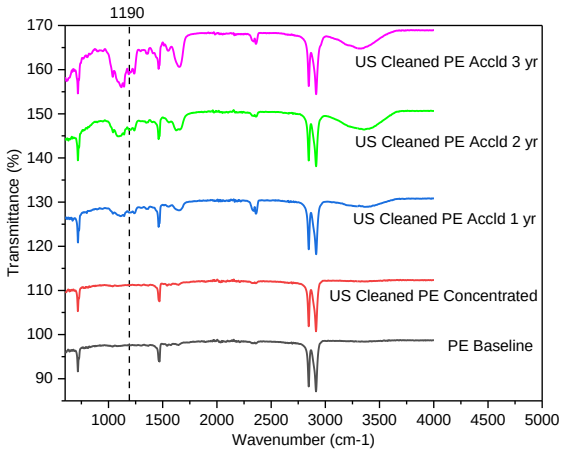

b)

Figure 50: Comparison of FTIR spectra of different polyethylene samples a) exposed to AFFF and b) after ultrasonic cleaning.

C.3.1.2. Polypropylene

For polypropylene samples the infrared spectra are shown in Figure 51a with peak assignment description given in Figure 51. Symmetric bending vibration mode of $–CH_3$ group is detected at 1375 cm^{-1}. The peaks at 1459, 2844 and 2915 cm^{-1} are attributed to $–CH_2–$ symmetric bending, $–CH_2–$ symmetric stretching and $–CH_2–$ asymmetric stretching; respectively Absorption peak observed at 2950 cm^{-1} is related to $–CH_3$ asymmetric stretching vibration [25]. The specific vibration bands of the perfluorinated chains are in the frequency range of 1030 – 1242 cm^{-1}, and peaks are observed for all the AFFF exposed samples (PP concentrated, PP Accld 1 yr, PP Accld 2 yr, and PP Accld 3 yr). The band at 1120-1175 cm^{-1} is characterized by the transmittance (%) for C-F bond [26]. Other bands that show variation from the baseline sample to the AFFF exposed samples include 1658 cm^{-1} which highlights C=C stretching may be a double bond from the polymer chain or PFAS and 3365 cm^{-1} that corresponds to O-H stretching.

Table 20: FTIR peak assignment and description for polypropylene samples.

Sample Name	**Peak Position, Wavenumber (cm^{-1})**							
PP Baseline	No Peak	1375	1459	No Peak	2844	2915	2950	No Peak
PP Concentrate	1120-1175			1658				3365
PP Accld 1 yr								
PP Accld 2 yr								
PP Accld 3 yr								
Bond Type	C-F stretching	CH3 Vibration	CH_2 Symmetric bending	C=C stretching	CH_2 Symmetric stretching	CH_2 Asymmetric stretching	CH_2 Asymmetric stretching	O-H stretching

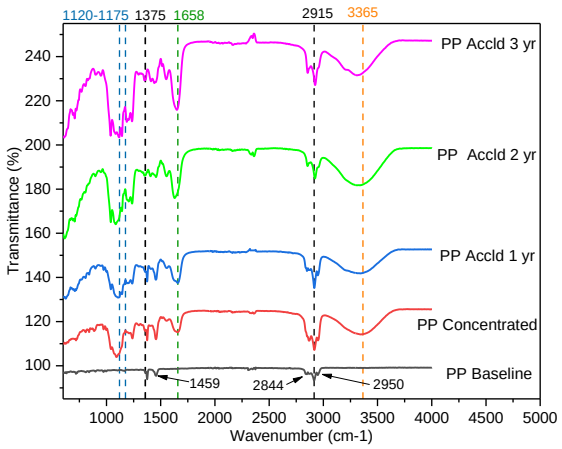

a)

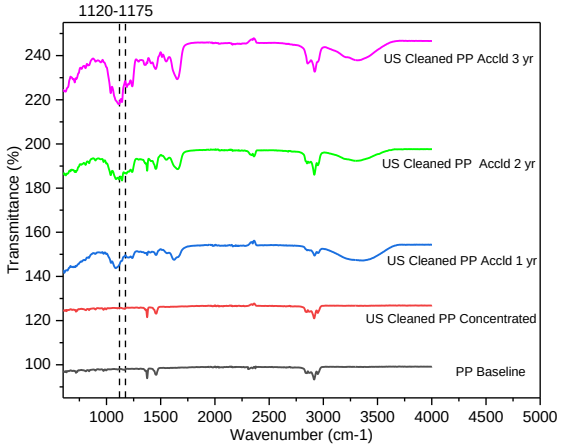

b)

Figure 51: Comparison of FTIR spectra of different polypropylene samples a) exposed to AFFF and b) after ultrasonic cleaning.

Measured spectra for the cleaned samples are provided in Figure 51b. Like polyethylene, polypropylene samples with long term AFFF exposure still exhibited peaks corresponding to the fluorine bond at 1085 cm^{-1} but no peak for the short-term exposure after cleaning.

C.3.1.3. Nylon

The infrared spectra for nylon samples exposed to AFFF are presented in Figure 52a with the peak assignment. FTIR results indicated the chemical structure of the baseline with the certain chemical groups such as N–H stretching peaks at 3297 cm^{-1}, C–H stretching at 2931 cm^{-1}, amide-I at 1630 cm^{-1}, amide-II

at 1542 cm^{-1}, and amide-III at 1370 cm^{-1}. A peak at 1089 cm^{-1} corresponding to the presence of C-F bond was measured on the surface of samples with long term exposure.

Figure 52b represents the FTIR results for cleaned nylon samples. Similar to polyethylene and polypropylene, the long-term exposure samples have peaks at 1089 cm^{-1} corresponding to the fluorinated chain [27] indicating the PFAS remains on the surface even after ultrasonic cleaning. No peak was observed in this range for samples with short term exposure after cleaning.

Table 21. FTIR peak assignment and description of nylon samples.

Sample Name	**Peak Position, Wavenumber (cm^{-1})**						
Ny Baseline	No Peak	1370	1542	1630	2931	3297	No Peak
Ny Concentrate	1089					No Peak	3297
Ny Accld 1 yr							
Ny Accld 2 yr							
Ny Accld 3 yr							
Bond Type	C-F stretching	Amide-III	Amide-II	Amide-I	CH_2 stretching	N-H stretching	O-H stretching

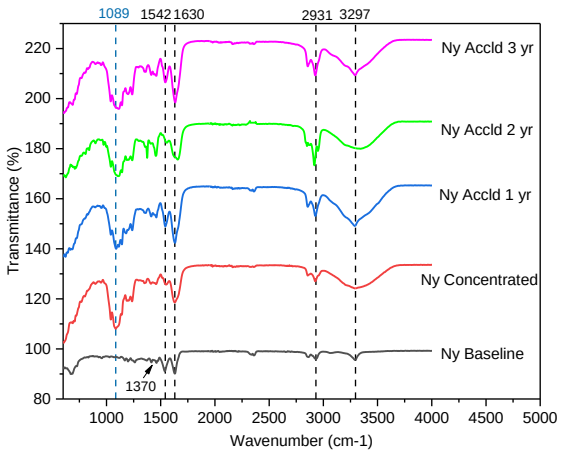

a)

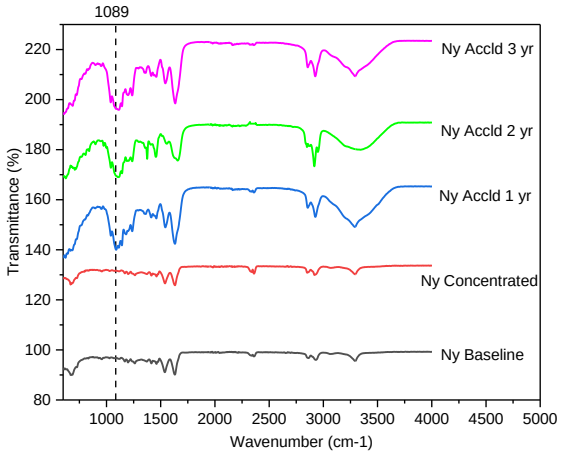

b)

Figure 52: Comparison of infrared spectra of different nylon samples a) exposed to AFFF and b) after ultrasonic cleaning.

C.3.2. Raman Spectroscopy

Raman Spectroscopy was employed to detect the existence of fluorinated compounds and quantification of their concentration on the polymer surface. The Raman spectra were detailed for the baseline, fluorinated, and ultrasonicated cleaned polyethylene (PE), polypropylene (PP) and nylon (Ny) samples. The spectra for the samples were presented for Raman shift of 1200–2800 cm^{-1}.

C.3.2.1. Polyethylene

The Raman spectra measured for the samples are provided in Figure 53 and Table 22 lists the peak positions and assignment descriptions. The Raman spectra of polyethylene has a few characteristic features. The

scattering spectra in the range of 1200 – 2800 cm^{-1}, three peaks at about 1296, 1439 and 2700 cm^{-1} are fixed for all types of samples. The bands at Raman Shift 1297cm^{-1} and 1439 cm^{-1} are subsequent to the twisting and bending modes of CH_2 [28, 29], while the band at 2700 cm^{-1} is due to C-H vibration.

For AFFF exposed samples, the peak at 1297 cm^{-1} is due to the presence of the C-F bond [30, 31]. The more molecules in the measurement volume the higher the intensity. Hence, the fluorinated peak intensity has increased with increasing exposure duration. The increasing peak at 1439 and 2700 cm^{-1} is attributed to the hydrocarbon surfactants or other hydrocarbon-based additives in the AFFF.

Raman spectra for ultrasonic cleaned samples are presented in Figure 53b. Similar to the results from the FTIR, the ultrasonic cleaning was not able to remove the fluorinated compounds for the long-term exposure but was effective at removing them after a short-term exposure.

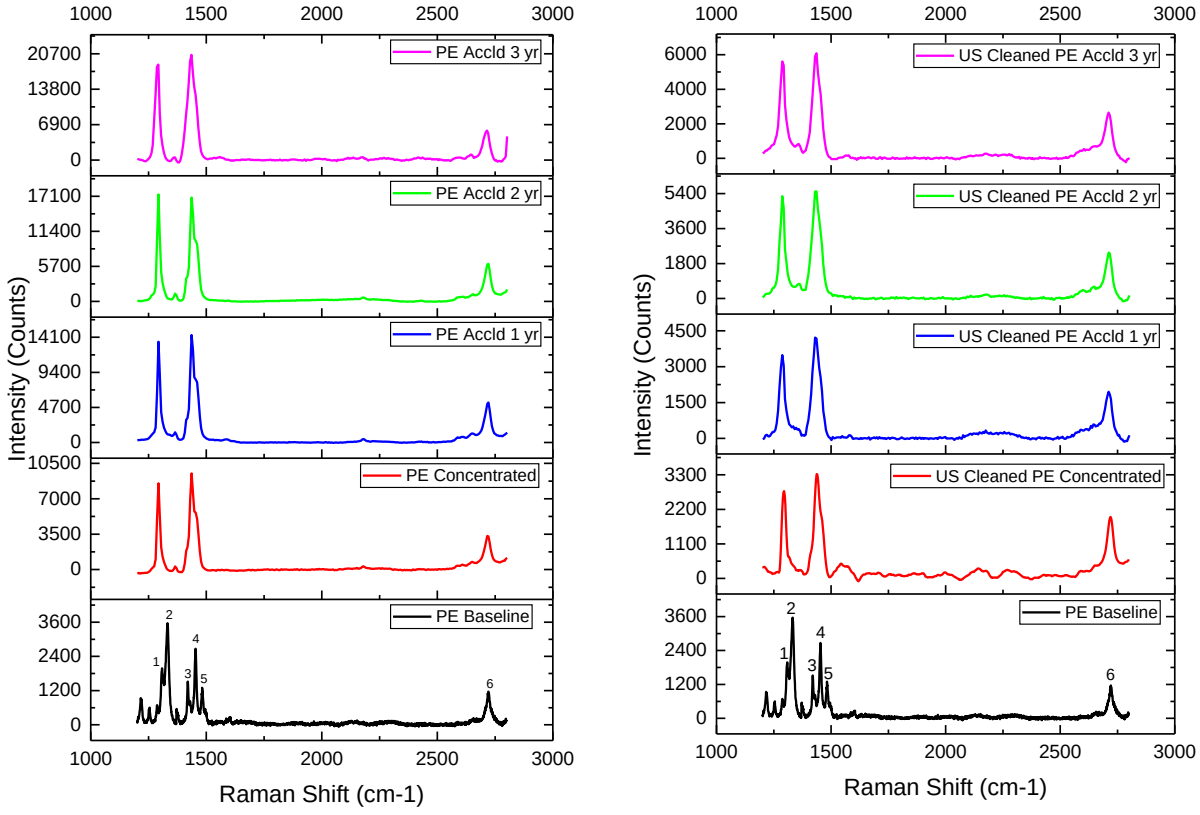

a) b)

Figure 53: Raman Spectra polyethylene samples a) exposed to AFFF and b) after ultrasonic cleaning.

Table 22: Raman spectroscopy for polyethylene samples with assignment.

Sample Name	Polyethylene					
	Peak Position, Raman Shift (cm^{-1})					
	1	2	3	4	5	6
Baseline	1296.07	1332.18	1415.84	1439.59	1457.37	2718.81
Concentrated	1292.97	No Peak	1412.77	1436.54	No Peak	2721.28
Accld 1 yr	1292.97	No Peak	No Peak	1436.54	No Peak	2716.2
Accld 2 yr	1292.97	No Peak	No Peak	1436.54	No Peak	2721.28
Accld 3 yr	1292.51	No Peak	No Peak	1435.98	No Peak	2715.02
Assignment	C-C twisting	CH_2 bending	CH_2 bending + CH_2 rocking	CH_2 bending	CH_2 bending	C-H vibration

The variation of the results at different locations on the sample surface is shown through the results in Figure 54. The error bars in the plot represent the standard deviation of the intensity for three different locations measured. The intensity at the peaks were typically within ±15%. This was typical for all polymer samples measured in this study.

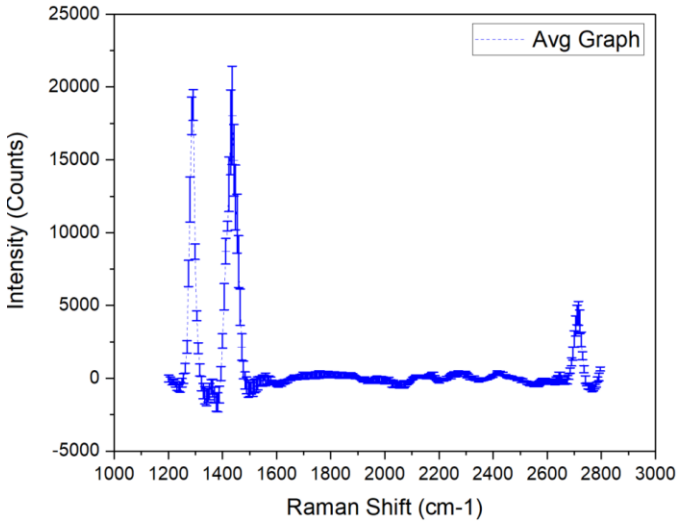

Figure 54: Raman Spectra standard deviation for three different reading of PE Accld 3 yr Sample.

C.3.2.2. Polypropylene

The characteristics features of Raman spectra of polypropylene is provided in Figure 55 for AFFF exposed and cleaned samples. Figure 55a contains Raman spectra for baseline polypropylene with bands at Raman shifts of 1218, 1297, 1357, 1459 and 2727 corresponding to the twisting and bending vibration modes of hydrocarbon as indicated in Table 6 [32, 33].

For AFFF exposed samples, the peak at 1327 cm^{-1} is due to the presence of C-F bond [34]. Increasing the aging period increased the number of C-F groups on the surface resulting in a higher measured intensity. Raman spectra for cleaned samples presented in Figure 55 contains lower peaks at 1297, 1439, and 2700 cm^{-1} compared with samples before cleaning. However, samples with long term exposure continue to show elevated intensity peaks at 1297 cm^{-1} relative to the baseline sample, indicating the presence of PFAS on the surface following ultrasonic cleaning. The samples with short term exposure had a similar spectrum compared with the baseline indicating the PFAS was removed through ultrasonic cleaning.

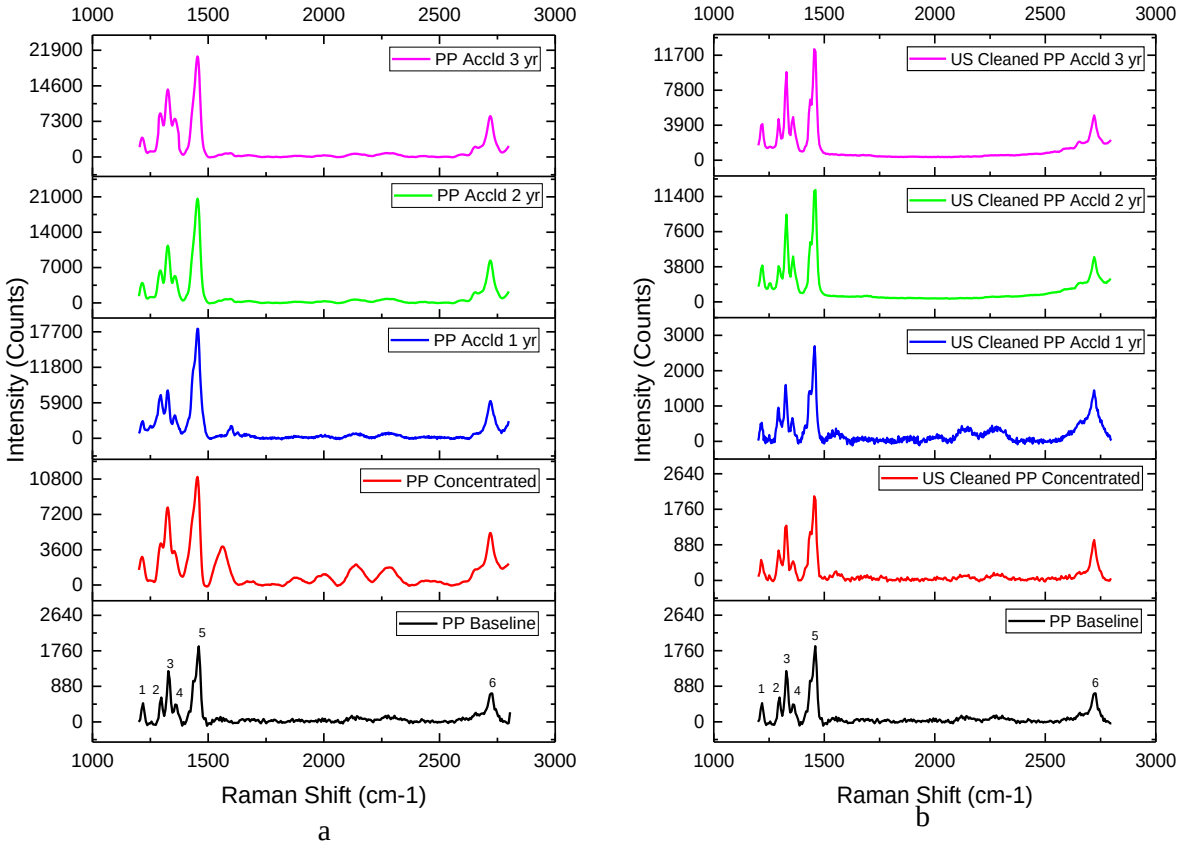

Figure 55: Raman Spectra polypropylene samples a) with AFFF exposure and b) following ultrasonic cleaning.

Table 23: Raman spectroscopy of polypropylene samples with assignment.

Sample Name	Polypropylene					
	Peak Position, Raman Shift (cm^{-1})					
	1	**2**	**3**	**4**	**5**	**6**
Baseline	1218.69	1297.64	1327.81	1357.88	1459.34	2727.91
Concentrated	1217.53	1303.52	1328.3	1353.01	1456.44	2720.71
Accld 1 yr	1217.53	1295.24	1325.55	1355.75	1456.44	2724.4
Accld 2 yr	1214.74	1292.48	1328.3	1361.23	1456.44	2722.12
Accld 3 yr	1214.74	1295.24	1328.3	1358.49	1451.04	2722.12
Assignment	CH_2 twisting + CH sym bending + C-C	CH_2 rocking + CH sym bending	CH2 rocking + CH2 twisting	CH_3 sym ben + CH sym bending	CH_3 asym twisting + CH_2 sym bending	CH_2 vibration

C.3.2.3. Nylon

The Raman spectra for nylon are shown in Figure 56. Table 24 includes the peak positions and their corresponding assignment to vibrational bands for the peaks and bond associated to baseline nylon samples. Figure 56 represented Raman spectra for baseline, as observed the bands at Raman Shift 1306, 1416/65, 1444, 1472 are due to the twisting and bending modes of CH_2 [28, 29]. The band at 1636 due to amide I, whereas 2745 cm^{-1} due to combination band [35].

For AFFF exposed samples, the peak at 1306 cm^{-1} is due to the presence of C-F bond [36]. The more molecules in the measurement volume the higher the intensity. As seen from the figure, the longer exposure to AFFF resulted in a higher intensity thus an increase in concentration on the surface.

Raman spectra for cleaned samples are contained in Figure 56b. The results show that the peaks at 1297, 1439, and 2700 cm^{-1} had similar intensity to the samples with long term AFFF exposure. As a result, the ultrasonic cleaning was not as effective on the nylon samples compared with polyethylene and polypropylene. Similar spectra were obtained for the baseline and cleaned short term exposure sample.

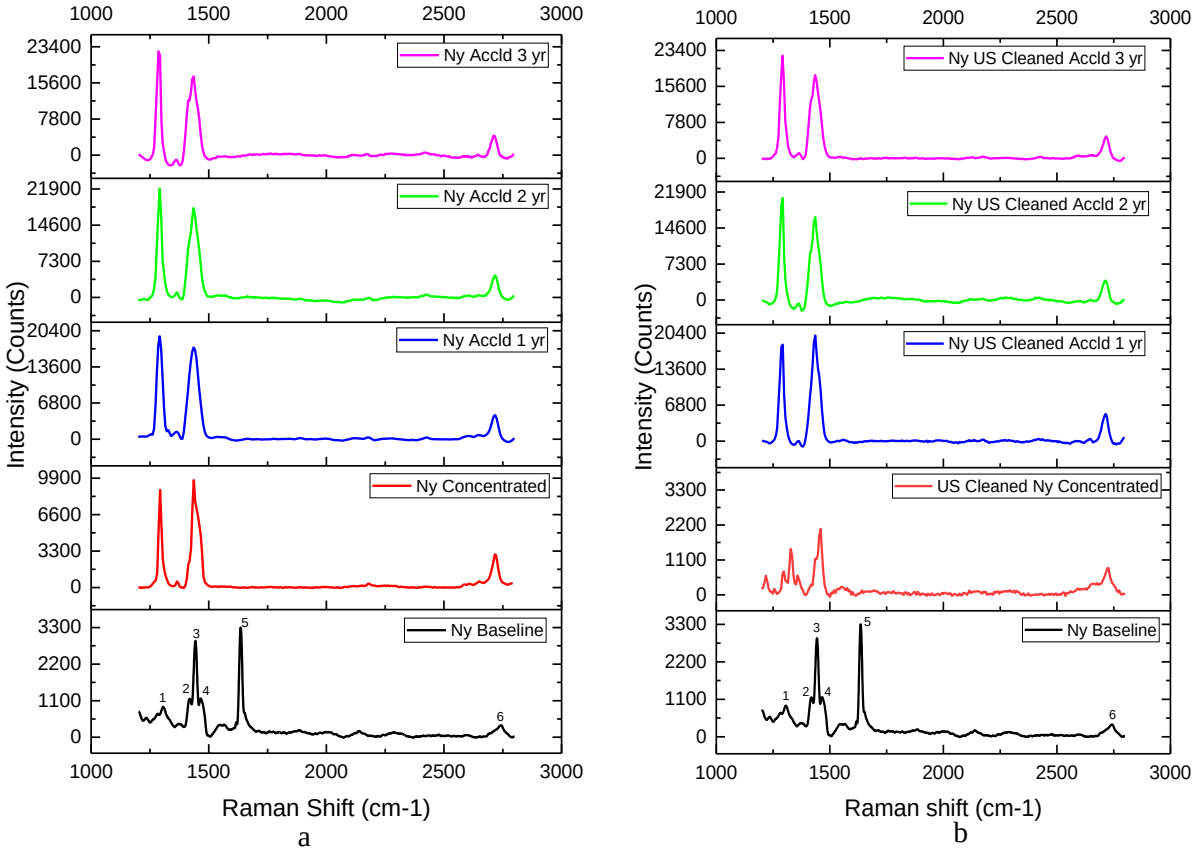

Figure 56: Raman spectra for nylon samples a) with AFFF exposure and b) following ultrasonic cleaning.

Table 24: Raman spectroscopy of nylon with assignment.

Sample Name	Nylon					
	Peak Position, Raman Shift (cm^{-1})					
	1	2	3	4	5	6
Baseline	1306.13	1416.55	1444.71	1472.63	1636.1	2745.31
Concentrated	1292.45	No Peak	1454.32	No Peak	No Peak	2715.76
Accld 1 yr	1292.51	No Peak	1435.98	No Peak	No Peak	2715.02
Accld 2 yr	1292.51	No Peak	1435.98	No Peak	No Peak	2720.1
Accld 3 yr	1286.48	No Peak	1435.98	No Peak	No Peak	2715.02
Assignment	CH_2 twisting	CH_2 bending	CH_2 bending	CH_2 bending	Amide I	Combination band

C.4. Discussion

The spectra for different polymers exposed to AFFF over a range of durations indicate that the PFAS adsorption onto the surface is dependent on exposure duration and polymer type. In addition, the removal of PFAS from the polymer surface was also found to vary based on polymer type.

Figure 57 and Figure 58 provide the net intensity of fluorinated peaks for Nylon (1306 cm^{-1}), Polyethylene (1297 cm^{-1}), Polypropylene (1327 cm^{-1}) before and after ultrasonicated cleaning based on the Raman spectroscopy results. Net intensity was determined by subtracting the baseline intensity of the polymer (i.e., no AFFF exposure) from the intensity of samples exposed to AFFF for different durations.

As seen in Figure 57, nylon had the highest intensity while polypropylene had the lowest with the preference for adsorption of PFAS from AFFF being nylon>polyethylene>polypropylene. The measured preferential adsorption for PFAS for different polymers is similar to that measured in other studies with pure chemical PFAS compounds in Refs. [13, 17]. The higher adsorption for nylon has been attributed to reactions with the N-H bonds in the polymer chain [17]. The differences in adsorption for polyethylene and polypropylene may also be due to their chemical composition. Xrd results for the polyethylene used in this study (see Table 1) indicate that it contains 20% C_{60} (Fullerene) reinforcement. Based on the results in Ref. [37], these C_{60} bonds provide bonding sites for the fluorinated compounds resulting in polyethylene having higher adsorptions. Data in Figure 57 also shows an increasing amount of fluorinated compound on the surface with exposure time up to 3 years for all polymers. This is somewhat different compared with the results in Ref. [17] where the adsorption was observed to reach a plateau after about 10 days of exposure. The different trend in adsorption with time may be due to the other additives in AFFF resulting having an impact on adsorption. In addition, the research in Ref. [17] also showed that the presence of a biofilm due to environmental conditioning in water also increased the adsorption of PFAS onto the surface compared with samples prepared in the laboratory. This implies the fact that plastics with biofilms on to the surface exposed to AFFF may adsorb even more PFAS [17].

The removal of PFAS from the surface through ultrasonic cleaning is shown in Figure 58. As previously indicated, a significant fraction of PFAS can be removed from the surface after a short exposure (2 days). The percent reduction in PFAS from the surface with exposure duration is more clearly seen in Figure 59. PFAS is most effectively removed from polyethylene, with 70-80% removal for all long duration exposures. The effectiveness of removing PFAS from nylon and polypropylene through ultrasonic cleaning decreases

with exposure duration. This is most pronounced in nylon where the effectiveness is less than 10% for longer duration exposures. For polypropylene, ultrasonic cleaning becomes less effective for exposure durations longer than 1 year. These trends for removal of PFAS based on polymer type are similar to that reported in Ref. [17] for desorption of pure PFAS compounds in seawater following a 48-hour soak. In addition, Ref. [17] found that the presence of a biofilm also decreases the amount of desorption compared with laboratory prepared samples. This indicates that the data in Figure 9 may be best case scenario for removal of PFAS from the surface using the ultrasonic cleaning procedure adopted in this study. The trends in the removal of PFAS from the surface for different polymers are in line with the preferential bonding that may occur between the different polymers and PFAS as described previously. The N-H bonds in nylon may bond more with the PFAS resulting in it being more difficult to remove PFAS from the surface, especially after prolonged exposure. Similarly, the C_{60} (Fullerene) reinforcement in the polyethylene may bond more with PFAS making it more difficult to remove compared with the polypropylene which does not have the C_{60}.

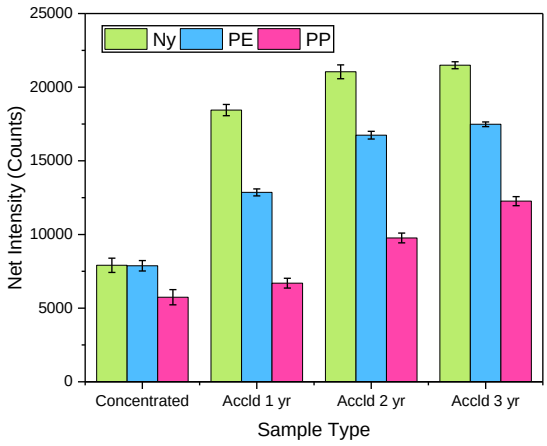

Figure 57: Comparison of intensity for different exposure durations for peak: Ny (1306 cm^{-1}), PE (1297 cm^{-1}), PP (1327 cm^{-1}).

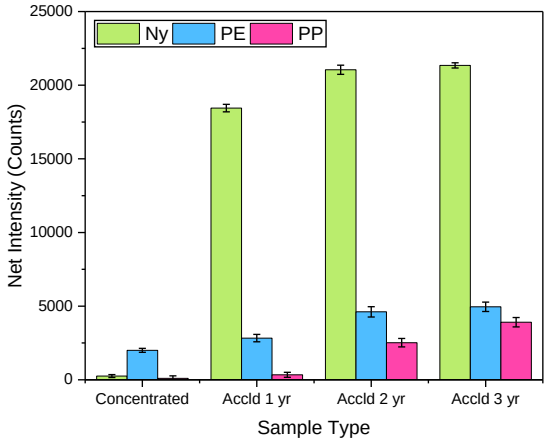

Figure 58: Comparison of intensity at fluorinated peak for ultrasonic cleaned samples fluorinated peak: Ny (1306 cm^{-1}), PE (1297 cm^{-1}), PP (1327 cm^{-1}).

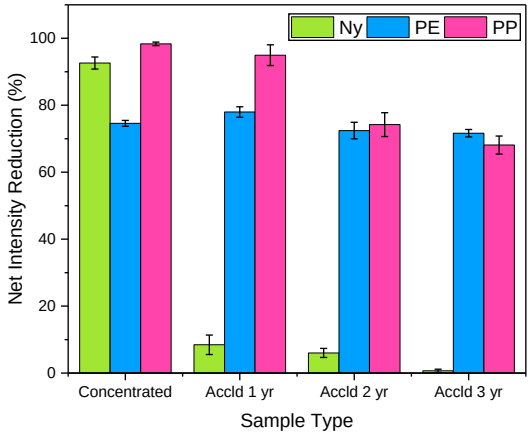

Figure 59: Intensity reduction from fluorinated to Ultrasonicated cleaned samples fluorinated peak: Ny (1306 cm^{-1}), PE (1297 cm^{-1}), PP (1327 cm^{-1}).

C.5. Conclusion

PFAS from AFFF firefighting foam is being phased out due to environmental concerns and equipment that has contained AFFF needs to be cleaned to remain in use. The focus of this research was to explore the impact of polymer type and duration on the sorption of AFFF derived PFAS onto the polymer surface. Three different polymers (polyethylene, polypropylene, and nylon) were exposed to AFFF for effective durations of 2 days to 3 years. The effects of ultrasonic cleaning of the samples were also explored.

The exposure duration had a significant impact on the amount of PFAS at the sample surface. Increasing the exposure duration resulted in an increase in fluorine at the surface for all polymers. Nylon was measured to have the highest adsorption of fluorine on the surface while polypropylene had the least adsorption of fluorine. These results were consistent with measurements in both a FTIR and Raman Spectroscopy. The high adsorption values for nylon were attributed to the possibility of chemical reactions taking place at the surface resulting in stronger bonds between the nylon and PFAS. More PFAS adsorb onto surface if the plastic has been environmentally aged causing a biofilm to form on the surface.

The degree to which PFAS could be removed from the surface through ultrasonic cleaning was dependent both on AFFF exposure duration and polymer type. Increasing the exposure duration resulted in more PFAS remaining on the surface following ultrasonic cleaning. For short term exposure (2 days), the fluorine could be effectively removed from the surface using ultrasonic cleaning (80-90% reduction in Raman intensity for the C-F bond). For longer duration exposures, the reduction was less. Both polyethylene and polypropylene resulted in a reduction in the Raman intensity for the C-F bond of 70-90% depending on the exposure duration. However, nylon resulted in intensity reductions of 0-10%. This was attributed to the stronger bond that forms between the PFAS and nylon. Less removal of PFAS may occur if plastics have been environmentally aged resulting in a biofilm on the surface.

References

[1] L. P. Turner *et al.*, "Mechanochemical remediation of perfluorooctanesulfonic acid (PFOS) and perfluorooctanoic acid (PFOA) amended sand and aqueous film-forming foam (AFFF) impacted soil by planetary ball milling," *Sci Total Environ,* vol. 765, p. 142722, Apr 15 2021, doi: 10.1016/j.scitotenv.2020.142722.

[2] C. Baduel, J. F. Mueller, A. Rotander, J. Corfield, and M. J. Gomez-Ramos, "Discovery of novel per- and polyfluoroalkyl substances (PFASs) at a fire fighting training ground and preliminary investigation of their fate and mobility," *Chemosphere,* vol. 185, pp. 1030-1038, Oct 2017, doi: 10.1016/j.chemosphere.2017.06.096.

[3] B. J. Place and J. A. Field, "Identification of novel fluorochemicals in aqueous film-forming foams used by the US military," *Environ Sci Technol,* vol. 46, no. 13, pp. 7120-7, Jul 3 2012, doi: 10.1021/es301465n.

[4] W. J. Backe, T. C. Day, and J. A. Field, "Zwitterionic, cationic, and anionic fluorinated chemicals in aqueous film forming foam formulations and groundwater from U.S. military bases by nonaqueous large-volume injection HPLC-MS/MS," *Environ Sci Technol,* vol. 47, no. 10, pp. 5226-34, May 21 2013, doi: 10.1021/es3034999.

[5] B. N. Nzeribe, M. Crimi, S. Mededovic Thagard, and T. M. Holsen, "Physico-Chemical Processes for the Treatment of Per- And Polyfluoroalkyl Substances (PFAS): A review," *Critical Reviews in Environmental Science and Technology,* vol. 49, no. 10, pp. 866-915, 2019, doi: 10.1080/10643389.2018.1542916.

[6] W. A. Gebbink, S. Ullah, O. Sandblom, and U. Berger, "Polyfluoroalkyl phosphate esters and perfluoroalkyl carboxylic acids in target food samples and packaging--method development and screening," *Environ Sci Pollut Res Int,* vol. 20, no. 11, pp. 7949-58, Nov 2013, doi: 10.1007/s11356-013-1596-y.

[7] K. A. Barzen-Hanson *et al.*, "Discovery of 40 Classes of Per- and Polyfluoroalkyl Substances in Historical Aqueous Film-Forming Foams (AFFFs) and AFFF-Impacted Groundwater," *Environ Sci Technol,* vol. 51, no. 4, pp. 2047-2057, Feb 21 2017, doi: 10.1021/acs.est.6b05843.

[8] J. Gluge *et al.*, "An overview of the uses of per- and polyfluoroalkyl substances (PFAS)," *Environ Sci Process Impacts,* vol. 22, no. 12, pp. 2345-2373, Dec 1 2020, doi: 10.1039/d0em00291g.

[9] R. C. Buck *et al.*, "Perfluoroalkyl and polyfluoroalkyl substances in the environment: terminology, classification, and origins," *Integr Environ Assess Manag,* vol. 7, no. 4, pp. 513-41, Oct 2011, doi: 10.1002/ieam.258.

[10] R. Mahinroosta and L. Senevirathna, "A review of the emerging treatment technologies for PFAS contaminated soils," *J Environ Manage,* vol. 255, p. 109896, Feb 1 2020, doi: 10.1016/j.jenvman.2019.109896.

[11] J. Becanova, L. Melymuk, S. Vojta, K. Komprdova, and J. Klanova, "Screening for perfluoroalkyl acids in consumer products, building materials and wastes," *Chemosphere,* vol. 164, pp. 322-329, Dec 2016, doi: 10.1016/j.chemosphere.2016.08.112.

[12] R. M. Janousek, S. Lebertz, and T. P. Knepper, "Previously unidentified sources of perfluoroalkyl and polyfluoroalkyl substances from building materials and industrial fabrics," *Environ Sci Process Impacts,* vol. 21, no. 11, pp. 1936-1945, Nov 1 2019, doi: 10.1039/c9em00091g.

[13] J. W. Scott, K. G. Gunderson, L. A. Green, R. R. Rediske, and A. D. Steinman, "Perfluoroalkylated Substances (PFAS) Associated with Microplastics in a Lake Environment," *Toxics,* vol. 9, no. 5, May 11 2021, doi: 10.3390/toxics9050106.

[14] H. Zhu and K. Kannan, "A pilot study of per- and polyfluoroalkyl substances in automotive lubricant oils from the United States," *Environmental Technology & Innovation,* vol. 19, 2020, doi: 10.1016/j.eti.2020.100943.

[15] M. Llorca, M. Farre, H. K. Karapanagioti, and D. Barcelo, "Levels and fate of perfluoroalkyl substances in beached plastic pellets and sediments collected from Greece," *Mar Pollut Bull,* vol. 87, no. 1-2, pp. 286-291, Oct 15 2014, doi: 10.1016/j.marpolbul.2014.07.036.

[16] M. Llorca, G. Schirinzi, M. Martinez, D. Barcelo, and M. Farre, "Adsorption of perfluoroalkyl substances on microplastics under environmental conditions," *Environ Pollut,* vol. 235, pp. 680-691, Apr 2018, doi: 10.1016/j.envpol.2017.12.075.

[17] G. Bhagwat *et al.*, "Biofilms Enhance the Adsorption of Toxic Contaminants on Plastic Microfibers under Environmentally Relevant Conditions," *Environ Sci Technol,* vol. 55, no. 13, pp. 8877-8887, Jul 6 2021, doi: 10.1021/acs.est.1c02012.

[18] S. Lath, E. R. Knight, D. A. Navarro, R. S. Kookana, and M. J. McLaughlin, "Sorption of PFOA onto different laboratory materials: Filter membranes and centrifuge tubes," *Chemosphere,* vol. 222, pp. 671-678, May 2019, doi: 10.1016/j.chemosphere.2019.01.096.

[19] M. A. Uriakhil, T. Sidnell, A. De Castro Fernandez, J. Lee, I. Ross, and M. Bussemaker, "Per- and poly-fluoroalkyl substance remediation from soil and sorbents: A review of adsorption behaviour and ultrasonic treatment," *Chemosphere,* vol. 282, p. 131025, Nov 2021, doi: 10.1016/j.chemosphere.2021.131025.

[20] H. Cao, W. Zhang, C. Wang, and Y. Liang, "Sonochemical degradation of poly- and perfluoroalkyl substances - A review," *Ultrason Sonochem,* vol. 69, p. 105245, Dec 2020, doi: 10.1016/j.ultsonch.2020.105245.

[21] C. Farber *et al.*, "Complementarity of Raman and Infrared Spectroscopy for Structural Characterization of Plant Epicuticular Waxes," *ACS Omega,* vol. 4, no. 2, pp. 3700-3707, 2019, doi: 10.1021/acsomega.8b03675.

[22] J. Zięba-Palus, "The usefulness of infrared spectroscopy in examinations of adhesive tapes for forensic purposes," *Forensic Science and Criminology,* vol. 2, no. 2, 2017, doi: 10.15761/fsc.1000112.

[23] J. Maity, C. Jacob, C. K. Das, S. Alam, and R. P. Singh, "Homocomposites of chopped fluorinated polyethylene fiber with low-density polyethylene matrix," *Materials Science and Engineering: A,* vol. 479, no. 1-2, pp. 125-135, 2008, doi: 10.1016/j.msea.2007.06.045.

[24] A. P. Kharitonov and L. N. Kharitonova, "Surface modification of polymers by direct fluorination: A convenient approach to improve commercial properties of polymeric articles," *Pure and Applied Chemistry,* vol. 81, no. 3, pp. 451-471, 2009, doi: 10.1351/pac-con-08-06-02.

[25] A. Gopanna, R. N. Mandapati, S. P. Thomas, K. Rajan, and M. Chavali, "Fourier transform infrared spectroscopy (FTIR), Raman spectroscopy and wide-angle X-ray scattering (WAXS) of polypropylene (PP)/cyclic olefin copolymer (COC) blends for qualitative and quantitative analysis," *Polymer Bulletin,* vol. 76, no. 8, pp. 4259-4274, 2018, doi: 10.1007/s00289-018-2599-0.

[26] G. Acik, C. E. Cansoy, and M. A. Tasdelen, "Synthesis of fluorinated polypropylene using CuAAC click chemistry," *Journal of Applied Polymer Science,* vol. 136, no. 7, 2018, doi: 10.1002/app.47072.

[27] J. Yang, C. Feng, J. Dai, N. Zhang, T. Huang, and Y. Wang, "Compatibilization of immiscible nylon 6/poly(vinylidene fluoride) blends using graphene oxides," *Polymer International,* vol. 62, no. 7, pp. 1085-1093, 2013, doi: 10.1002/pi.4396.

[28] S. Affatato, E. Modena, S. Carmignato, and P. Taddei, "The use of Raman spectroscopy in the analysis of UHMWPE uni-condylar bearing systems after run on a force and displacement control knee simulators," *Wear,* vol. 297, no. 1-2, pp. 781-790, 2013, doi: 10.1016/j.wear.2012.10.002.

[29] F. Fleissner, K. E. Napp, B. Wezisla, and L. Völker-Pop, "Combined Raman Spectroscopy and Rheology for Characterizing Polymer Melts," *Spectroscopy,* vol. 34, p. 9, 2019.

[30] F. Withers, S. Russo, M. Dubois, and M. F. Craciun, "Tuning the electronic transport properties of graphene through functionalisation with fluorine," *Nanoscale research letters,* vol. 6, no. 1, pp. 1-11, 2011.

[31] M. L. Shofner, V. N. Khabashesku, and E. V. Barrera, "Processing and mechanical properties of fluorinated single-wall carbon nanotube− polyethylene composites," *Chemistry of Materials,* vol. 18, no. 4, pp. 906-913, 2006.

[32] M. A. De Baez, P. Hendra, and M. Judkins, "The Raman spectra of oriented isotactic polypropylene," *Spectrochimica Acta Part A: Molecular and Biomolecular Spectroscopy,* vol. 51, no. 12, pp. 2117-2124, 1995.
[33] S. R. Ahmad, R. J. Young, and I. A. Kinloch, "Raman Spectra and Mechanical Properties of Graphene/Polypropylene Nanocomposites," *International Journal of Chemical Engineering and Applications*, vol. 6, no. 1, pp. 1-5, 2015, doi: 10.7763/ijcea.2015.V6.440.
[34] D. McIntosh, V. N. Khabashesku, and E. V. Barrera, "Nanocomposite fiber systems processed from fluorinated single-walled carbon nanotubes and a polypropylene matrix," *Chemistry of Materials*, vol. 18, no. 19, pp. 4561-4569, 2006.
[35] B. Stuart, "A Fourier transform Raman study of water sorption by Nylon 6," *Polymer bulletin*, vol. 33, no. 6, pp. 681-686, 1994.
[36] V. K. Rangari, M. Yousuf, S. Jeelani, M. X. Pulikkathara, and V. N. Khabashesku, "Alignment of carbon nanotubes and reinforcing effects in nylon-6 polymer composite fibers," *Nanotechnology*, vol. 19, no. 24, p. 245703, Jun 18 2008, doi: 10.1088/0957-4484/19/24/245703.
[37] S. Amarantov *et al.*, "Investigation of fluorinated C60 by means of optical spectroscopy," *Nuclear Instruments and Methods in Physics Research Section A: Accelerators, Spectrometers, Detectors and Associated Equipment*, vol. 470, no. 1-2, pp. 318-322, 2001.